UNCLASSIFIED

SECURITY CLASSIFICATION OF THIS PAGE (When Data Entered)

DTIC FILE COPY

1

AD-A197 218

REPORT DOCUMENTATION PAGE

READ INSTRUCTIONS BEFORE COMPLETING FORM

1. REPORT NUMBER: AFIT/CI/NR 88- 133

2. GOVT ACCESSION NO.

3. RECIPIENT'S CATALOG NUMBER

4. TITLE (and Subtitle): THE EFFECT OF VERTICAL WIND SHEAR ON TROPICAL CYCLONE MOVEMENT

5. TYPE OF REPORT & PERIOD COVERED: MS THESIS

6. PERFORMING ORG. REPORT NUMBER

7. AUTHOR(s): KIM MARGARET TALBERT

8. CONTRACT OR GRANT NUMBER(s)

9. PERFORMING ORGANIZATION NAME AND ADDRESS: AFIT STUDENT AT: NORTH CAROLINA STATE UNIVERSITY.

10. PROGRAM ELEMENT, PROJECT, TASK AREA & WORK UNIT NUMBERS

11. CONTROLLING OFFICE NAME AND ADDRESS

12. REPORT DATE: 1988

13. NUMBER OF PAGES: 111

14. MONITORING AGENCY NAME & ADDRESS (if different from Controlling Office): AFIT/NR, Wright-Patterson AFB OH 45433-6583

15. SECURITY CLASS. (of this report): UNCLASSIFIED

15a. DECLASSIFICATION/DOWNGRADING SCHEDULE

16. DISTRIBUTION STATEMENT (of this Report): DISTRIBUTED UNLIMITED: APPROVED FOR PUBLIC RELEASE

DTIC ELECTE AUG 0 2 1988 S D CSD

17. DISTRIBUTION STATEMENT (of the abstract entered in Block 20, if different from Report): SAME AS REPORT

18. SUPPLEMENTARY NOTES: Approved for Public Release: IAW AFR 190-1
LYNN E. WOLAVER
Dean for Research and Professional Development
Air Force Institute of Technology
Wright-Patterson AFB OH 45433-6583

19. KEY WORDS (Continue on reverse side if necessary and identify by block number)

20. ABSTRACT (Continue on reverse side if necessary and identify by block number): ATTACHED

DD FORM 1 JAN 73 1473 EDITION OF 1 NOV 65 IS OBSOLETE

UNCLASSIFIED

SECURITY CLASSIFICATION OF THIS PAGE (When Data Entered)

Abstract

TALBERT, KIM M. The Effect of Vertical Wind Shear on Tropical Cyclone Movement (Under the direction of Mark DeMaria).

Tropical cyclone motion is investigated using a three-dimensional primitive equation model based upon Ooyama's three-layer incompressible fluid model. The governing equations are solved on a doubly periodic midlatitude f-plane using a spectral method with Fourier basis functions. Numerical f-plane simulations are run which successively include a nearly linear horizontal barotropic basic current, surface drag, and cumulus convection. Simulations are then run, under identical conditions, with increasingly greater magnitudes of westerly vertical wind shear. [i.e. $U_{layer\ 2} - U_{layer\ 1} > 0$]. All simulations are repeated using a variable Coriolis parameter to incorporate the β-effect.

Relative vorticity advection had the most dominant effect on tropical cyclone motion followed by the β-effect. The inclusion of the physical processes of surface drag and cumulus convection also had significant effects. Surface drag retarded vortex speed and resulted in a rightward deviation of the vortex relative to the direction of the basic current. Cumulus convection also resulted in vortex deviations to the right of the track towards the regions of diabatic heating associated with areas of maximum boundary layer convergence. These results are in agreement with numerous other studies.

The effect of unidirectional vertical wind shear on cyclone movement is twofold. The primary effect, evident in all shear simulations, results in an initial deviation of the simulated cyclone towards the right of the direction of the wind shear vector. This deviation is directed towards

enhanced environmental temperatures. The magnitude of the deviation increases as the magnitude of the shear increases.

A secondary effect is observed in some cases. This effect results from vertical vortex tilt due to the differential motion between the upper and lower layer vortices caused by vertically varying winds. Cyclone movement induced by this effect generally acts in the same direction as the primary effect. A time lag of about 6 hours between maximum vortex tilt and directional changes is observed. Depending upon the direction of the shear vector and basic current, the effects of vertical shear can either enhance the effects of other factors or work against them. These results indicate that, in some cases, vertical wind shear may be responsible for seemingly anomalous turning motion observed in tropical cyclone paths.

These shear results were verified in variable origin simulations incorporating vertical shear that varied both in direction and speed. The sensitivity of a cyclone's track to initial placement is less for the primitive equation model than that observed for a nondivergent barotropic model and is partially due to the inclusion of vertical shear.

The sensitivity of simulated cyclone to sea surface temperature is investigated. Results show the intensity of the storm to increase as the sea surface temperature increases. The track remains relatively unaffected indicating that the modeling of storm intensity may not be extremely important for track forecasting in some cases.

The Effect of Vertical Wind Shear on Tropical Cyclone Movement

by

Kim Margaret Talbert

A thesis submitted to the Graduate Faculty of
North Carolina State University
in partial fulfillment of the
requirements for the Degree of
Master of Science

Department of Atmospheric Sciences

Raleigh

1987

Approved by:

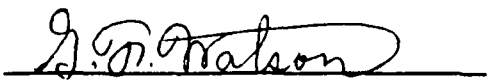

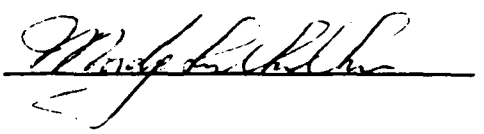

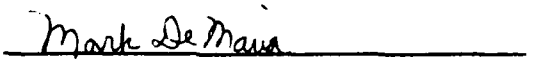

Chairman of Advisory Committee

Table of Contents

1. Introduction

Because of the potentially devastating threat that tropical cyclones pose to life and property, a great amount of effort has been expended to accurately predict their tracks. Dynamical models are currently being used operationally to forecast tropical cyclone movement and, in research, to increase the understanding of factors affecting this movement. All these models utilize various forms of some, or all, of the equations governing conservation of momentum, mass and energy in the atmosphere. The simplest operational model, SANBAR (for Sanders Barotropic) originally developed by Sanders and Burpee (1968), is a one-layer model which uses the barotropic vorticity equation to forecast the vertically averaged vorticity field. One of the most complex models is the Movable Fine Mesh model (MFM) developed by Hovermale and Livezey (1977). The MFM, currently used by the National Meteorological Center, is a ten-layer three-dimensional model utilizing the full set of the primitive equations and a fine mesh that moves with the cyclone. Theoretical and observational studies suggest that there are many different factors, acting simultaneously and interactively, which can affect the movement of a tropical cyclone. These factors include: vortex advection by the large scale horizontal wind, the variation of the Coriolis parameter with latitude (the β-effect), the physical processes of the cyclone, the structure of the vortex, and the vertical shear of the large scale horizontal winds. A complete understanding of these factors, facilitated by the use of research models, is necessary for the improvement of tropical cyclone forecasting.

The most dominant factor affecting tropical cyclone movement is the advection of the cyclone by the large scale current in which it is embedded. This concept, commonly referred to as the steering current principle, originated in conjunction with the movement of extratropical cyclones and was later expanded for use in the tropics. As observational methods in the tropics improved, much research was devoted towards the specification of a best steering layer or best level for use in tropical cyclone track prediction (e.g., George and Gray, 1976). Recognizing that cyclone motion was the result of complex interactions between the tropical cyclone and the larger scale environment, researchers began to work towards the determination of factors which could modify cyclone movement. With the advent of numerical predication methods, it became possible to test these concepts.

Numerical studies (Kasahara, 1957; Kasahara and Platzman, 1963; DeMaria, 1985) indicated that the center of a vortex moved with the mean flow in a constant or horizontally linear basic current. However, these studies also indicated that this movement would be modified by a component down and to the left of a vorticity gradient associated with a nonlinear basic current. This same principle can be applied to the planetary vorticity gradient which arises from the variation of the Coriolis parameter with latitude. Many numerical studies have shown that the inclusion of a variable Coriolis parameter induces a northwestward movement of a vortex at speeds between 1 and 3 ms^{-1}.

In further attempts to define an adequate steering current, Anthes and Hoke (1975) isolated the effect of the horizontal divergence of the large scale winds upon vortex motion on a ß-plane. By comparing the tracks of

cyclones simulated in divergent and nondivergent models, they found that the inclusion of divergent winds slowed the westward component of vortex motion. The inclusion of divergence in a barotropic model resulted in vortex movement similiar to that observed with a three-dimensional model.

Physical processes such as surface drag and cumulus convection are fundamental to the existence of tropical cyclones. Frictionally induced low-level convergence of the large scale horizontal winds leads to the forced ascent of saturated air parcels and cumulus convection occurs. The latent heat release from the cumulus clouds drives the cyclone circulation which in turn leads to increased low-level convergence. Charney and Eliassen (1964) first discerned this cooperative interaction between different scales of motion, commonly referred to as Conditional Instability of the Second Kind (CISK). It is this interaction which, combined with the presence of low level moisture, is responsible for the maintenance of a tropical cyclone. Studies have indicated that the inclusion of physical processes in dynamical models can significantly change the track of a cyclone (DeMaria, 1984).

Kuo (1968) showed theoretically that a cyclonically rotating vortex in a basic flow would deflect to the right of, and move slower than, the defined steering current, if the surface drag on the base of the vortex exceeded that on the environment. The inclusion of the diabatic effects of cumulus convection in a dynamical model directly influences the size, intensity, and symmetry of a simulated cyclone. Changes in any one of the factors could further effect the path of a cyclone.

While much research has been conducted with respect to the foregoing factors, very little has been directed towards isolating the effects of the vertical shear of the large scale horizontal wind upon tropical cyclone motion. A study by Jones (1977a) used several different vertically sheared environments to define an appropriate steering current but did not attempt to separate the effects of the wind shear. Other research concentrated more upon cyclone intensity and development rather than track forecasting. For example, Madala and Piacsek (1975) showed that tropical cyclones do not develop in regions of large vertical wind shear (>1.25 ms^{-1}/km). Recent observational studies indicate that storms in nature exhibit anomalous motion which has yet to be explained (e.g., Chan, 1986). In some cases vertical wind shear may be an important factor in explaining this motion. This thesis utilizes a three-dimensional primitive equation model (PEMOD) to investigate the effects of vertical wind shear on a simulated vortex by successively including the effects of surface drag, cumulus convection, a linear barotropic basic current, and a unidirectional vertically sheared basic current. All simulations are made on an f-plane and then repeated on a β-plane to incorporate the effects of planetary vorticity advection. These simulations are then compared to simulations run under similar initial conditions, using a nondivergent barotropic spectral model (NDBM).

The model chosen for this study was developed by DeMaria and Schubert (1984) and is a generalization of the three-layer, axisymmetric model developed by Ooyama (1969). Ooyama's model was one of the first to successfully simulate the life cycle of tropical cyclones. The model uses a simple cumulus parameterization scheme which treats the diabatic

effects of cumulus convection as a mass flux between layers of different density and is proportional to the vertical velocity at the top of the boundary layer and the vertical distribution of equivalent potential temperature. The model also uses the minimum vertical resolution necessary for tropical cyclone simulations (three layers). The lowest layer represents a constant thickness boundary layer, the middle layer is representative of the 600 mb mean pressure level, and the top layer represents the 200 mb outflow layer. Expanding Ooyama's model to three dimensions was necessary to simulate interactions between the vortex and large scale winds as well as asymmetries. The balance approximation was relaxed and more general primitive equations were used since the balance equations are much more difficult to solve in three--dimensions.

In a departure from the norm in numerical tropical cyclone prediction, DeMaria (1983) and DeMaria and Schubert (1984) solved the primitive equation models using the Spectral Galerkin method. This method was chosen over the more commonly used finite-difference methods because it reduces computational dispersion, eliminates nonlinear instabilities, and is more accurate per degree of freedom. In this method, the spatially dependent variables are expanded in a series of orthogonal basis functions which satisfy the boundary conditions of the dependent variables. Because these equations are solved on a doubly periodic midlatitude ß-plane, Fourier components were chosen as the basis functions. Periodic boundary conditions were chosen to simulate an infinite domain and the disturbance, the simulated cyclone in this case, is considered small with respect to the domain size in order to circumvent boundary problems.

After the spatially dependent variables are expanded in truncated double Fourier series, they are substituted back into the governing equations and an inner product is taken with each basis function. The result is a set of ordinary differential equations for the time dependent series amplitudes. The equations, in spectral form, are then integrated forward in time using the forward time differencing scheme for the first time step and the Adams-Bashforth scheme thereafter. In order to accomplish the integration, the nonlinear terms must be calculated at each time step. This is accomplished by transforming the dependent variables from spectral space to physical space at specified grid points. The nonlinear products of the dependent variables are calculated and then an inverse transform, using a numerical quadrature rule, is used to transform back to spectral space (Orzag, 1970). A detailed description of the spectral method may be found in DeMaria (1983).

In Chapter 2, the governing equations and model parameters are presented along with a brief description of the parameterization schemes used for the physical processes. Results of cyclone simulations, made under resting basic state conditions to test the cyclone features, are also presented. Chapter 3 investigates the effects of the physical processes on tropical cyclone movement by successively including the parameterizations for surface drag and cumulus convection for simulations run under nonresting barotropic basic flow conditions. In Chapter 4, results of simulations with a vortex embedded in easterly and westerly currents with varying magnitudes of vertical wind shear are presented. The vortex center in each layer is tracked separately in an effort to

understand how the vertical structure is effected by vertical wind shear and how this change of structure affects the movement of a cyclone.

To test the findings of this preliminary research on the effect of vertical wind shear, experiments are made with a vortex embedded on the periphery of a simulated subtropical anticyclone where the vertical wind shear is allowed to change both direction and magnitude. Prediction of cyclone tracks by numerical models tend to be sensitive to errors made in the specification of the initial conditions. To investigate this sensitivity, the origin of the vortex is changed in the north-south and east-west directions while all other conditions are kept constant. The results of these experiments are presented in Chapter 5 along with a comparison with experiments run under similar conditions using a nondivergent barotropic version of the model (NDBM).

Sea surface temperatures are known to affect the intensity of a tropical cyclone (Ooyama, 1969; Kitade, 1980). Several experiments are conducted with differing values of sea surface temperature specified in order to examine the effect upon tropical cyclone movement. The results of these experiments are also presented in Chapter 5. Finally, in Chapter 6, a summary of the research findings will be presented along with a discussion of their significance.

2. Model Summary

2.1 Summary of the Governing Equations

The equations governing the motion of the three-layer incompressible rotating fluid system are given in vector form by:

$$\frac{\partial \mathbf{V}_0}{\partial t} + f\hat{k} \times \mathbf{V}_0 + \nabla\phi_0 = -(\mathbf{V}_0\cdot\nabla)\mathbf{V}_0 + \mathbf{F}_0 - \frac{w^-}{H_0}(\mathbf{V}_0 - \mathbf{V}_1) \tag{2.1}$$

$$\frac{\partial \mathbf{V}_1}{\partial t} + f\hat{k} \times \mathbf{V}_1 + \nabla\phi_1 = -(\mathbf{V}_1\cdot\nabla)\mathbf{V}_1 + \mathbf{F}_1 + \frac{w^+}{(H_1+h_1)}(\mathbf{V}_0 - \mathbf{V}_1) \tag{2.2}$$

$$\frac{\partial \mathbf{V}_2}{\partial t} + f\hat{k} \times \mathbf{V}_2 + \nabla\phi_2 = -(\mathbf{V}_2\cdot\nabla)\mathbf{V}_2 + \mathbf{F}_2 \tag{2.3}$$

$$H_0\nabla\cdot\mathbf{V}_0 + w = 0 \tag{2.4}$$

$$\frac{\partial h_1}{\partial t} + H_1\nabla\cdot\mathbf{V}_1 - w = -\nabla\cdot(h_1\mathbf{V}_1) - Q \tag{2.5}$$

$$\frac{\partial h_2}{\partial t} + H_2\nabla\cdot\mathbf{V}_2 = -\nabla\cdot(h_2\mathbf{V}_2) + \frac{Q}{e} \tag{2.6}$$

where

$\mathbf{V}_i = u_i\hat{i} + v_i\hat{j}$ = horizontal velocity of layer i (i=0,1,2)

u_i = eastward component of velocity

v_i = northward component of velocity

w = vertical velocity at the top of the boundary layer

H_i = mean thickness of layer i

h_i = thickness deviation from mean thickness

f = Coriolis parameter

g = acceleration of gravity

ρ_i = density of layer i

IF_i = friction term of layer i

$$\epsilon = \frac{\rho 2}{\rho 1}$$

$Q = Q^+ - Q^-$ = diabatic flux

$$\phi_0 = \phi_1 = g(h_1 + \epsilon h_2)$$

$$\phi_2 = g(h_1 + h_2)$$

$$w^+ = \frac{1}{2}(|w| + w)$$

$$w^- = \frac{1}{2}(|w| - w)$$

$$\nabla = \frac{\partial}{\partial x}\hat{i} + \frac{\partial}{\partial y}\hat{j}$$

Equations (2.1)-(2.3) are the momentum equations for each fluid layer in cartesian coordinates. Because the density is assumed to be the same in layers 0 and 1, the last terms on the right hand side of equations (2.1) and (2.2) are included so that momentum is conserved in those layers when a positive vertical motion exists at the top of the boundary layer. Equations (2.4)-(2.6) are the mass continuity equations for each layer where the boundary layer equation (2.4) takes a simple form because it is assumed to have a constant thickness (i.e. $h_0 = 0$). The continuity equations for layers 1 and 2 include the mass transport term Q which allows for the inclusion of the diabatic effects of heating Q^+ and cooling Q^-. In an incompressible system, these effects allow parcels to move between fluid layers of different density. Both Q and IF_i represent the effects of many small scale motions that must be formulated in terms of the large scale

variables in order to close the set of governing equations. The parameterization of these terms will be discussed in the next section.

To incorporate the effects of a variable Coriolis parameter, the midlatitude ß-plane approximation is applied to the model. In this approximation, the Coriolis parameter f is approximated by $f_o+ßy$ where ßy is neglected compared to f_o except where f is differentiated. This approximation is necessary to satisfy the doubly periodic boundary conditions of the model. To incorporate this approximation into the model, the momentum equations (2.1)-(2.3) must be used in differentiated form. Therefore, they are replaced by the vorticity ζ_i and the divergence δ_i equations. These equations are derived in each layer by calculating the right hand side of the following equations

$$\frac{\partial \zeta_i}{\partial t} = \frac{\partial}{\partial x}\left(\frac{\partial v_i}{\partial t}\right) - \frac{\partial}{\partial y}\left(\frac{\partial u_i}{\partial t}\right) \tag{2.7}$$

$$\frac{\partial \delta_i}{\partial t} = \frac{\partial}{\partial x}\left(\frac{\partial u_i}{\partial t}\right) + \frac{\partial}{\partial y}\left(\frac{\partial v_i}{\partial t}\right) \tag{2.8}$$

where $\frac{\partial u_i}{\partial t}$ and $\frac{\partial v_i}{\partial t}$ are the two scalar equations obtained by expanding the vector form of the momentum equations for each layer into their x and y components. Furthermore, a streamfunction ψ_i and a velocity potential χ_i relating the velocity components to the vorticity and divergence may be defined as follows:

$$u_i = -\frac{\partial \psi_i}{\partial y} + \frac{\partial \chi_i}{\partial x} \tag{2.9}$$

$$v_i = \frac{\partial \psi_i}{\partial x} + \frac{\partial \chi_i}{\partial y} \tag{2.10}$$

$$\zeta_i = \nabla^2 \psi_i = \frac{\partial v_i}{\partial x} - \frac{\partial u_i}{\partial y} \tag{2.11}$$

$$\delta_i = \nabla^2 \chi_i = \frac{\partial u_i}{\partial x} + \frac{\partial v_i}{\partial y} \tag{2.12}$$

These diagonostic relationships are used to specify the divergence, vorticity, and horizontal velocity components in terms of the streamfunction and velocity potential when the Fourier Galerkin solution method is applied.

Aside from the parameterizations of the physical processes and the ß-plane approximation, only one other approximation is made to the governing equations. In the calculated version of (2.7), the velocity potential contribution to βv_i is neglected, as is the streamfunction contribution to the βu_i term in (2.8). This approximation is necessary so that nonoscillating solutions to the linearized equations do not occur (Stevens, et al., 1977)

2.2 Summary of Parameterization of Physical Processes

In order to close the set of equations, the friction and mass transport terms must be formulated in terms of the large scale field variables. The friction terms, following DeMaria (1983), are parameterized by:

$$\mathbb{F}_0 = -\frac{C_D}{H_0}|\mathbb{V}_0|\mathbb{V}_0 + \lambda_2\nabla^2\mathbb{V}_0 \tag{2.13}$$

$$\mathbb{F}_1 = \lambda_2\nabla^2\mathbb{V}_0 - \mu\frac{(\mathbb{V}_1 - \mathbb{V}_2)}{(H_1+h_1)} \tag{2.14}$$

$$\mathbb{F}_2 = \lambda_2\nabla^2\mathbb{V}_2 + \mu\frac{(\mathbb{V}_1 - \mathbb{V}_2)}{\epsilon(H_2+h_2)} + Q^+\frac{(\mathbb{V}_1 - \mathbb{V}_2)}{\epsilon(H_2+h_2)} \tag{2.15}$$

(A) (B) (C) (D)

where

$|\mathbb{V}_0|$ = the magnitude of the horizontal boundary layer wind

C_D = coefficient of momentum exchange

λ_2 = horizontal eddy diffusion coefficient

μ = shear stress coefficient

Term A specifies the surface drag calculated from the bulk aerodynamic formula. The B terms represent the effect of the horizontal eddy diffusion of momentum. Vertical diffusion effects resulting from velocity shear between layers 1 and 2 are represented by the C terms. Term D arises from the mixing of momentum that occurs when mass is transported from layer 1 to layer 2. Constant values of .0015 and 10^3 m^2s^{-1} were assumed for the frictional coefficients C_D and λ_2, respectively and were so chosen based upon experimental evidence by Ooyama (1969) and DeMaria (1983). The shear stress coefficient μ assumes a constant value of 1.5×10^{-4} ms^{-1}.

The diabatic effects of cumulus clouds are treated collectively and represented by a mass transport Q^+ from layer 1 to layer 2 in this model. As previously discussed, cumulus convection on the tropical cyclone scale can occur only if convectively unstable air is continuously supplied through low level convergence. Therefore, following Ooyama (1969), Q^+ is given by:

$$Q^+ = \begin{cases} \eta w & w>0 \\ 0 & w\leq 0 \end{cases} \tag{2.16}$$

where

$$\eta = 1 + \frac{\Lambda_0 - \Lambda_2}{\Lambda_2 - \Lambda_1}. \tag{2.17}$$

The equivalent potential temperature deviations are given by the following relations:

$$\Lambda_0 = (\theta_e)_0 - \Theta$$

$$\Lambda_1 = (\theta_e)_1 - \Theta \qquad (2.18)$$

$$\Lambda_2 = (\theta_e^*)_2 - \Theta$$

where $(\theta_e)_0$ and $(\theta_e)_1$ are the equivalent potential temperatures of the ambient air in layers 0 and 1. $(\theta_e^*)_2$ is the saturated equivalent potential temperature in layer 2 based on the assumption that the environmental and saturated cloud air have the same temperature at this level. The term Θ represents a constant reference temperature set to 342K.

The proportionality factor η is derived from moist static energy considerations. This measure of convective instability depends upon the vertical distribution of the equivalent potential temperature given by equation (2.17). Again, following Ooyama (1969), the temperature distribution must include the stabilizing effect of upper level (layer 2) warming in order to check the uncontrolled growth of a model vortex. Also, variations in the boundary layer equivalent potential temperature must be represented, otherwise η would decrease unrealistically with the establishment of a warm core. The equivalent potential temperature in each layer is therefore determined by the following:

$$\frac{\partial \Lambda_0}{\partial t} = -u_0\frac{\partial \Lambda_0}{\partial x} - v_0\frac{\partial \Lambda_0}{\partial y} - \frac{\bar{w}}{H_0}(\Lambda_0 - \Lambda_1) + \lambda_2\nabla^2\Lambda_0 + \frac{C_E}{H_0}|V_0|(\Lambda_S - \Lambda_0) \qquad (2.19)$$

$$\Lambda_1 = -10K \qquad (2.20)$$

$$\Lambda_2 = \bar{\Lambda}_2 + \frac{gy}{c_p}(1 - e)h_2 \qquad (2.21)$$

where $$\Lambda_S = \bar{\Lambda}_S - \frac{g\alpha}{c_p}(h_1 - h_2) \qquad (2.22)$$

Equation (2.19) is the thermodynamic energy equation for the boundary layer, from which the boundary layer potential temperature deviation is predicted. The first two terms on the right hand side represent the horizontal advection of the equivalent potential temperature, while the third term represents its vertical advection. Horizontal eddy diffusion is represented by the fourth term. The last term represents the surface flux of the equivalent potential temperature. C_E is the air-sea exchange coefficient which is assumed equivalent in value to the surface drag coefficient.

Λ_S is the sea surface saturated equivalent potential temperature deviation and is given by equation (2.22). The mean sea surface temperature deviation $\bar{\Lambda}_S$ is a function of the sea surface temperature T_S. The constant α has a value of 1.87 and c_p is the specific heat at constant pressure. All model simulations use $\bar{\Lambda}_S$ = 30K, which corresponds to a sea surface temperature of 27.5°C, except in Chapter 5 where the effects of the sea surface temperature on tropical cyclone movement is investigated. Since Λ_0 is now a prognostic variable, it is initially set to 15K corresponding to a boundary layer equivalent potential temperature of 357K.

Ooyama (1969) argued that the mid-level layer 1 equivalent potential temperature deviations were not of critical importance to the dynamics of the tropical cyclone so Λ_1 is given a constant value of -10K. This value corresponds to a constant midlevel θ_e value of 332K. Finally, the saturated equivalent potential temperature deviation for layer 2, Λ_2, can be

diagnosed using equation (2.21). $\bar{A}_2$ is a function of the standard value for the layer 2 equivalent potential temperature at large distances from the storm center and is assumed constant at 0K. The constant γ has a value of 8.6 and is derived from an analogy with compressible fluids and the assumption that layers 1 and 2 are representative, respectively, of the 600mb and 200mb pressure levels. For a complete discussion on the formulation of equations (2.16)-(2.22), the reader is referred to the original paper by Ooyama (1969) and to DeMaria (1983).

The diabatic effect of radiative cooling, Q^-, is also parameterized in this model by crudely simulating a mass transport from layer 2 to layer 1. The inclusion of this term is required to offset the net heating of the model domain that occurs with the establishment of a warm core and allows for longer integration times (DeMaria, 1984). Therefore, to allow the layer between 200mb and 600mb to cool by 1°C per day, Q^- is given by:

$$Q^- = \frac{\epsilon R \ln\left(\frac{600}{200}\right)}{g(1-\epsilon)} \frac{1^\circ C}{day} \qquad (2.23)$$

where R is the gas constant for dry air.

In summary, equations (2.13)-(2.15) define the friction terms of the momentum equations while equations (2.16)-(2.22) give the diabatic effects of cumulus convection in terms of large-scale variables. Radiative cooling is crudely simulated through the inclusion of (2.23) into the mass continuity equations for layers 1 and 2. The vector form of the momentum equations (2.1)-(2.3) are then expanded into their appropriate components, after which the vorticity and divergence equations can be calculated using (2.7) and (2.8). The boundary layer equivalent potential

temperature deviation must now be predicted, and the layer 2 saturated temperature diagnosed, at every time step. If the vertical velocity w is eliminated, the resulting equations (2.5)-(2.8) and (2.19) become a system of nine equations in x,y and t with nine unknowns ψ_0, χ_0, ψ_1, χ_1, h_1, ψ_2, χ_2, h_2, and Λ_0.

2.3 Solution Method

To obtain the approximate solutions to the governing equations, the Spectral Galerkin method described in Chapter 1 is applied. The resulting equations are then transformed in the vertical so that the dependent variables are the amplitudes of the model normal modes. Three vertical modes exist in this model, two of which have shallow water equations describing the horizontal structure. The last mode is an inertial oscillation mode arising due to the use of a constant bounday layer thickness. Given the mean thickness for each layer, the solutions to the shallow water equations yield an external gravity wave speed of 287 ms^{-1} and an internal gravity wave speed of 52 ms^{-1}. A more complete description of the spectral solution to the governing equations and the derivation of the model normal modes can be obtained in DeMaria (1983) and DeMaria and Schubert (1984).

All model simulations use a series truncation limit of M=N=35. The dependent variables are doubly periodic in the east-west and north-south directions on the respective intervals of $[0,L_x]$ and $[0,L_y]$ where $L_x = L_y = 4000$km. The resolution, using a 3M+1 point physical grid in conjunction with the above Fourier truncation limit and domain size, is approximately 38 km. This resolution is adequate for examining the large

scale tropical cyclone features. The average simulation was integrated for 72 hours on the Cray-XMP and took approximately 9 minutes of CPU time using a 90 second time step.

DeMaria (1983) discusses the phenomena of spectral blocking which is the tendency for larger amounts of energy to accumulate in the higher wave numbers due to the sharp gradients of the dependent variables that develop as the cyclone intensifies. In order to filter this excess energy without affecting the larger scales of motion, fourth-order horizontal diffusion terms are added to equations (2.4)-(2.8) and (2.19). Throughout this study, the model uses a value of $.3 \times 10^{14}$ $m^4 s^{-1}$ in all simulations which results in an e-folding time of 1.02 hours for the amplitude of the highest mode in the simplest one-dimensional case. Table 1 gives the values of the parameters used in a typical model simulation.

2.4 Initial Conditions

The primitive equation model is initialized, in all layers, with an axisymmetric barotropic vortex of the form:

$$V(r) = V_m(\frac{r}{r_m})\exp[1 - \frac{r}{r_m}] \tag{2.24}$$

where

$$r = [(x - x_o)^2 + (y - y_o)^2]^{1/2} \tag{2.25}$$

The maximum tangential wind V_m is equal to 25 ms^{-1} at a radius, r_m, of 100 km from the vortex center. The coordinates of the vortex center are represented by $(x_o\ y_o)$, which is normally the exact center of the model domain unless otherwise specified. Because the movement of a vortex is dependent upon the vortex structure outside the radius of maximum

winds, (e.g., Fiorino and Elsberry, 1987; DeMaria, 1985), the same initial vortex structure was used for all simulations made in this study. A fairly strong initial vortex was chosen in order to hold to a minimum, the time needed for cyclone intensification to a mature stage. An exponential vortex allows for the velocity to rapidly approach zero at large distances from the cyclone center so that periodic boundary conditions are satisfied.

As mentioned in Section 2.1, the governing equations are written in terms of the streamfunction and velocity potential, therefore, equation (2.24) cannot be used directly and is replaced by

$$\zeta(r) = \frac{2V_m e}{r_m}[1 - \frac{1}{2}(\frac{r}{r_m})]\exp[-(\frac{r}{r_m})] \tag{2.26}$$

which gives the vorticity of the initial vortex as a function of radius. To specify the initial mass field, the nonlinear balance equation is used:

$$\nabla^2\phi_i = f_o\zeta_i - \frac{\partial(u_i\zeta_i)}{\partial y} + \frac{\partial(v_i\zeta_i)}{\partial x} - \nabla^2\left(\frac{u_i^2+v_i^2}{2}\right) \tag{2.27}$$

which can be solved for ϕ using the spectral method. Equation (2.27) must be used in order to incorporate the asymmetric initial conditions which arise when the vortex is superimposed upon a large scale basic current and can be derived from (2.8) under the assumption that the divergence, time rate of change of the divergence, friction, and vertical velocity are initially zero. Since the streamfunction contribution to the βu_i term was neglected in the divergence equation, the initial conditions are axisymmetric on both the f-plane and β-plane if the mean wind is zero.

Table 1. Values for parameters used in a typical model run.

Symbol	Value	Description
M, N	35, 35	series truncation limits in x,y
L_x, L_y	4000, 4000 km	x,y domain size
Δt	90 s	time step
λ_2	10^3 m^2s^{-1}	2nd order diffusion coefficient
λ_4	$.3 \times 10^{14}$ m^4s^{-1}	4th order diffusion coefficient
H_0	1000 m	Layer 0 mean thickness
H_1	4543 m	Layer 1 mean thickness
H_2	3127 m	Layer 2 mean thickness
	20°N	Evaluation latitude for f and β
g	9.8 ms^{-1}	acceleration of gravity
R	287 $JK^{-1}kg^{-1}$	gas constant for dry air
c_P	1004 $Jkg^{-1}deg^{-1}$	specific heat at constant pressure
C_D	.0015	drag coefficient
C_E	.0015	air-sea exchange coefficient
μ	1.5×10^{-4} ms^{-1}	shear stress coefficient
ϵ	.8715	density ratio ($= \frac{\rho 2}{\rho 1}$)
$\bar{\Lambda}_2$	0K	
Λ_1	-10K	
$\bar{\Lambda}_S$	30K	
γ	8.6	
α	1.87	

2.5 Results of Numerical Simulations with a Resting Basic State

A strong barotropic vortex, with initial mass and wind fields given by (2.26) and (2.27), was placed in the center of a 4000 km by 4000 km domain under resting basic state conditions. The model was integrated for 4 days in order to test the features of a simulated cyclone. The fully parameterized simulation was first run on the f-plane and then repeated on the ß-plane (case NS) to isolate the effect of a latitudinally variable Coriolis parameter. Both f and ß are evaluated at 20°N.

Figure 1 shows the 96-hour tracks of the vorticity maximum in layers 1 and 2 for the ß-plane case. In the absence of a basic current, cyclone movement is due to the advection of planetary vorticity by the tangential wind which immediately induces a westward component of motion for a vortex in the North Hemisphere. As discussed by Anthes and Hoke (1975) and Holland (1983), the asymmetries introduced by this effect will create two opposing circulations to the west and east of the vortex. These opposing circulations result in a southerly wind through the vortex which then advects the vortex poleward. The result of the two effects is a northwestward acceleration of the vortex. Holland (1983) showed analytically that this movement on a ß-plane is further modified by the radial inflow of a convergent vortex. This inflow introduces cyclonic vorticity asymmetries to the north and anticyclonic to the south. The greater the inflow angle, the greater the northward displacement of the vortex and speed which with it moves. These analytical results showed agreement with numerical results by Anthes and Hoke (1975).

Because ß=0 for the f-plane simulation, the vortex remains stationary throughout the integration under no basic flow conditions. However, in

qualitative agreement with the above theory and numerical results by Jones (1977a) and Kitade (1980), the layer 1 vortex on the ß-plane moves north of northwest initially with the direction becoming more northwesterly after 66 hours. The average speed of this vortex center is 2.8 ms^{-1} over the course of the 96-hour integration. Figure 2 (top) shows a breakdown of the 6-hourly speed and direction of the layer 1 vorticity maximum. The speed of the layer 1 vortex approaches values of 4 ms^{-1} after 48 hours in response to increased boundary layer convergence 24 hours prior.

Because the radial structure of the layer 2 vortex changes in response to the transport of momentum from layer 1, the movement induced by the ß-effect of the layer 2 vortex is different from that in layer 1. The vortex will no longer be vertically aligned, however, momentum will still be transported upwards causing deviation dependent changes in the upper level radial structure. In this simulation, the upper layer maximum vorticity center oscillates about the lower layer track after the first 24 hours with an intial displacement towards the west. This oscillation is similar to that observed by Yeh (1950) and may be a response to the nonlinear interactions with the current. This oscillation is evident, however, in the upper layer and not in the surface track. The layer 2 vortex center reaches a maximum deviation from the lower vortex after 96 hours, this deviation is 43 km to the southwest. Figure 2 (bottom) gives the deviation of the upper layer vortex center from the lower layer vortex center at 6-hour intervals. Positive values for Δx and Δy indicate that the layer 2 vortex is displaced east or north of the layer 1 vortex, respectively. There appears to be a correlation between large eastward

deviations of the upper vortex and significant changes in the direction of the lower level vortex, which will be investigated further in later chapters.

Figure 3 (top) shows the time evolution of the minimum surface pressure perturbation on both the f-plane and ß-plane. This perturbation is a..ually given in terms of the deviation of the computed surface pressure P_S from the mean surface pressure $\bar{P}_S$ which is taken to be about 1010mb. The surface pressure P_S in the incompressible system is given by

$$P_S = \rho g \left[H_0 + H_1 + h_1 + \epsilon(H_2 + h_2)\right] \qquad (2.28)$$

and $\bar{P}_S$ is the value of P_S when $h_1 = h_2 = 0$. For the first 24 hours, the cyclone intensifies rapidly and at the same rate in both cases. After that time, the ß-plane case stops intensifying and levels off for the rest of the integration while the f-plane case continues to intensify but at a slower rate than before. These results are in qualitative agreement with the study by Madala and Piaseck (1975), which showed that the inclusion of the ß-effect inhibited cyclone intensification.

The time evolution of the maximum tangential winds in layer 1 is shown at the bottom of Figure 3. The maximum tangential winds increase from 25 ms^{-1} to 62 ms^{-1} and 50 ms^{-1} on the f- and ß-plane, respectively. After 4 days, the minimum surface pressure drops from 991 mb to 914 mb on the f-plane and to 954 mb on the ß-plane. The ß-plane simulation lies well within the range of wind and pressure values observed in Atlantic hurricanes based on a study by Shea and Gray (1973).

As examplified by Figures 1 and 3, the upper and lower vortex is not always vertically aligned. Huntley and Diercks (1981) presented

observational evidence of vortex tilt, which they attributed to vertical wind shear, in three tropical storms. In order to examine this phenomena more closely, the layer 1 and layer 2 vortices are tracked separately. Values of the dependent variables in each layer are calculated relative to a cylindrical grid always centered upon their respective streamfunction minimums as the storm moves. The variables are displayed at the initial time and again after 72 hours to facilitate discussion of 3-day simulations presented in later chapters.

Figure 4 shows the radial structure of the maximum tangential winds in each of the three layers for both cases. All values displayed for the dependent variables are azimuthal averages, calculated on a cylindrical grid, using eight values at each of the radial points. The radial structure in the bottom layers are very similar for both simulations with the f-plane case being more intense than that of the ß-plane. However, at 72 hours the tangential winds in layer 2 differ dramatically. For the f-plane case, the maximum winds are 38 ms^{-1} at a radius of 80 km and the winds become anticyclonic at a radius of 450 km. The ß-plane case, on the other hand, has a layer 2 maximum tangential wind of only 20 ms^{-1} at a radius of 80 km with an anticyclone developing around 300 km from the upper level storm center.

The convective stability and vertical velocities are given in Figure 5 as a function of radius. The radial convective stability profiles, given at the top of Figure 5, are initially constant at 2.5 (non-dimensional units) because the vortex used is initially barotropic, consequently no upper level thickness deviations occur. After 72 hours, both cases showed lower values due to the establishment of a warm core and the occurrence of

subsidence. At the bottom of Figure 5, the vertical velocities for the f and ß cases are shown at left and right, respectively. Both have a maximum occurring inside the radius of the maximum winds with the f-plane case having greater values. Negative values also occur near the vortex center indicating sinking motion. These features are seen in naturally occurring tropical storms and similiar numerical results obtained by Ooyama (1969) and DeMaria (1983). In those studies, the upper level vortex develops from momentum transports whereas in this study an upper level vortex was included in the initial condition.

In summary, a brief description of the primitive equation spectral model was presented in this chapter with an explanation of the simple cumulus parameterization scheme used. Although more sophisticated models exist, this model is capable of simulating tropical cyclones which exhibit many features that occur in nature as examplified by the results of the no basic flow simulations. DeMaria and Pickle (1987), who developed an axisymmetric analog to this model which utilized isentropic coordinates in order to make the inclusion of thermodynamics more straightforward, showed similar developmental results. The use of a strong initial vortex in all levels did not adversely affect these features and led to an efficient use of computer time by cutting out unnecessarily long intensification periods. The movement of the simulated vortex on the ß-plane with no basic flow is generally northwest at a speed of approximately 3 ms^{-1}, in agreement with theory. The upper level vortex center is tracked separately and oscillates about the layer 1 center with an average deviation of 15 km over the 96-hour integration.

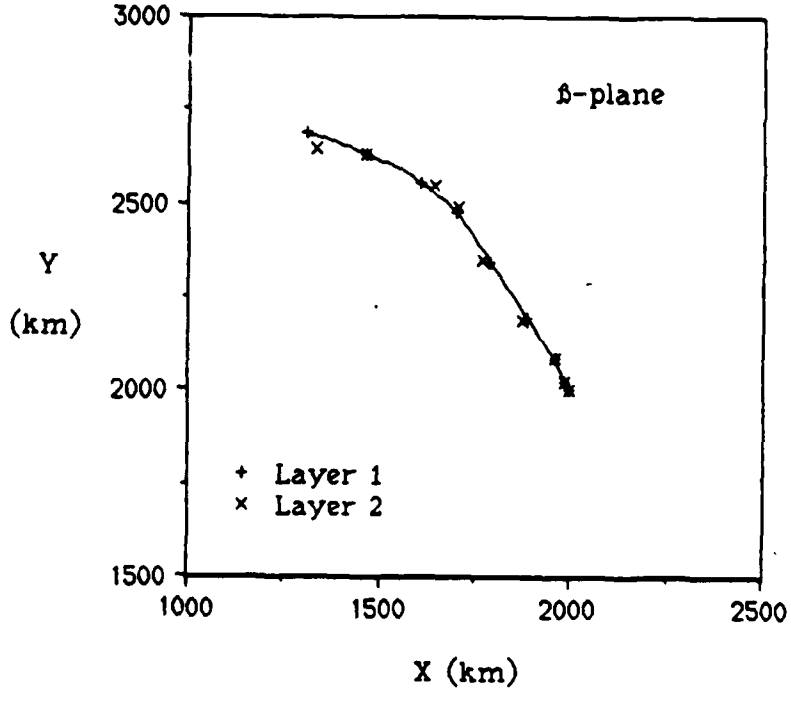

Figure 1 The 96-hour track of the layer 1 vorticity maximum (solid line) with crosses representing the position of the layer 2 maximum for NS case. Symbols mark the vortex positions at 12-hour intervals.

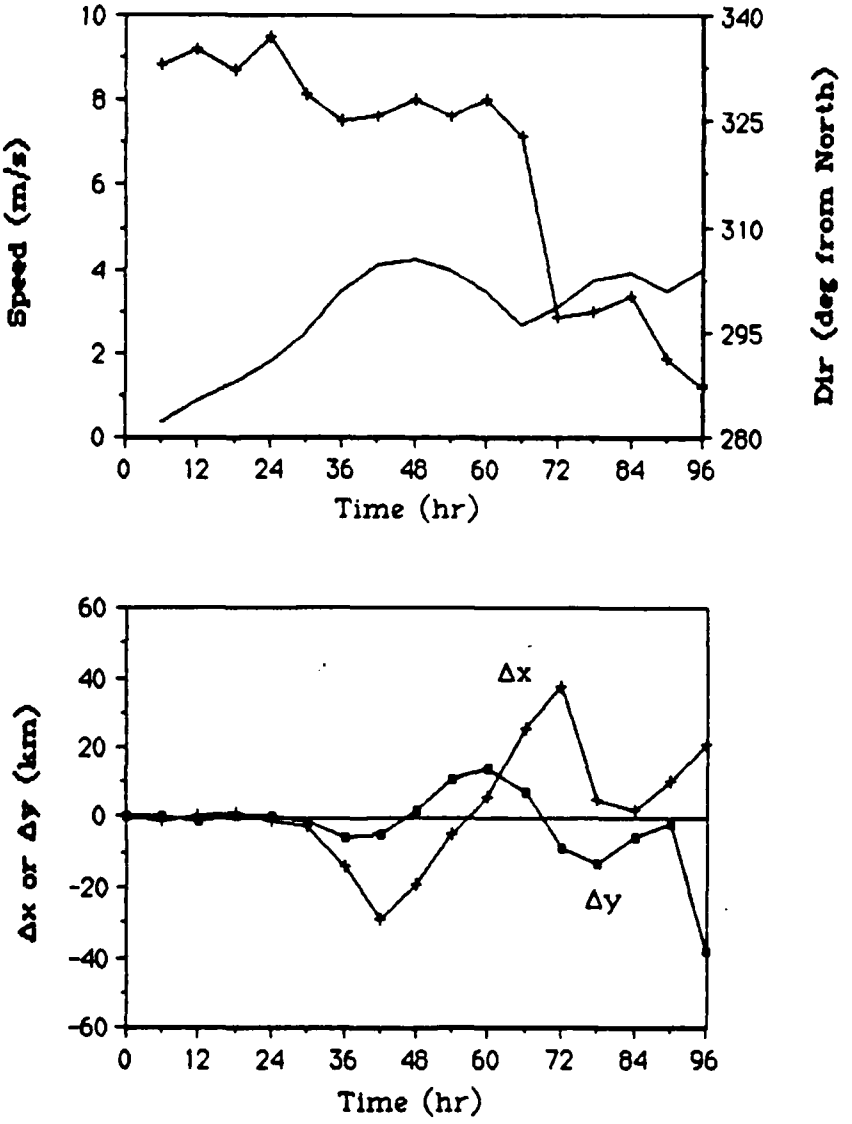

Figure 2 Time evolution of the speed (solid) and direction (hatched) of the layer 1 vorticity maximum (top). Upper and lower vortex positional deviations (bottom), Δx or Δy indicates an eastward or northward displacement of the layer 2 vortex relative to the layer 1 vortex for the NS case.

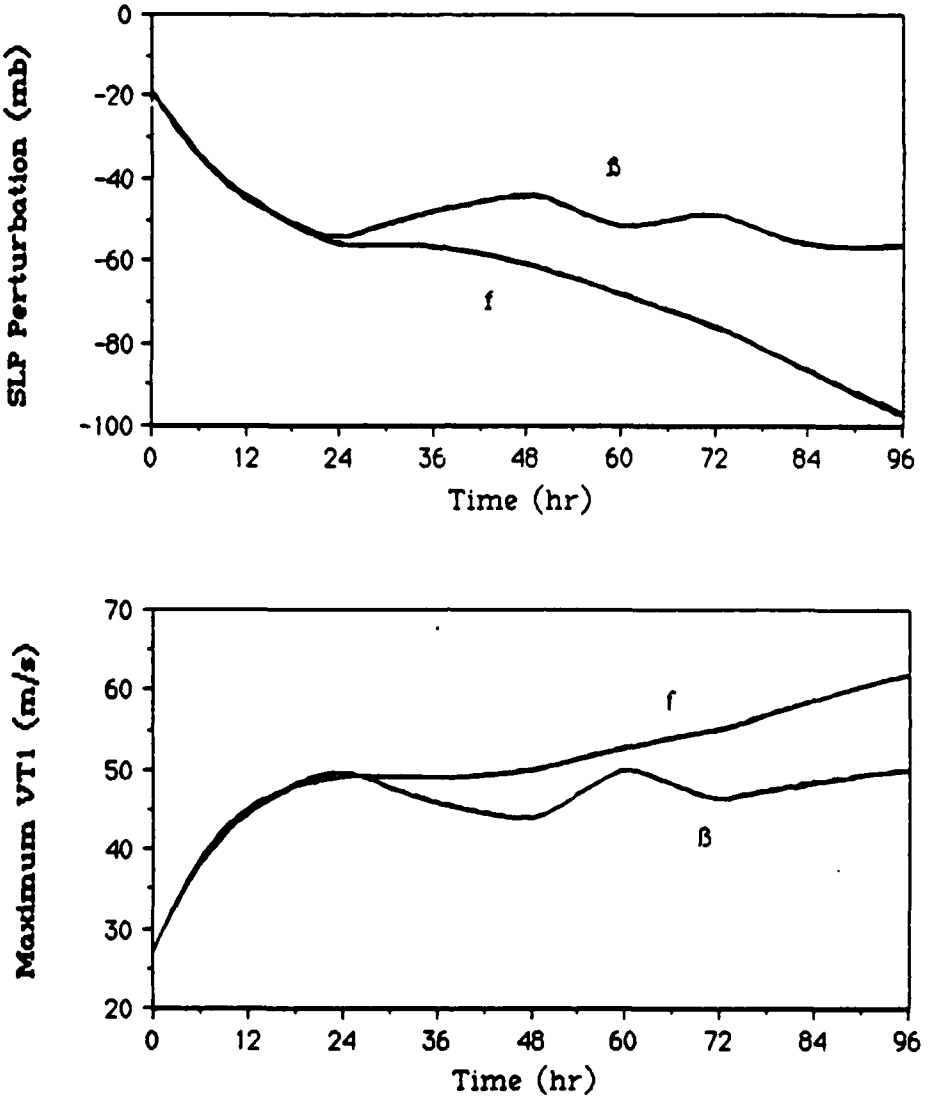

Figure 3 Time evolution of the minimum surface pressure perturbation (top) and the maximum layer 1 tangential wind VT1 (bottom) for f-plane and ß-plane resting basic state simulations.

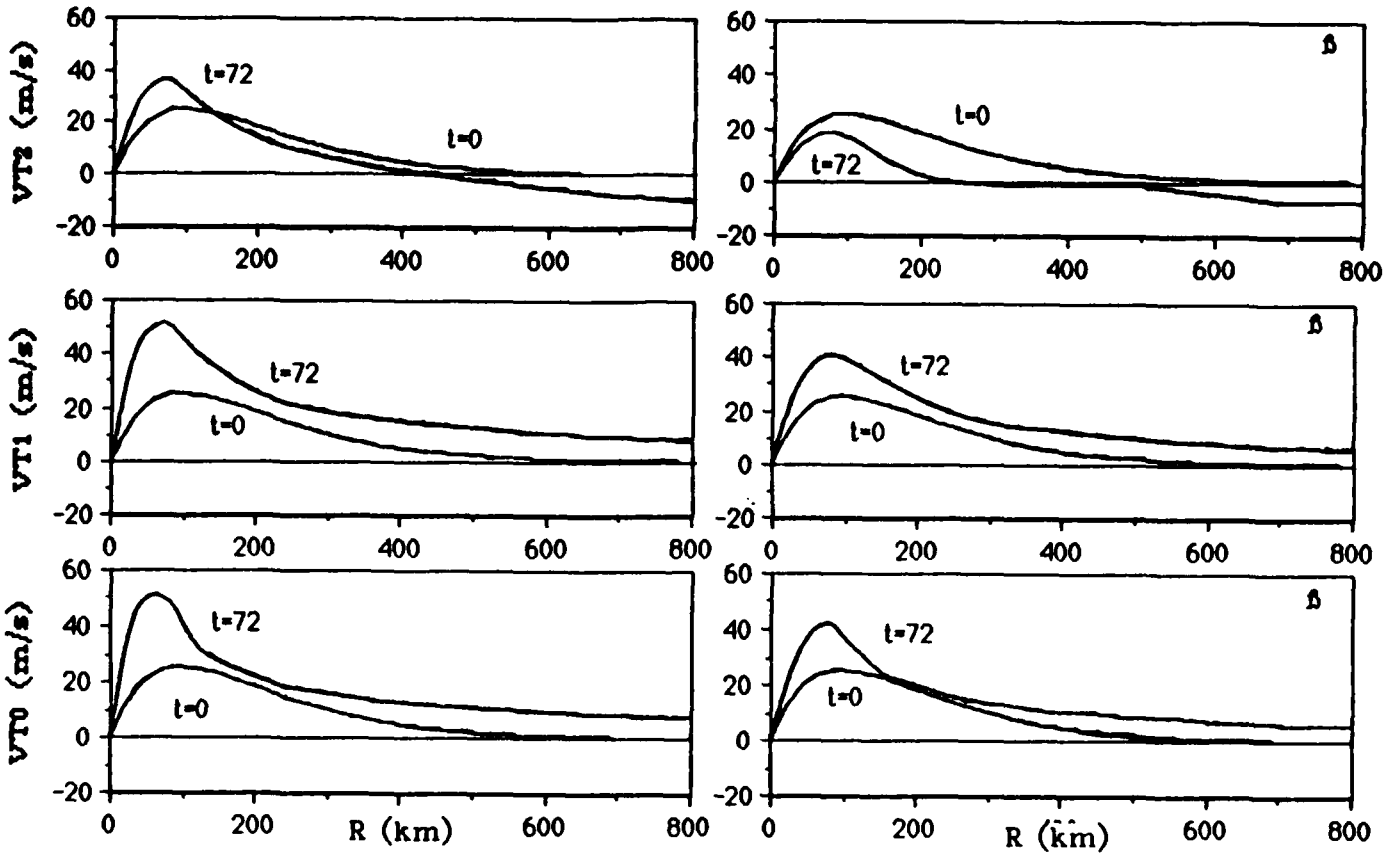

Figure 4 Radial profiles of the azimuthally averaged tangential wind VT for each layer at 0 hours and at 72 hours for the f-plane (left) and β-plane (right) resting basic current simulations.

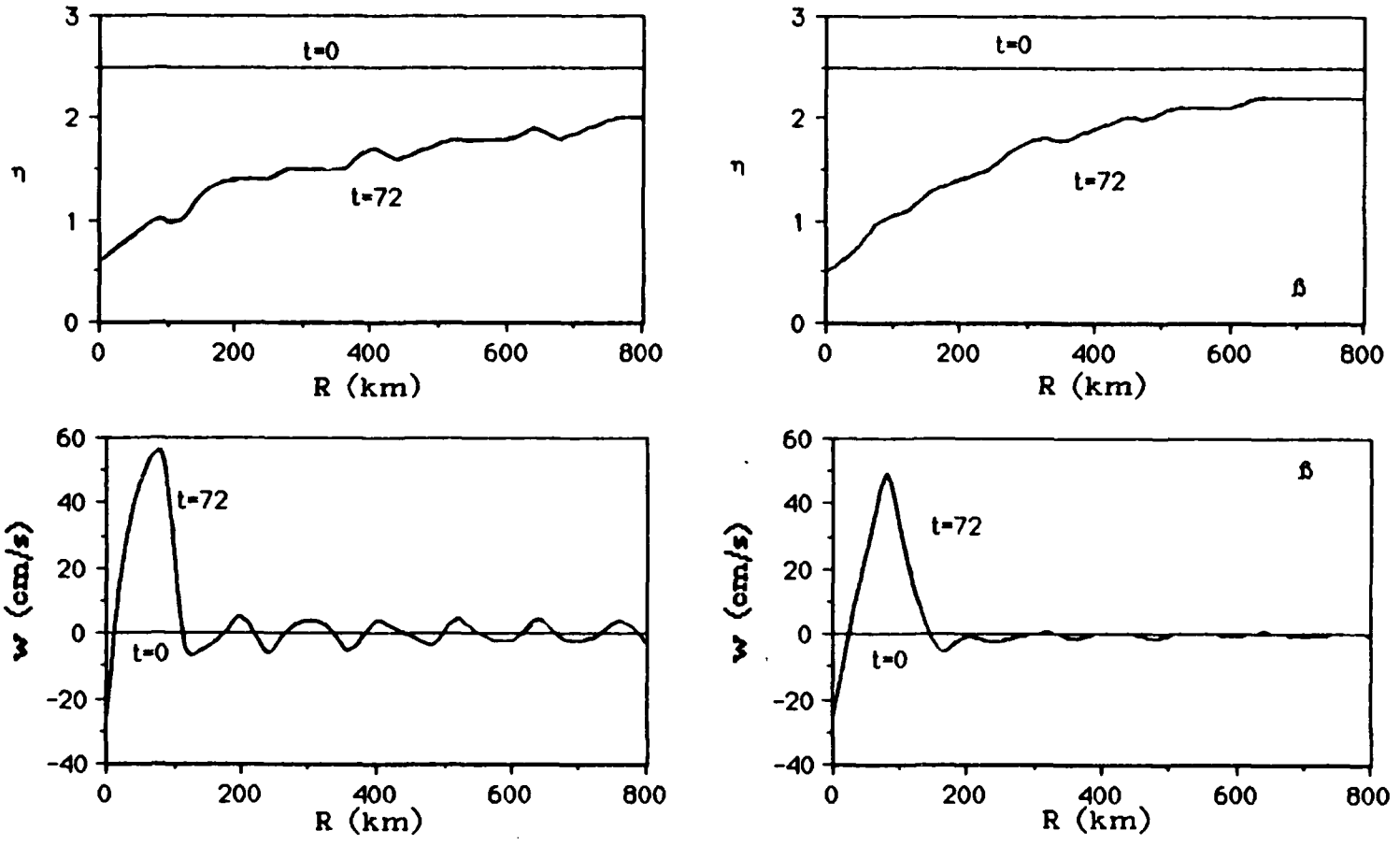

Figure 5 Radial profiles of the vertical stability parameter η (top) and vertical velocity w at the top of the boundary layer (bottom) at 0 hours and at 72 hours for the f-plane (left) and ß-plane (right) resting basic state simulations.

3. Numerical Simulations with Varying Physical Processes

3.1 Description of the Non-resting Basic Current

One of the advantages of using numerical models for research is the ability to change physical parameters at will. The use of a three-layer primitive equation model allows for the addition, in each layer, of a large scale horizontal wind. The three dimensionality of the model allows these winds to interact with the storm circulation. The horizontal structure and magnitude of these winds can be specified separately in each layer to simulate various atmospheric conditions, however, doubly periodic boundary conditions for the dependent variables limit the horizontal structure that these winds can assume. To satisfy these conditions, all simulations made in Chapters 3 and 4 use a large scale polynomial zonal wind with the structure specified, in each layer, by the following:

$$U_i = A_i - (n+1)By'^{n} + (n+3)Cy'^{n+2} \tag{3.1}$$

where

$$B = \frac{A_i(n+2)}{F(n)(n+1)\left(\frac{L_y}{2}\right)^n}$$

$$C = \frac{A_i}{F(n+3)\left(\frac{L_y}{2}\right)^{n+2}} \tag{3.2}$$

$$F = \frac{(n+2)}{n(n+1)} - \frac{1}{(n+3)}$$

$$y' = y - \frac{L_y}{2} .$$

The subscript i (=1 or 2) indicates the appropriate layer. A_i is the amplitude of the zonal wind at the center of the domain and n=6 for all simulations, therefore, the wind field is described by an eighth-order polynomial. Figure 6 shows this zonal wind profile in y with $A=-8\ ms^{-1}$ as well as the normalized vorticity and vorticity gradients associated with it. As evident in the figure, this zonal wind structure was chosen because it is approximately constant for a 1000 km swath in y thus eliminating any relative vorticity gradients which could arise from the horizontal shear of the horizontal wind. In addition, the first and second derivatives of U are continuous across the periodic boundaries. It must also be recognized that by using this wind structure, the validity of data obtained when a simulated vortex strays out of this 1000 km region must be held suspect. Not only are vorticity gradients introduced which complicate the movement of the cyclone, but the vorticity and vorticity gradients are unrealistic as a result of the large magnitudes of wind velocity near the boundaries. In light of this, simulations are terminated when the vortex passes out of the central uniform wind region.

In this chapter, the strong initially axisymmetric nondivergent vortex described in Section 2.4 is superimposed upon the nearly linear steering current described previously. The introduced current is barotropic, i.e. there is no vertical shear of the horizontal wind, with the magnitude of the zonal flow being $8\ ms^{-1}$ in each layer. In order to examine the effect of a barotropic basic current on cyclone movement, numerical experiments are made with a simulated easterly basic current and then repeated with a westerly current on both the f- and ß-plane with the sea surface temperature held constant at 27.5° C. Experiments are run initially

without physical processes (ND cases), then repeated with the effect of surface drag included (DD cases), and finally run with the full parameterizations of surface drag and cumulus convection included (F cases). Table 2 gives a summary of the numerical simulations presented in this chapter.

3.2 Results of f-plane Simulations

The effect of surface drag in the primitive equation model is neglected by setting the surface drag coefficient C_D and boundary layer modes equal to zero, while cumulus convection is turned off by holding the boundary layer equivalent equivalent potential temperature Λ_0 constant throughout the simulation and setting the mass transport term Q^+ to zero. As a result, for the ND cases, there is very little boundary layer convergence and subsequent vertical motions and the cyclone fails to intensify. For an initially axisymmetric cyclonic vortex embedded in a barotropic basic current, the tangential winds become asymmetric about the vortex axis. This occurs as a result of the addition of the basic flow to the vortex flow with a maximum occurring on the righthand side of the vortex relative to the direction of the basic flow. However, for a constant flow simulation made in the absence of modeled physics and with a constant Coriolis parameter, these asymmetries do not advect the basic flow. Therefore, the cyclone motion is a result of linear advection by the basic current. In agreement, the vortex center, taken to be the vorticity maximum, of a vortex embedded in a barotropic easterly current (ND1 case) moves with a constant speed of 8 ms^{-1} towards the west with negligible deviations of speed or direction from the basic state current. An examination of the

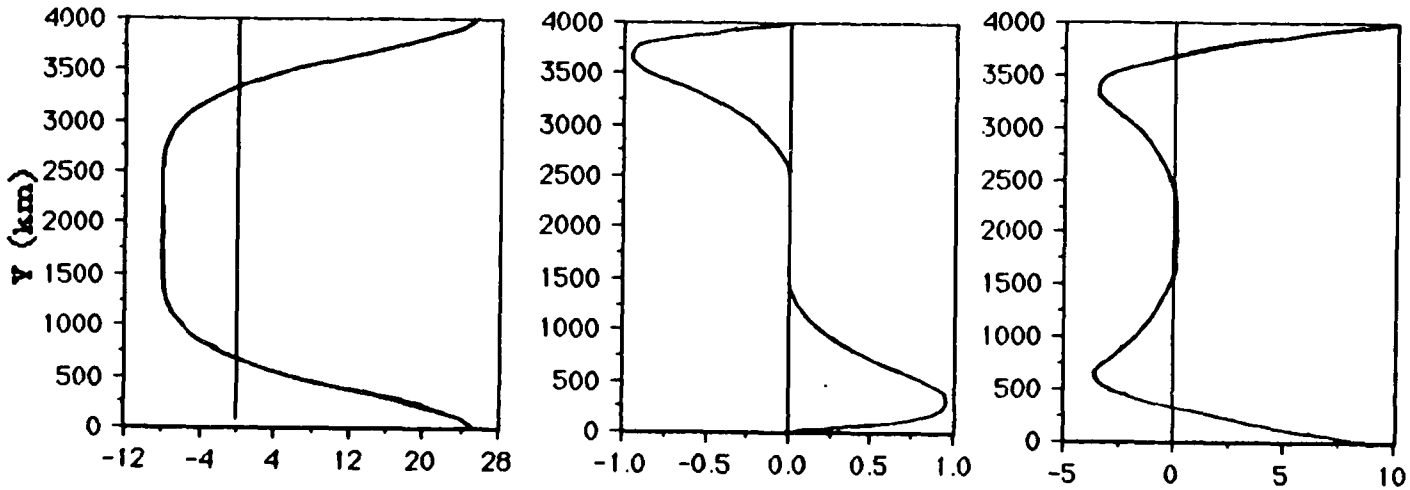

Figure 6 Zonal wind field (a), normalized relative vorticity (b), and normalized relative vorticity gradient (c) for easterly current given by equation (3.1) with A=-8 ms^{-1}.

Table 2. Summary of the numerical simulations presented in Chapter 3.

Simulation	Physical Processes		Basic Current (ms-1)	Coriolis Parameter
	Drag	Moisture		
ND1	No	No	-8î	ß=0
DD1	Yes	No	-8î	ß=0
F1	Yes	Yes	-8î	ß=0
NDBM1	-	-	-8î	ß=0
ND2	No	No	-8î	ß≠0
DD2	Yes	No	-8î	ß≠0
F2	Yes	Yes	-8î	ß≠0
NDBM2	-	-	-8î	ß≠0
ND3	No	No	8î	ß≠0
DD3	Yes	No	8î	ß≠0
F3	Yes	Yes	8î	ß≠0
NDBM3	-	-	8î	ß≠0

upper layer vortex track indicates that it is advected in the same manner. Vertical alignment of the vortex is maintained and, after 72 hours, a maximum deviation of only 11 km is observed. Identical tangential wind structures are observed in both layers throughout the integration. In Figure 7, the 72-hour track of the ND1 vortex center, originating at (2000 km, 2000 km), is displayed on a segment of the model domain along with the tracks of the surface drag (DD1) and fully parameterized (F1) cases.

Next, the effect of surface drag on a vortex in easterly flow is investigated on the f-plane in the absence of cumulus effects, case DD1. In this model, the frictional effect of surface drag is incorporated by using the bulk aerodynamic formula for the boundary layer momentum equation given by term (A) in equation (2.13). When surface drag is introduced, the layer 1 vortex deviates to the right of the defined basic current by an average of 5°. In addition, the speed of the layer 1 vortex is on the average 24% slower than the initial basic flow and is reduced by 42% at the end of the 72-hour integration. Figure 8 (bottom) shows the speed and direction of the DD1 vortex center as a function of time.

This slowing of the vortex speed by the surface drag is a nonlinear effect that is proportional to the squared boundary layer wind. Layer 1 vortex motion, in this case, is in agreement with theory advanced by Kuo (1969) that a cyclonically rotating vortex in a constant flow with friction will deviate to the right of the direction of the flow. Jones (1977a) presented similar f-plane results where simulations including surface drag deviated 5° to the right of the basic advecting current. However, it must be noted, those simulations implicitly incorporated the effects of vertical

wind shear by defining a basic current to be the vertical average of the horizontal winds used in each layer.

Interestingly, an examination of the tracks of the upper level vortex reveals that it does not continue to advect precisely with the upper level basic current. A comparison of the upper and lower vortex tracks are shown at the top of Figure 8. In this simulation, the layer 2 vorticity maximum moves slightly slower than, and approximately 3° to the left of, the basic current. This deviation is first observed after 12 hours into the integration, until this time the layer 2 vortex moved in the same direction but faster than the layer 1 vortex.

The vertical alignment of the vortex is not maintained because of the lack of cumulus convection and the resulting mass and momentum transports. However, the absence of these transports raises the question of the cause behind this observed directional deviation between the upper and lower vortex. Because deviations are not observed in the ND1 case, it seems reasonable to assume that the upper level directional deviation from the basic current results from factors arising in conjunction with its displacement from the lower level vortex. It can also be speculated that with the addition of mass and momentum transports, a combination of the effects in each layer would serve to lessen slightly the rightward deviation from the basic current due to surface drag. This immediately leads to implications that the inclusion of vertically varying horizontal winds would also affect vortex motion. This phenomena will be investigated more fully in the succeeding chapters.

While the ND1 and DD1 simulations never intensified, the fully parameterized case, F1, intensified to cyclone strength with maximum

tangential winds of 51 ms^{-1} and a minimum sea level pressure of 967 mb occurring 18 hours into the integration. By the end of the 72-hour integration, the vortex is a minimal tropical cyclone with a 985 mb central pressure and 35 ms^{-1} tangential winds. The vortex center moves at an average speed of 5.9 ms^{-1} in a northwesterly direction. Figure 9 (top) gives the speed and direction of this vortex center in the F1 simulation as a function of time. As illustrated in Figure 7, the inclusion of cumulus convection induces a significant northward propagation of the simulated tropical cyclone. This deflection is a direct result of the intensification of the cyclone and is explained by asymmetries in diabatic heating rate caused by asymmetries in boundary layer convergence. As explained previously, a vortex embedded in easterly flow will exhibit asymmetric winds about its axis with a maximum occurring on the righthand side in relation to the direction of motion. With the addition of surface drag, winds directed toward low pressure will result in order to maintain balanced flow. This radial inflow leads to boundary layer convergence which induces vertical motions. Since the diabatic heating rate is proportional to positive vertical motions at the top of the boundary layer, a maximum will occur towards the front and right of a translating vortex. Shapiro (1983) showed that maximum convergence occurs in an arc in the right front of a vortex in constant flow in a slab boundary layer. The resulting asymmetries in the heating results in greater convergence in the low levels and an increase in the local rate of change of vorticity with time. Since a vortex will follow the greatest increase in vorticity, the cyclone begins to move towards the right and front of the vortex center.

The motion of the F1 simulation verifies this. Initially, when compared to the surface drag case, DD1, the vortex moves at a faster rate for the first 18 hours and in a more northerly direction. After this time, as intensification drops off, the vortex moves at a slightly slower rate and moves more towards the west due to advection by the basic current. The upper level vortex generally moves with the layer 1 vortex but displays the same oscillation about the lower level track as in the no basic flow case on the ß-plane with maximum deviation of the layer 1 and layer 2 vortex being 31 km. An oscillatory period of approximately 54 hours is observed. The deviations in the north-south and east-west directions between the upper and lower vortex are presented at the bottom of Figure 9. Because these deviations are so small in comparison to the overall movement of the cyclone, they cannot be resolved by presenting both tracks on the same graph. A comparison of these deviations with the time evolution of the speed and direction of the layer 1 vorticity maximum, given at the top of Figure 9, indicate a slight correlation between the north-south component of motion and the west-east deviation between the upper and lower vortex. The importance of cumulus convection is illustrated by the coupling effect it has on the vortex in that the layer 1 and layer 2 vortex maintain a vertical integrity and move together unlike the surface drag case.

For f-plane simulations in westerly flow (not shown), the results are identical to the easterly flow simulations when explained with respect to the basic current direction. To summarize the effects of varying physical processes for f-plane simulations made with a nonresting barotropic basic current, the dominant factor is advection by the basic current as

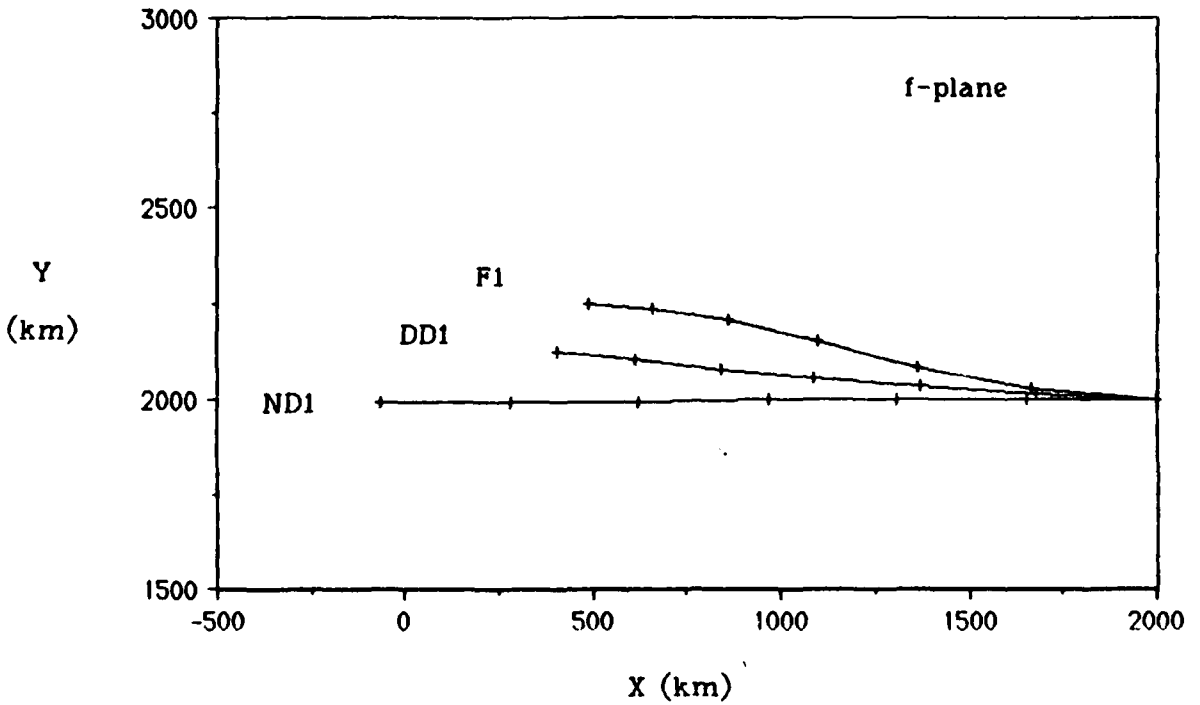

Figure 7 The 72-hour tracks of the layer 1 vorticity maximum for simulations ND1, DD1 and F1. Symbols mark the vortex position at 12-hour intervals.

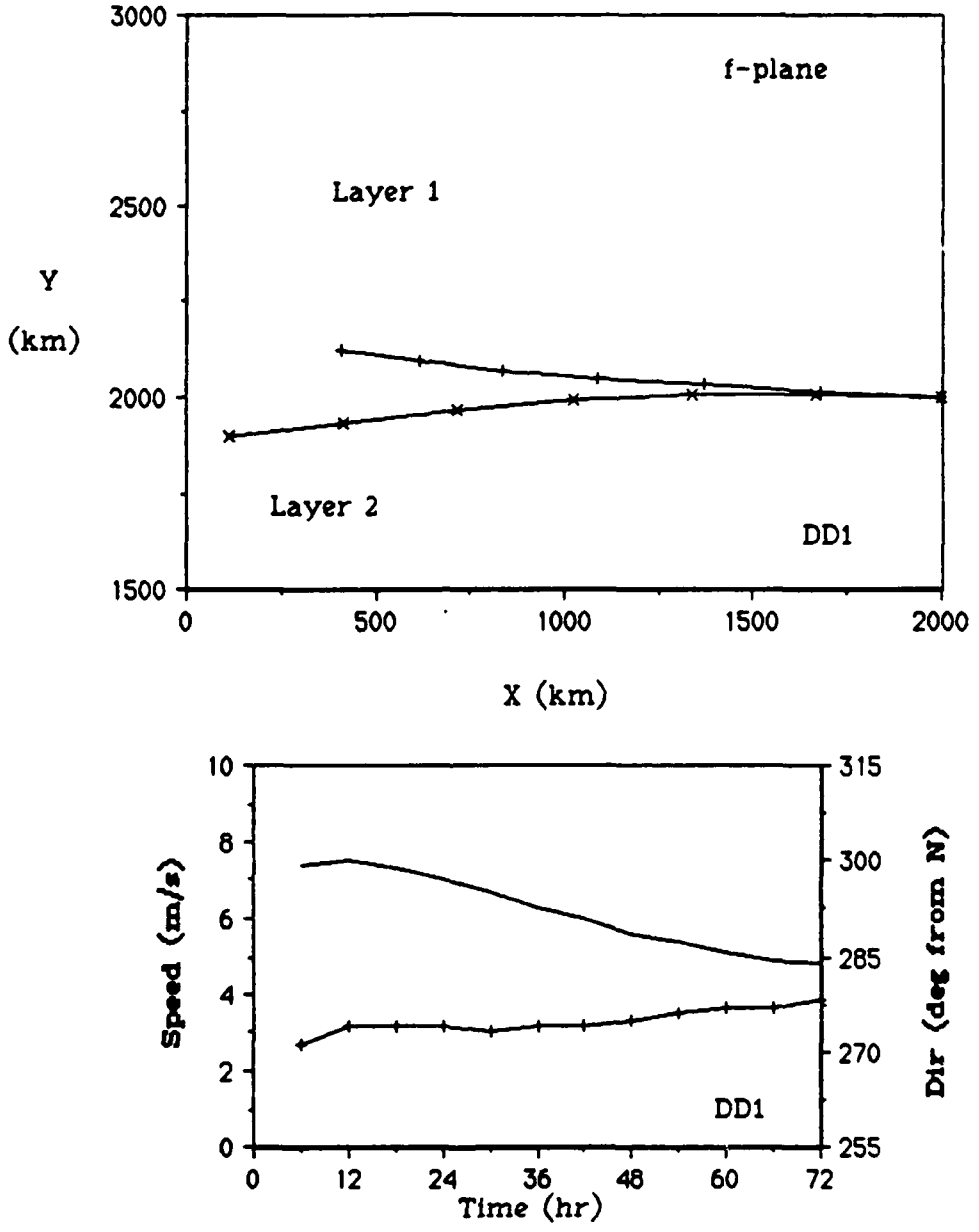

Figure 8 The 72-hour tracks of the vorticity maximum in each layer (top) and the speed (solid) and direction (hatched) of the layer 1 vorticity maximum (bottom) for the DD1 case. Symbols appear at 12-hour intervals.

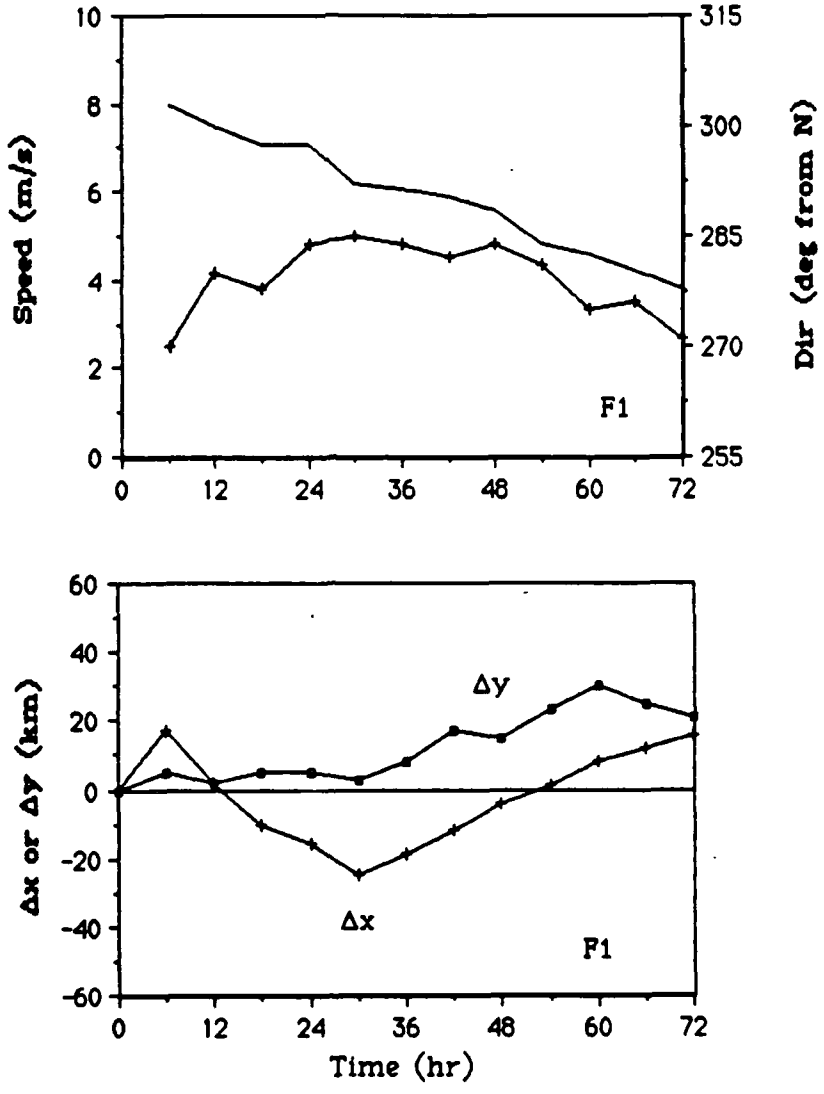

Figure 9 Time evolution of the speed (solid) and direction (hatched) of the layer 1 vorticity maximum (top). Upper and lower vortex positional deviations (bottom), Δx or Δy indicates an eastward or northward displacement of the layer 2 vortex relative to the layer 1 vortex for the F1 case.

evidenced in the ND case with no model physics. In easterly (westerly) flow, the vortex is advected towards the west (east) by the constant basic current. Surface drag slows this westward (eastward) component of motion and causes the vortex to deviate, to the right of its direction of motion, towards the north (south). The addition of cumulus convective effects induces a further deviation to the north (south) due to asymmetries in the diabatic heating rates.

3.3 ß-plane Simulations in an Easterly Current

Figure 10 shows the vortex tracks for all simulations made in easterly flow that include the effect of a variable Coriolis parameter. The simulation with no model physics (case ND2) shows an overall motion of 8.9 ms^{-1} towards 279°. This represents a northwestward acceleration due to the inclusion of the ß-effect when compared to the f-plane case, ND1. After 72 hours, the inclusion of a variable Coriolis parameter causes the cyclone to move towards 329° at an average speed of 1.6 ms^{-1} without physical effects included. The induced northerly component of motion is approximately 1.4 ms^{-1}.

For the DD2 case, the magnitude of the surface drag effect is larger than the DD1 case because of its proportionality to the increased speed of the vortex due to ß-effect. The direction of the layer 1 vortex is deviated by an average of 5° from the ND2 case, or 14° from the basic flow direction. Again, a directional deviation is observed between the upper and lower vortex centers, as displayed at the top of Figure 11, with the layer 2 vortex displaying a 72-hour average rightward deviation of 7° from the direction of the basic current. The inclusion of a variable Coriolis

parameter induces a northwestward component of motion for the vortex center in both layers. As in the f-plane simulations, ND2 and DD2 failed to intensify.

In the ß-plane case with full parameterization, F2, a further northward deviation of the vortex from the surface drag case DD2 is observed. This track of this vortex is terminated in Figure 10 after 60 hours because the vortex center had moved into regions of large vorticity gradients associated with the flow field. The speed of the vortex is greater than the surface drag case at nearly all times, until the vortex begins to weaken after 42 hours, as illustrated by comparing Figure 11 (bottom) with Figure 12 (middle). Again, this indicates that the heating asymmetries caused by greater boundary layer convergence to the right front of the cyclone are responsible for this further northward deviation, with advection by the basic current still dominating the cyclone motion. The layer 1 vortex moves, on the average, towards 293° at a speed of 7.2 ms^{-1}. Isolating the ß-effect after 60 hours shows that when physical processes are included the northwestward component of motion is enhanced over the f-plane case, F1, with the vortex velocity increasing towards 347° by 1.8 ms^{-1}. Since both the ß-effect and the physical processes effects act in the same direction for a cyclonically rotating vortex in easterly flow, the tendency will be towards the enhancement of the northward movement.

For this simulation, the upper level vortex moves in a manner similar to that exhibited in the other fully parameterized cases. The oscillation about the layer 1 vortex, illustrated at the bottom of Figure 12, has a

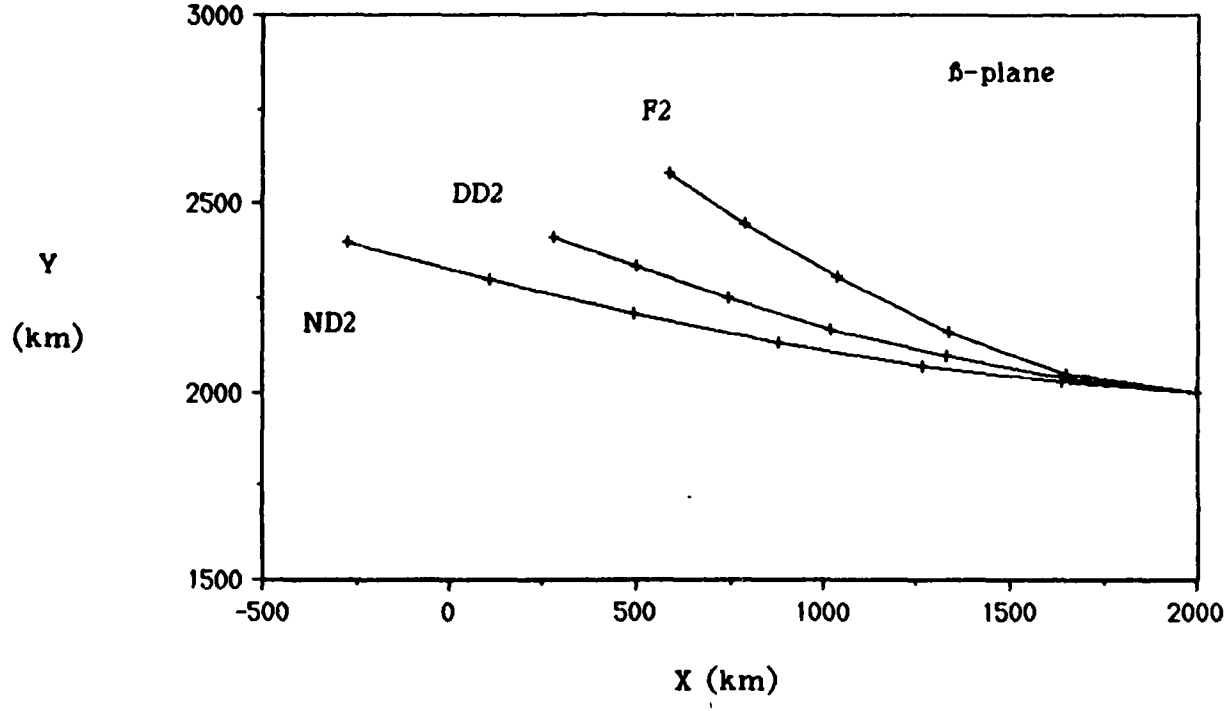

Figure 10 The 72-hour tracks of the layer 1 vorticity maximum for simulations ND2 and DD2, 60-hour track for F3. Symbols mark the vortex position at 12-hour intervals.

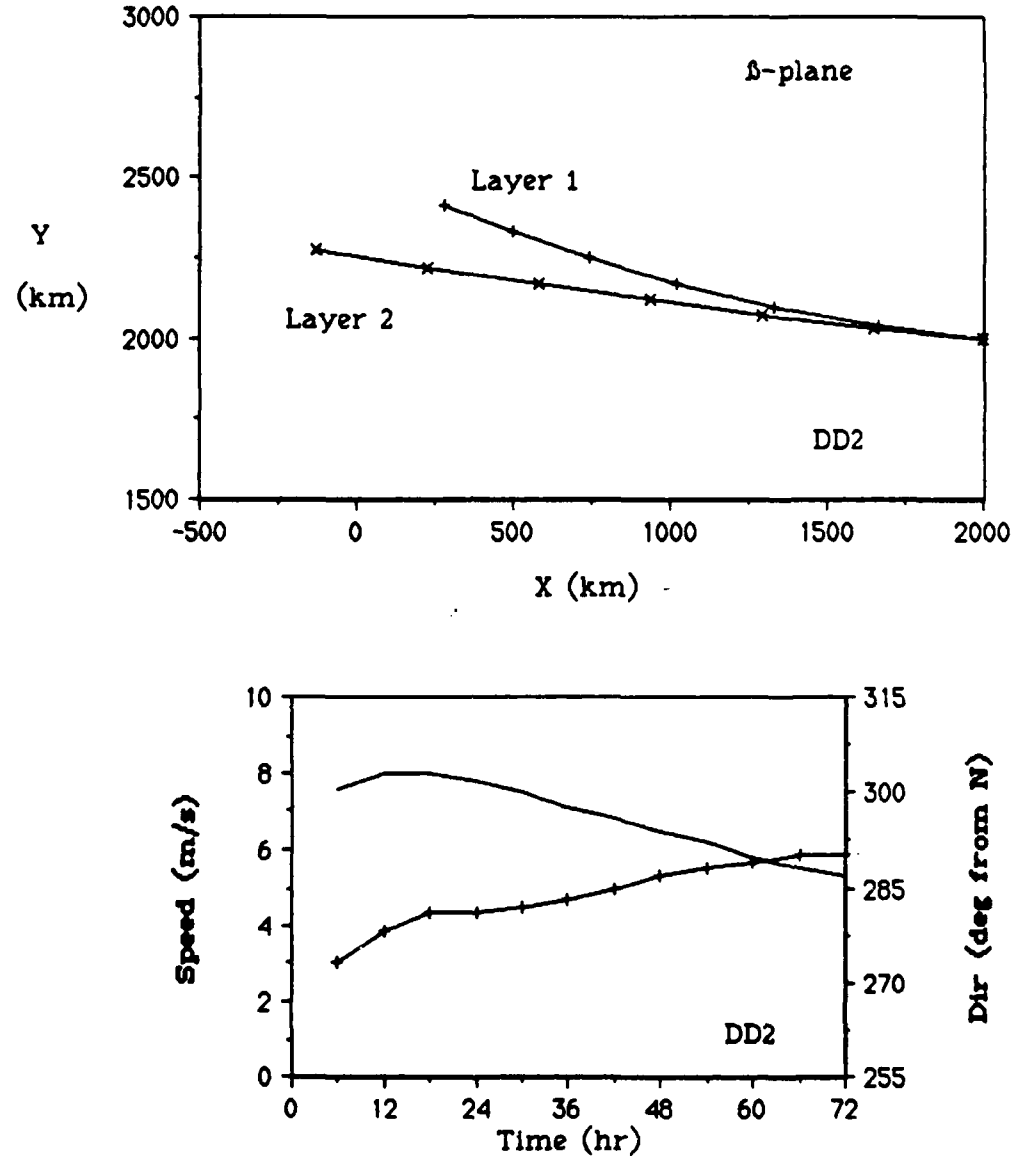

Figure 11 The 72-hour tracks of the vorticity maximum in each layer (top) and the speed (solid) and direction (hatched) of the layer 1 vorticity maximum (bottom) for the DD2 case. Symbols appear at 12-hour intervals.

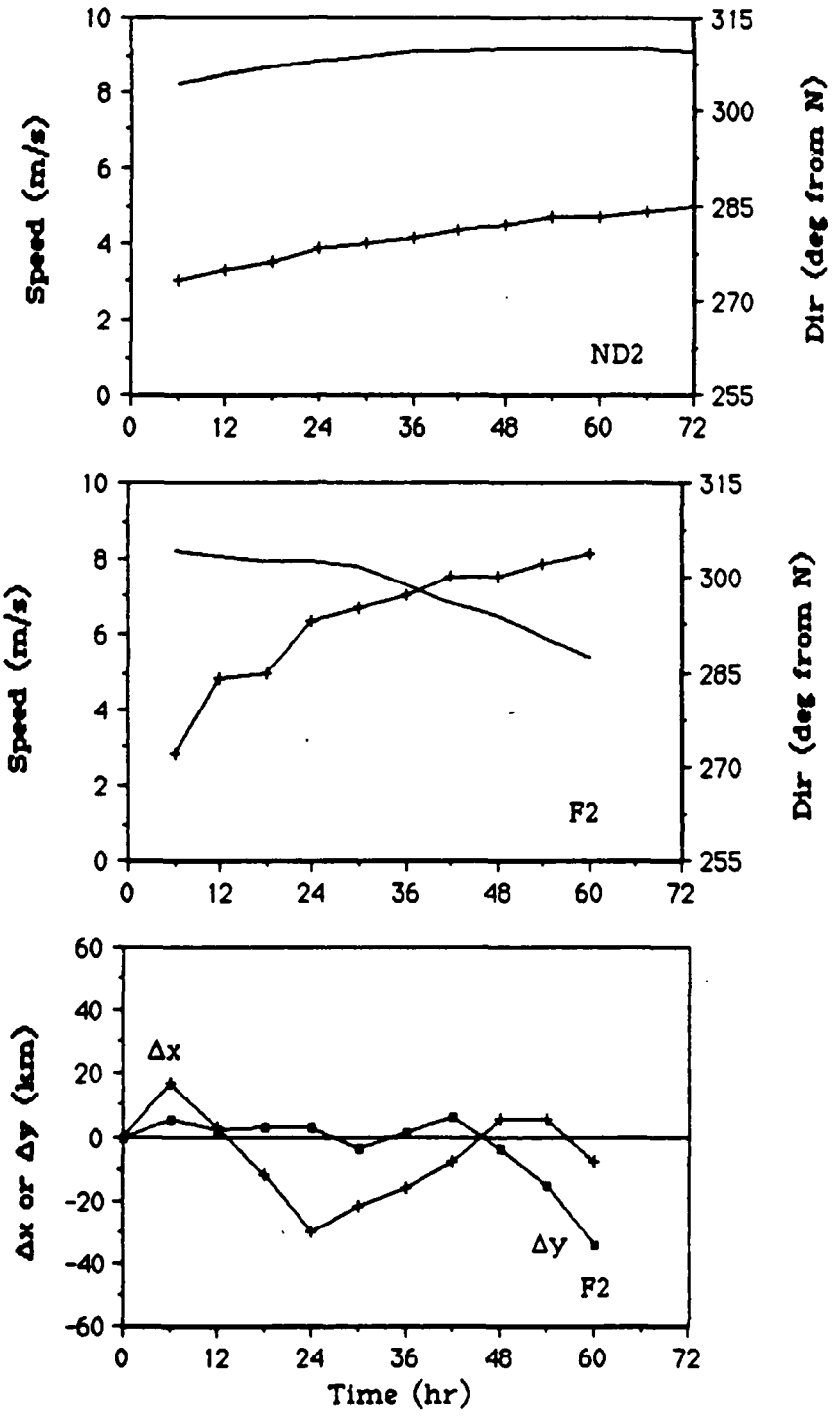

Figure 12 Time evolution of the speed (solid) and direction (hatched) of the layer 1 vorticity maximum (top). Upper and lower vortex positional deviations (bottom), Δx or Δy indicates an eastward or northward displacement of the layer 2 vortex relative to the layer 1 vortex for the F2 case.

period of 48 hours. The maximum displacement of 35 km occurs at 60 hours, the termination point for this experiment.

3.4 β-plane Simulations in a Westerly Current

The vortex tracks for the westerly simulations are shown in Figure 13. For the case with no model physics, ND3, the inclusion of a variable Coriolis parameter serves to induce a northwestward component of motion exactly as observed in the ND2 case. However, since the advection by the westerly current dominates, including a variable Coriolis parameter slows the eastward movement of the vortex while inducing a northward component of motion. The average speed of the vortex center is 7.3 ms^{-1} in a direction of 79° over the 72-hour integration, as can be seen in Figure 15 (top). Isolation of the β-effect shows it induces cyclone movement towards the northwest with exactly the same speed and direction as induced in the easterly case.

With the inclusion of surface drag, the cyclonically rotating layer 1 vortex should be deflected to right of the flow. As evidenced in Figure 13, DD3 is deflected to the right of the ND3 case by 5°, however, this still represents a deflection of 6° to the left of the basic current induced by the inclusion of the β-effect. The vortex speed consistently slows with time which is illustrated by Figure 14 (bottom).

An examination of the layer 2 vortex center shows a deflection of 9° to the left of the layer 1 vortex, which is to the left of the direction of the basic current. The movement in this case is the result of the β-effect, advection by the upper level current, and a response to the inclusion of

surface drag in the surface layer. In the upper level for the westerly current, the ß-effect and drag effect are in the same direction.

In the fully parameterized case, this interaction becomes more complex. Initially the cyclone deviates to the right of the surface drag case, however, about 36 hours into the integration the vortex begins to accelerate towards the north as the ß-effect begins to dominate over the physical effects. After 60 hours, the track of F3 crosses the surface drag track. Unlike the easterly case, ß and the physical processes now act in opposition. When isolated from a fully parameterized f-plane westerly current simulation (not shown), the ß-effect moves the vortex towards 336° at a speed of 1.7 ms^{-1}. The speed and direction of the layer 1 vortex are given in Figure 15 (middle).

This case is observed to be slightly more intense than F2 with maximum tangential winds of 50 ms^{-1} and a minimum sea level pressure of 966 mb occurring 18 hours into the integration. By the end of the 3-day integration, the cyclone exhibits a surface pressure of 980 mb and lower layer tangential winds of 38 ms^{-1}. As shown in Figure 15 (bottom) the upper level vortex oscillates about the lower level vortex with a maximum deviation of 31 km, similar to the F1 and F2 cases. A comparison with the direction of the layer 1 vortex indicates a good correspondence between the change in magnitude of the eastward deviation of the upper level vortex and directional changes of the lower level vortex.

3.5 Comparisons with NDBM Simulations

To illustrate the effect that the inclusion of physical processes has upon tropical cyclone movement, the fully parameterized cases run on the

primitive equation model (PEMOD) are compared to simulations run under identical initial conditions on a nondivergent barotropic model. The NDBM operates on the principle of the conservation of absolute vorticity and uses the barotropic vorticity equation given by

$$\frac{\partial \zeta}{\partial t} + \frac{\partial (u\zeta)}{\partial x} + \frac{\partial (v\zeta)}{\partial y} + \beta v = 0. \tag{3.3}$$

The components of the nondivergent wind are related to ζ by a streamfunction ψ where

$$u = -\frac{\partial \psi}{\partial y}, \quad v = \frac{\partial \psi}{\partial x} \tag{3.4}$$

$$\zeta = \frac{\partial^2 \psi}{\partial x^2} + \frac{\partial^2 \psi}{\partial y^2}. \tag{3.5}$$

The model uses one layer which represents the midtropospheric steering current and is solved using the Spectral Galerkin method. The NDBM is not capable of modeling changes in intensity because it does not incorporate any thermodynamics. In all simulations, the model is initialized with a vortex having the same radial structure and initial parameters as in the PEMOD simulations.

The β-plane simulation in easterly flow NDBM2 is nearly identical to the PEMOD experiment with no physical processes simulated, the ND2 case (refer to Figure 7 for this track). Deviations in the vortex positions between these two cases never exceeded 10 km in magnitude. Similarly, the westerly β-plane case, NDBM3, is nearly identical to the ND3 case with deviations in the vortex positions never exceeding 6 km in magnitude. The fact that the NDBM simulations are very similar to the PEMOD simulations

including no physical processes seems to indicate that the large-scale divergence effects are not very important.

The magnitude of the deviation observed between the two simulations, NDBM2 and F2, is 113 km after 24 hours, 382 km after 48 hours, and 561 km after 60 hours. The deviations between the NDBM3 and F3 vortex positions are 90 km at 24 hours, 286 km at 48 hours, and 394 km after 60 hours. These results indicate that the NDBM predicts the PEMOD position of a vortex in barotropic westerly flow on the β-plane better than any of the other cases. These results are in direct conflict with results of forecasts made by the SANBAR which consistently predicts the cyclone track in easterly flow better than in westerly flow (Anthes, 1982). In the next chapter, the effects of differing magnitudes of vertical wind shear are examined and the results used to help explain this dichotomy.

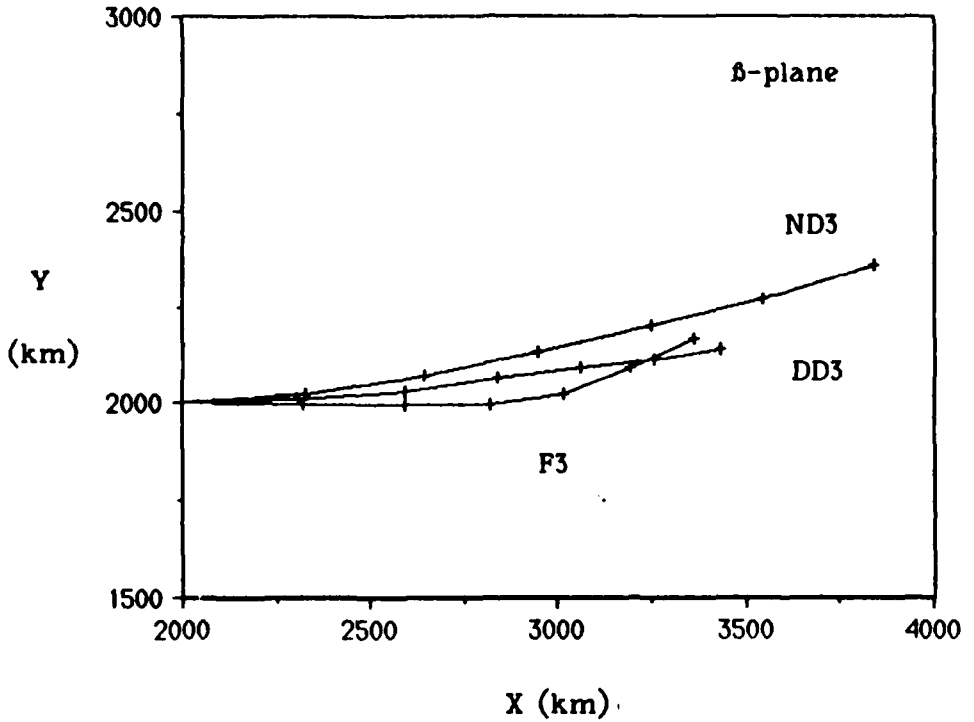

Figure 13 The 72-hour tracks of the layer 1 vorticity maximum for simulations ND3, DD3 and F3. Symbols mark the vortex position at 12-hour intervals.

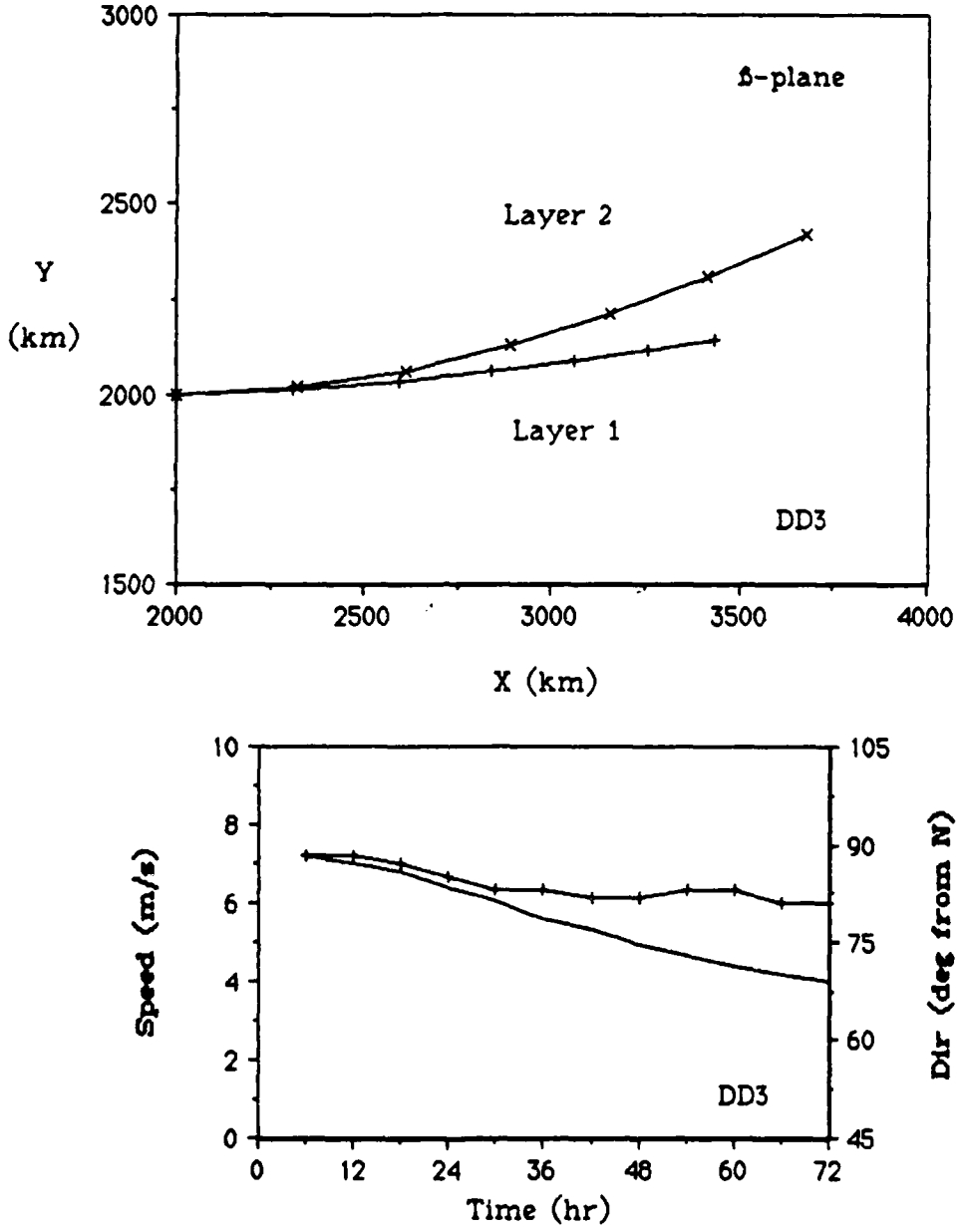

Figure 14 The 72-hour tracks of the vorticity maximum in each layer (top) and the speed (solid) and direction (hatched) of the layer 1 vorticity maximum (bottom) for the DD3 case. Symbols appear at 12-hour intervals.

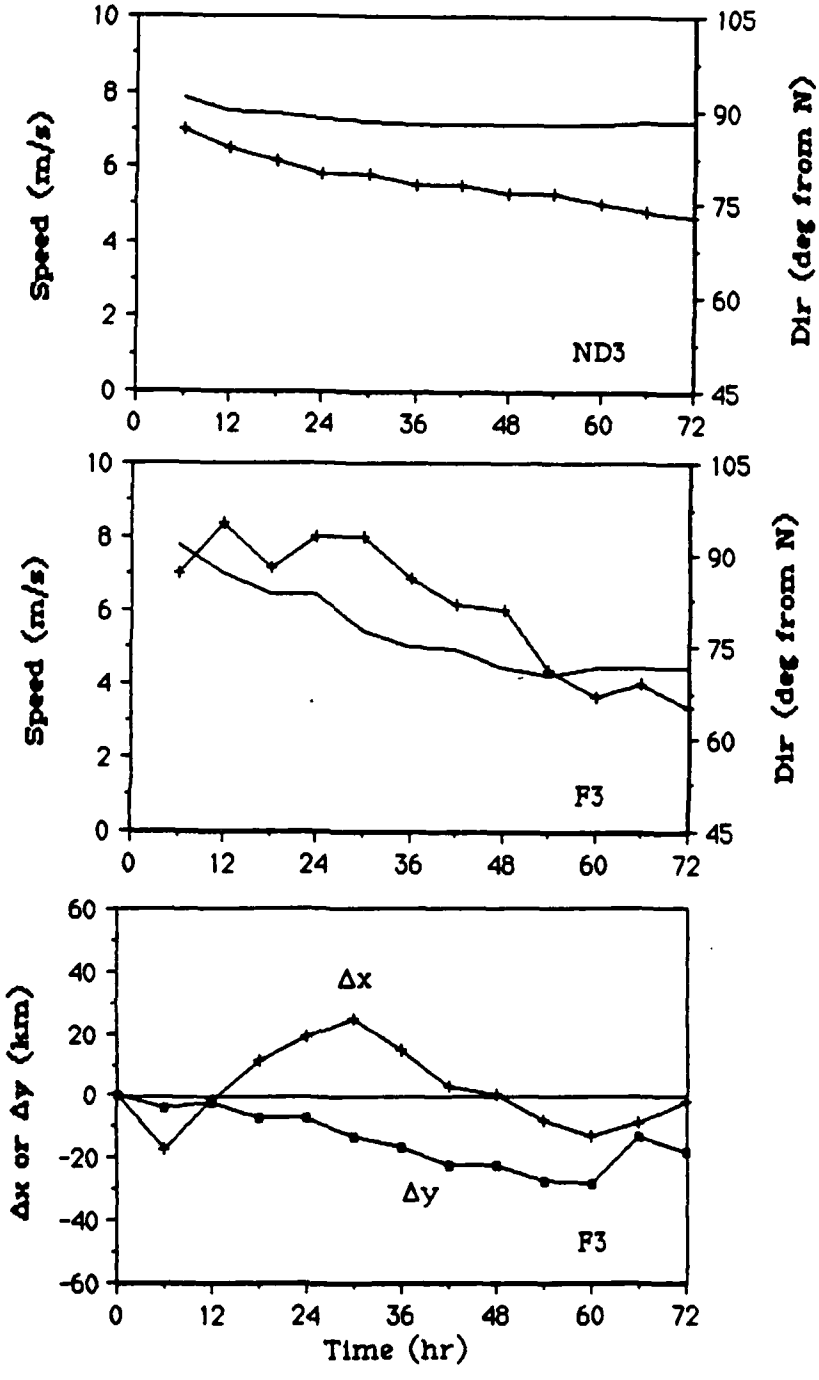

Figure 15 Time evolution of the speed (solid) and direction (hatched) of the layer 1 vorticity maximum for ND3 (top) and F3 (middle). Upper and lower vortex positional deviations (bottom), Δx or Δy indicates an eastward or northward displacement of the layer 2 vortex relative to the layer 1 vortex for the F3 case.

4. Numerical Simulations with Vertical Wind Shear

4.1 Description of the Shear Field

In order to isolate the effect of the vertical shear of the horizontal wind on tropical cyclone movement, numerous experiments are made utilizing increasingly greater magnitudes of shear. Zonal winds are added separately in layers 1 and 2 with the boundary layer winds being specified by the layer 1 wind. The structure of the horizontal wind U_i was described previously and is given by equation (3.3) in each layer. Only the simplest case of unidirectional shear of the zonal wind is considered in this chapter and is given by:

$$\mathbf{S} = \frac{U_2 - U_1}{\Delta Z}\,\hat{\imath} \tag{4.1}$$

where ΔZ is the geopotential height of the environmental layer between 200 mb and 600 mb and is the same for all simulations. Since the wind field is nearly constant throughout the central part of the domain (see Figure 6a), the shear field will also be constant in this region. Westerly wind shear is defined to be the positive value of equation (4.1), i.e. pointing towards the east from the west. This study concentrates upon the effect of westerly wind shear on tropical cyclone movement since the vertical wind structure required for westerly shear is very commonly found in the summertime tropical atmosphere. However, an example of a simulation using a current with easterly shear will be presented for illustrative purposes.

In the next section, the effects of physical processes on a simulated vortex embedded in a strongly sheared environment are investigated.

Similar in format to the experiments presented in Chapter 3, the movement is first investigated in the absence of physical processes, then with surface drag included, and finally with cumulus effects considered. Simulations are restricted to the simplest f-plane case. A summary of the simulations presented in Section 4.2 may be found in Table 3.

In Section 4.3, the results of fully parameterized simulations run on the f-plane with varying magnitudes of westerly wind shear are presented. The layer 1 wind magnitude of 8 ms^{-1} is held constant for all simulations requiring that the magnitude of the layer 2 zonal wind be different for every simulation in order to generate varying magnitudes of shear. The shear magnitudes were picked to crudely represent weak, moderately weak, average, and strong values of vertical synoptic scale wind shear present at 20° North latitude in the west Atlantic during the peak hurricane season (Hastenrath, 1985). Experiments are conducted with the shear magnitudes described above for a vortex embedded in easterly current simulated in all layers and then repeated for simulated westerlies. For this set of experiments, the layer mean wind, mass weighted in the vertical, given by

$$\bar{U} = \frac{(H_0+H_1)U_1 + \epsilon H_2 U_2}{H_0+H_1+\epsilon H_2} \tag{4.2}$$

is not equal to zero. Section 4.4 presents the same set of experiments repeated with the effect of a variable Coriolis parameter included. A summary of the simulations in Sections 4.3 and 4.4 may be found in Table 4.

A final set of experiments are presented in Section 4.5 where the mass weighted layer mean wind was zero. Therefore, from (4.2) the upper layer wind is given in terms of the lower layer winds by

$$U_2 = -\left(\frac{H_0+H_1}{\epsilon H_2}\right)U_1 \tag{4.3}$$

For these simulations, low level easterlies are chosen which requires that the upper levels winds be westerly. Experiments are run on the f-plane and repeated on the β-plane. These simulations are summarized in Table 6. The values for all parameters and initial conditions, other than the large scale winds, do not vary from those specified for preceeding simulations.

4.2 F-plane Simulations with Varying Physical Properties

Recalling the barotropic case run on the f-plane in the absence of physical processes, case ND1, the vortex in both layers advected with the basic current. One might expect that the same effect be evidenced when the basic currents are allowed to vary in the vertical in the absence of physical processes, i.e. that the vortex in each layer be advected precisely with its respective basic current. In order to test this, a simulation NDS1 is run with a vortex embedded in a strongly sheared basic current having a layer 1 basic current from the east at 8 ms^{-1} and no zonal flow in the upper layer. The 72-hour tracks of the upper and lower layer vortex centers for the NDS1 case are shown in Figure 16 (bottom). The upper layer tracks are represented by the lines with symbols and the lower layer tracks by the hatched lines. Results from this case show that the

Table 3. Summary of simulations presented in Section 4.2.

Simulation	Physical Processes		Basic Current		$\mathbb{S}$	$\bar{U}$	Coriolis
	Drag	Moisture	U_1 (ms^{-1})	U_2	(ms^{-1}/km)	(ms^{-1})	Parameter
NDS1	No	No	$-8\hat{i}$	$0\hat{i}$	$1.2\hat{i}$	$-5.4\hat{i}$	β=0
DDS1	Yes	No	$-8\hat{i}$	$0\hat{i}$	$1.2\hat{i}$	$-5.4\hat{i}$	β=0
SS1	Yes	Yes	$-8\hat{i}$	$0\hat{i}$	$1.2\hat{i}$	$-5.4\hat{i}$	β=0
NDS2	No	No	$-8\hat{i}$	$-16\hat{i}$	$-1.2\hat{i}$	$-10.6\hat{i}$	β=0

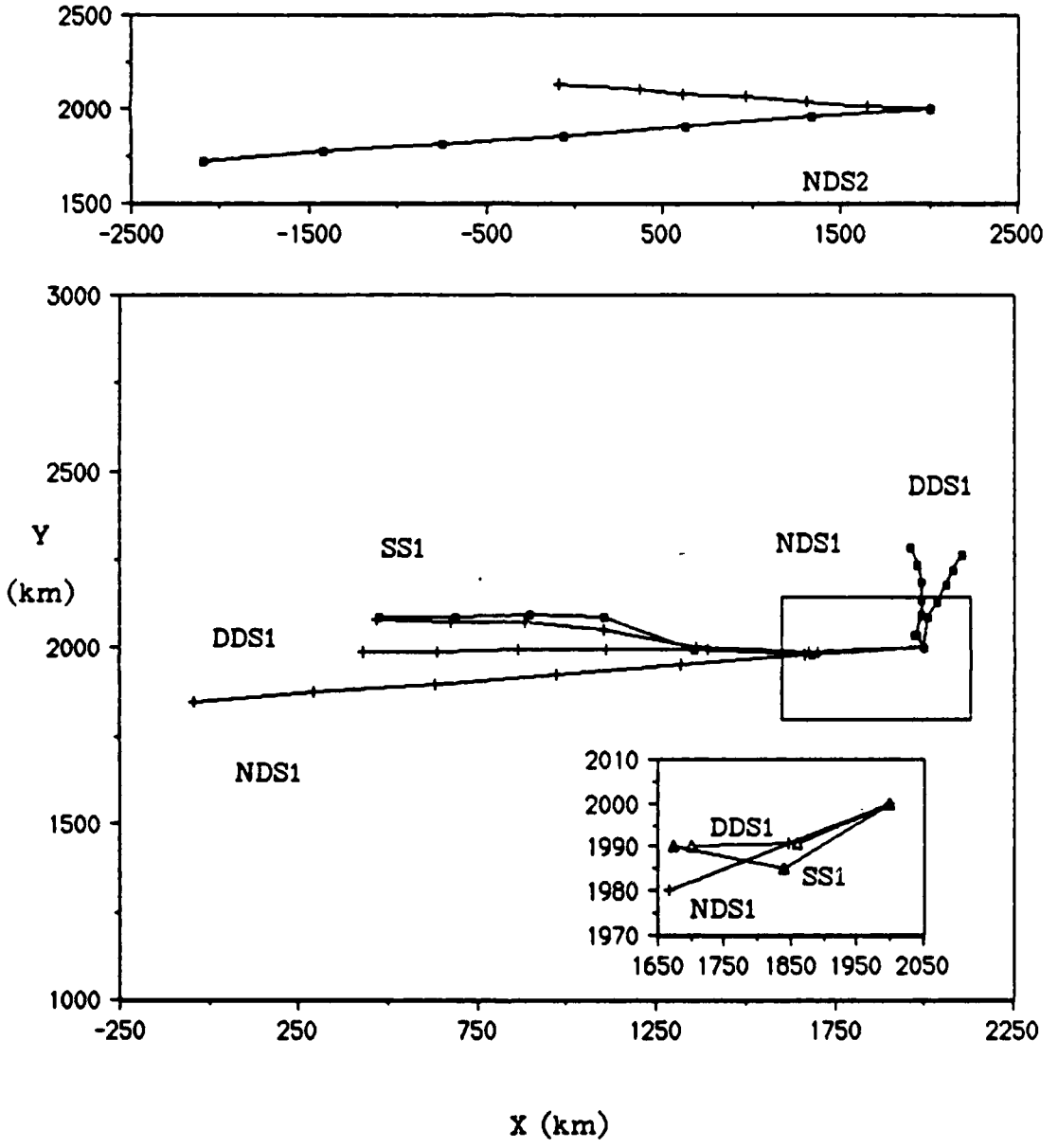

Figure 16 The 72-hour tracks of the vorticity maximum for NDS2 (top) and NDS1, DDS1, and SS1 cases (bottom), symbols mark position of layer 1 (hatches) and layer 2 (squares) vortices at 12-hour intervals. Magnification of boxed region shows initial tracks of the layer 1 vortices at 6-hour intervals (inset).

while the layer 1 vortex center moves with the same speed as the layer 1 basic current, its direction deviates to the left (south) of the basic current by 4.2°. The upper layer results are even more surprising. The vortex center moves with a component of motion slightly west of north at approximately 1.1 ms^{-1} even though no basic current was introduced in layer 2.

The movement described above must arise from the difference in the structure of the large scale environment that is due to the vertical wind shear. The inclusion of vertical wind shear indicates the presence of an horizontal temperature gradient. Using the thermal wind equation it can be determined that for westerly wind shear this temperature gradient would be positive to the right of the direction of the wind shear vector, towards the south in this case. The layer 1 vortex in case NDS1 displays a component of motion in this direction while ND1, the barotropic case which has no such gradient associated with it, shows no deviation from the basic current.

The movement of the layer 2 vortex seems to be in response to changes in the thickness fields caused by the motion of the layer 1 vortex. If an upper layer zonal current were used, the movement of the upper level vortex would be advected by that current in addition to this propagation opposite in direction to the layer 1 vortex propagation. This movement is similar to that observed in the upper levels for the surface drag cases presented in Chapter 3.

If the environmental temperature gradient does affect the motion of a vortex, easterly vertical shear of the horizontal winds should show results exactly opposite to those above since the horizontal temperature

gradient would now be directed towards the north. To verify the above hypothesis, a simulation was run under easterly shear conditions with no physical processes included (case NDS2). In this simulation, the layer 1 basic current is from the east at 8 ms^{-1} and the upper layer wind is from the east at 16 ms^{-1}. This choice of winds gives this simulation the same shear and, hence, temperature gradient magnitude as the above case but in the opposite direction. The tracks of the upper and lower layer vortex centers for the NDS2 case are shown at the top of Figure 16. The results of this simulation indicates that the lower layer vortex center deviates to the right of the basic current by an average of 3.5° with advection by the basic current dominating the motion. This observed deviation is towards the north, in the direction of the temperature gradient which is in agreement with the above arguement. However, this deviation is slightly less than the NDS1 case which has the same shear magnitude. This difference in deviations for the same shear magnitudes could occur as a result of the initial specification of the mass fields from the wind fields. In the upper layer, the vortex moves with the same speed as the upper layer current with a deviation towards the left of the basic current.

When surface drag is turned on, (DDS1), the layer 1 vortex is observed to move in the same direction as the layer 1 basic current but at a slower average speed of 6 ms^{-1}. In light of Chapter 3 simulations, this vortex movement must actually be considered a deviation to the right of its direction of motion, given by the layer 1 vortex in the NDS1 case. The effect of the surface drag acts in direct opposition to the effects of shear and, at least for this wind and shear configuration, cancels any directional changes in the track of a vortex on the f-plane. In the upper

layer, the vortex veers to right of the vortex in the NDS1 case leading further credence to the idea that in the absence of modeled physics, the layer 2 vortex moves in response to changes in the lower layer thickness field.

Finally, the effect of cumulus convection on the strong westerly sheared case SS1 is examined. The 72-hour tracks of the upper and lower layer vortices for all the westerly sheared cases are displayed in the middle of Figure 16. The boxed region is magnified and presented at the bottom to illustrate the layer 1 track differences during the first 12 hours. Initially, the lower layer vortex deviates more to the left of the basic current direction than does the vortex in the no physical processes case. This indicates that while the environmental factor still has an important effect on the cyclone's direction, the interaction between the upper and lower vortex must be considered also. Examining Figure 18 (bottom, at right), which presents the time evolution of the positional deviations between the upper and lower vortices for case SS1, it can be seen that the layer 2 vortex initially lagged 48 km behind, and slightly north of, the layer 1 vortex as a result of advection by their respective basic currents. After the first 12 hours, the period of rapid intensification, the vortex becomes vertically aligned due to mass transports which compensates for the initial shear effect and begins to move to the right of its initial direction of motion, due to the cumulus effect discussed in Chapter 3. After this time, oscillation of the layer 1 and 2 vortices is observed with changes in the direction of layer 1 correlated with large positional deviations in the vortices.

To summarize this section, the inclusion of vertical wind shear in this model produces a twofold effect. First, the inclusion of vertical wind shear induces a propagation of the simulated vortex that is to the right of the direction of the wind shear vector. This propagation is consistently observed for the layer 1 vortex center throughout simulations made in the absence of physical processes and with these processes included. Although more research is necessary to verify the exact mechanism causing this propagation, it appears to be a result of the structure of the larger scale environment. The track changes resulting from this effect should increase as the magnitude of the vertical wind shear increases. Although this appears to be the dominant factor, the difference in advection rates of the upper and lower vortices also results in short term directional changes observed in the track of the layer 1 vortex. These directional changes are highly dependent upon whether the upper layer vortex represents a source or sink of relative vorticity in the direction which the cyclone in layer 1 is moving and should be greater for larger shear magnitudes. These short term directional changes occur consistently in all model simulations whenever the upper and lower layer vortices deviate for whatever reason. However, the initial upper and lower layer displacements due to advection are quickly compensated by cumulus transports.

4.3 F-plane Simulations with Varying Magnitudes of Shear

As shown in the last section, the inclusion of a vertically varying basic state wind immediately introduces directional changes in the path of a simulated hurricane. According to the above arguement and with the

layer 1 basic current given the same magnitude throughout model simulations, a southward track deviation of a simulated cyclone in westerly shear from the barotropic case should be observed. This deviation should increase as the magnitude of the shear increases. This movement would be further tempered by the location of the upper level vortex in relation to the lower layer vortex. To further examine this influence, fully parameterized simulations are made with increasingly greater magnitudes of westerly vertical wind shear. In the first set of experiments, the basic current flow is easterly in all layers requiring that the upper layer wind speed be less than that in the lower layer. Such a structure allows the upper layer vortex to lag behind the layer 1 vortex position. The next set of experiments is run with westerly currents in each layer. This requires that the layer 2 wind speed be faster than the layer 1 wind speed. These simulations are summarized in Table 4.

4.3.1 Results of Easterly Current Simulations

Figure 17 displays the 72-hour tracks of two westerly shear cases in easterly flow. The weakest shear case WS1 and the greatest shear case SS1 are presented on a partial domain along with the barotropic case F1 for comparison. The moderate and average shear cases are not depicted on the plot, for the sake of clarity, but both had tracks running between the WS1 and SS1 tracks and exhibited some of the features of each. The time evolution of the direction and speed of the layer 1 vortex in each of these simulations are presented at the top of Figure 18. Deviations of the upper vortex from the lower vortex position are given at the bottom of

Table 4. Summary of simulations presented in Sections 4.3 and 4.4.

Simulation	Basic Current U_1 (ms^{-1}) U_2		$\mathbf{S}$ (ms^{-1}/km)	$\bar{U}$ (ms^{-1})	Coriolis Parameter
WS1	-8î	-6î	.3î	-7.3î	β=0
MS1	-8î	-4î	.6î	-6.7î	β=0
AS1	-8î	-2î	.9î	-6.0î	β=0
SS1	-8î	0î	1.2î	-5.4î	β=0
WS4	8î	10î	.3î	8.7î	β=0
MS4	8î	12î	.6î	9.3î	β=0
AS4	8î	14î	.9î	10.0î	β=0
SS4	8î	16î	1.2î	10.6î	β=0
WS2	-8î	-6î	.3î	-7.3î	$\beta\neq0$
MS2	-8î	-4î	.6î	-6.7î	$\beta\neq0$
AS2	-8î	-2î	.9î	-6.0î	$\beta\neq0$
SS2	-8î	0î	1.2î	-5.4î	$\beta\neq0$
WS3	8î	10î	.3î	8.7î	$\beta\neq0$
MS3	8î	12î	.6î	9.3î	$\beta\neq0$
AS3	8î	14î	.9î	10.0î	$\beta\neq0$
SS3	8î	16î	1.2î	10.6î	$\beta\neq0$

Figure 18. Positive values for Δx and Δy indicate a displacement of the layer 2 vortex to the east or north of the layer 1 vortex respectively.

For each simulation, the dominant factor influencing the vortex movement is advection by the basic current with the average speed of the layer 1 vortex decreasing with an increase in shear magnitude. Because of the surface drag effect, the vortex in all simulations moves slower than the basic current. As illustrated in these figures, as the shear magnitude increases, so does the initial southward deviation from the barotropic track. Further examination of the 6-hourly breakdown of the speed and direction of the vortex center shows remarkable similarities between shear cases. The strong northward movement during the first 30 hours is due to the cumulus effect discussed in Chapter 3 which quickly eliminates the initial vertical positional differences due to different advection rates. The effect of the large 6 hour positional differences are evident by the southward change in direction 12 hours into the integration. The results of the average and moderate shear cases (not shown) were consistent with the results obtained from the weakest and strongest shear cases.

Furthermore, all the simulations show an oscillation in the track of the type exhibited in the previous chapters that result from the nonlinear interactions with the environment. The period of the oscillation decreases as the shear magnitude increases, or as the layer 2 winds decrease in magnitude. Shifts in the direction of the layer 1 vortex seem to be related to the position of the upper layer vortex, the most obvious occurring 12 hours into the integration and explained above. Between 30 and 48 hours, all simulations show the upper layer vortex positioned to the southwest of the lower layer vortex and an associated northward movement.

An examination of the time evolution of the maximum tangential winds of the WS1, SS1 and F1 cases, given at the top of Figure 19, indicates that the inclusion of vertical wind shear not only effects the track but the intensity of the simulated cyclone as well. Madala and Piacsek (1975) showed that a cyclone did not intensify to hurricane strength for simulations with large vertical wind shear. Observational evidence also points to the fact that hurricanes do not develop in regions of large vertical wind shear (Anthes, 1975). For each simulation in this study, the simulated vortex (here, the initial vortex plus the non-resting basic current) is initially hurricane strength but continues to develop further. As the magnitude of the shear increased the value of the maximum tangential wind speed decreased and the time to intensify to that value increased. However, after the period of rapid intensification, the rate of deintensification became greater for the more weakly sheared cases which also became more asymmetric.

4.3.2 Results of Westerly Current Simulations

Figure 20 displays, on a portion of the model domain, the 72-hour tracks of the vortex centers for simulations made with westerly shear in westerly flow. Only the weakest WS4 and strongest SS4 shear cases are displayed along with the fully parameterized barotropic westerly flow case F4 for comparison. Figure 21 (top) shows the time evolution of the speed and direction of the layer 1 vortex for the WS4 and SS4 shear simulations. As evidenced by these figures, the most dominant influence upon the motion of the cyclone is advection by the basic current. However, unlike the easterly flow cases, the average speed of the vortex is nearly the

same, approximately 5.9 ms^{-1}, for each simulation with the initial speeds being greater in each case than the layer 1 wind speed because of the greater wind speeds aloft.

As the magnitude of the shear increases, the southward deviation from the barotropic case increases in agreement with the previous discussion. However, the magnitude of the deviations are not as great as those found in simulations utilizing the same shear values in easterly flow. This was observed previously in the simulations utilizing no physical processes and is probably due to the mass field specifications. Furthermore, an examination of the positional deviations between the upper and lower vortices (Figure 21 at bottom), indicate that the initial displacements are very small. Therefore, because of the faster vortex speed it would seem that stronger upper layer winds serve to drag the lower level vortex along with it. As a consequence, the shorter term directional changes in the layer 1 vortex are not observed during the first 24 hours as they were in the easterly flow case. The results of the average and moderate shear cases (not shown) were consistent with the results of the strong and weak shear cases.

An examination of the time evolution of the maximum tangential winds, illustrated at the bottom of Figure 19, shows that the barotropic case remains more intense throughout the integration than the sheared cases. The simulations all attain greater maximum tangential wind speeds than their easterly counterparts within the first 12 hours due to the greater magnitude of the upper level winds. Oscillations of the upper vortex about the lower vortex are observed later during the integration with directional changes occurring coincident with the larger displacements.

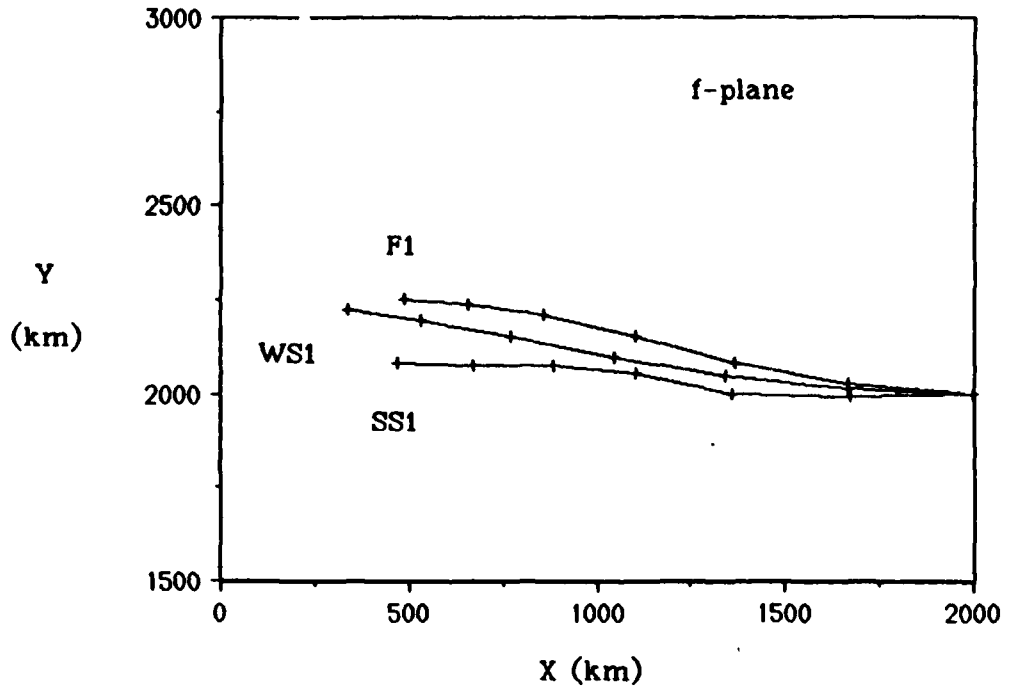

Figure 17 The 72-hour tracks of the layer 1 vorticity maximum for simulations WS1, SS1 and F1. Symbols mark the vortex position at 12-hour intervals.

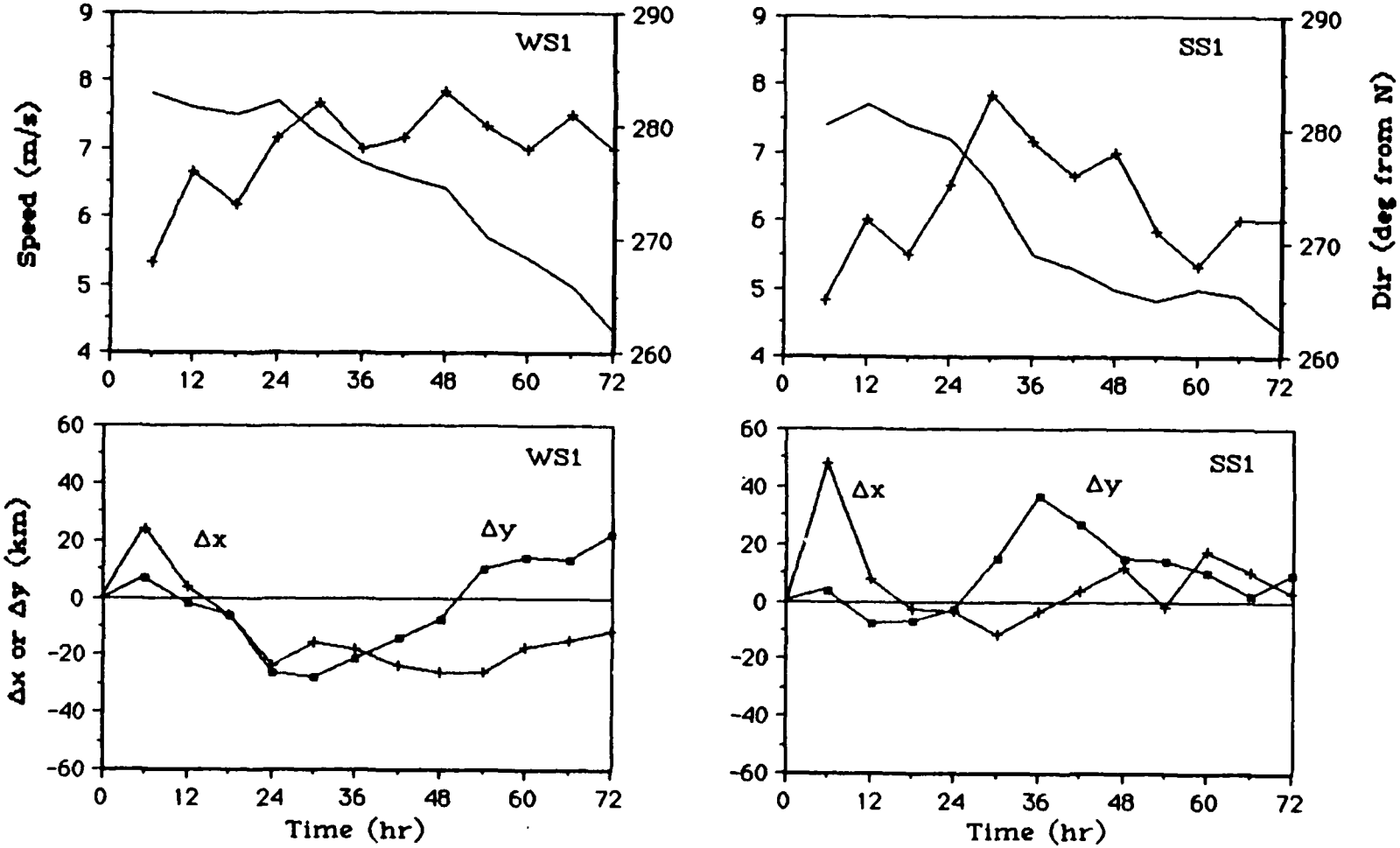

Figure 18 Time evolution of the speed (solid) and direction (hatched) of layer 1 vorticity maximum (top). Upper and lower vortex positional deviations (bottom), Δx or Δy indicates an eastward or northward displacement of the layer 2 vortex relative to the layer 1 vortex for WS1 (left) and SS1 (right).

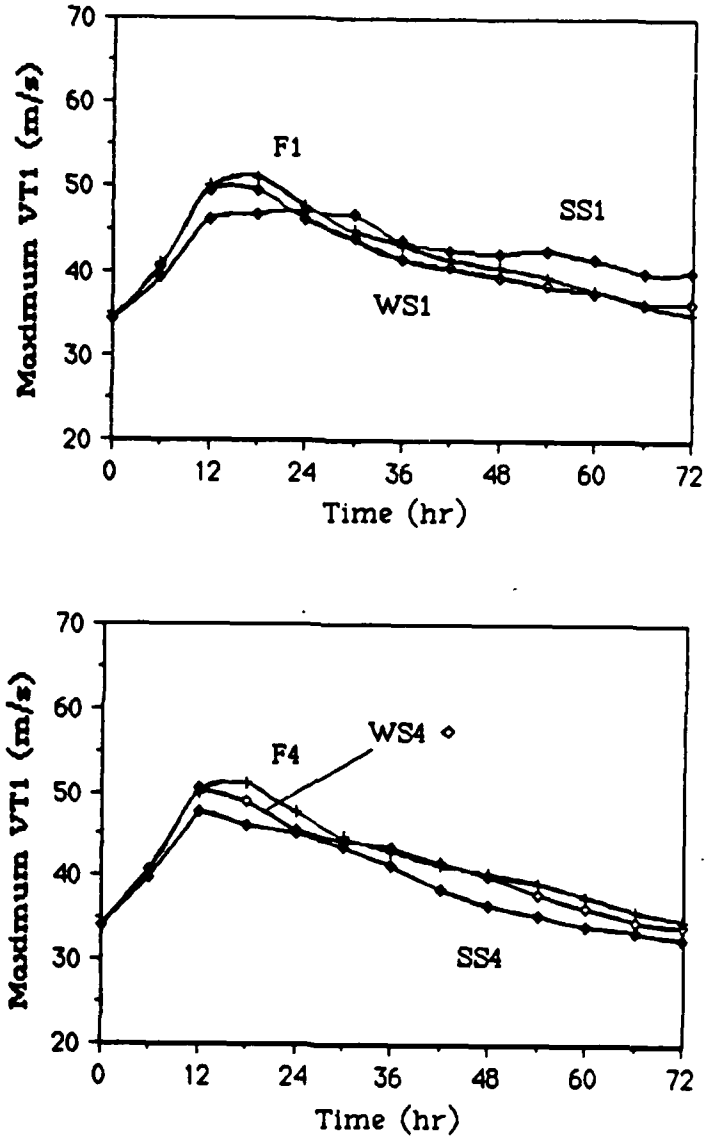

Figure 19 Time evolution of the maximum layer 1 tangential wind VT for cases F1, SS1, and WS1 (top) and F4, SS4, and WS4 (bottom).

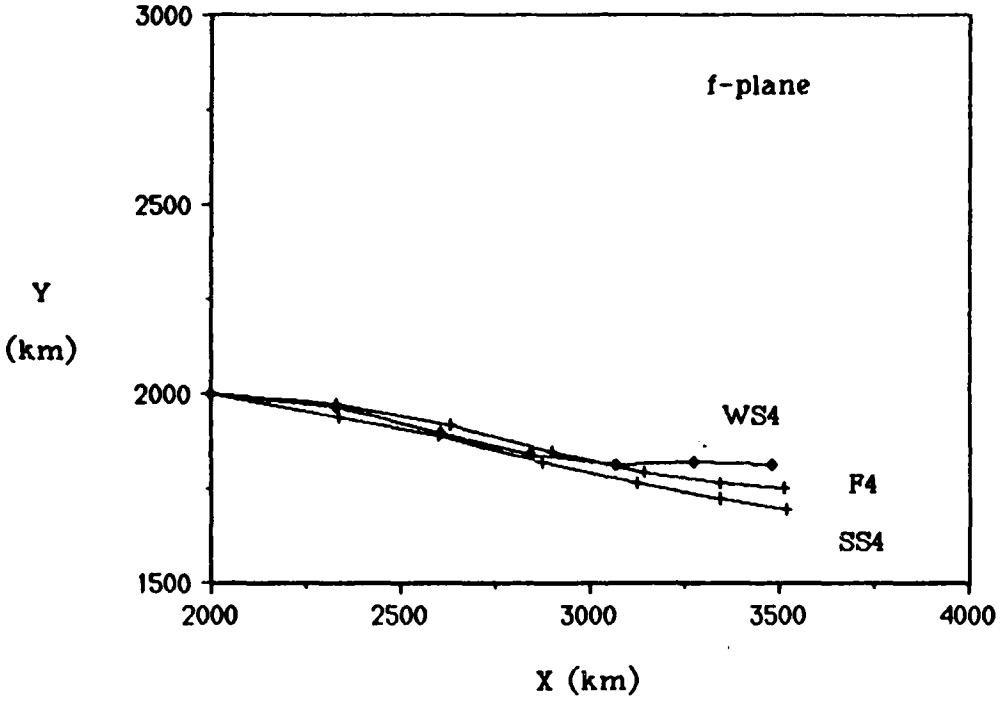

Figure 20 The 72-hour tracks of the layer 1 vorticity maximum for simulations WS4, SS4 and F4. Symbols mark the vortex position at 12-hour intervals.

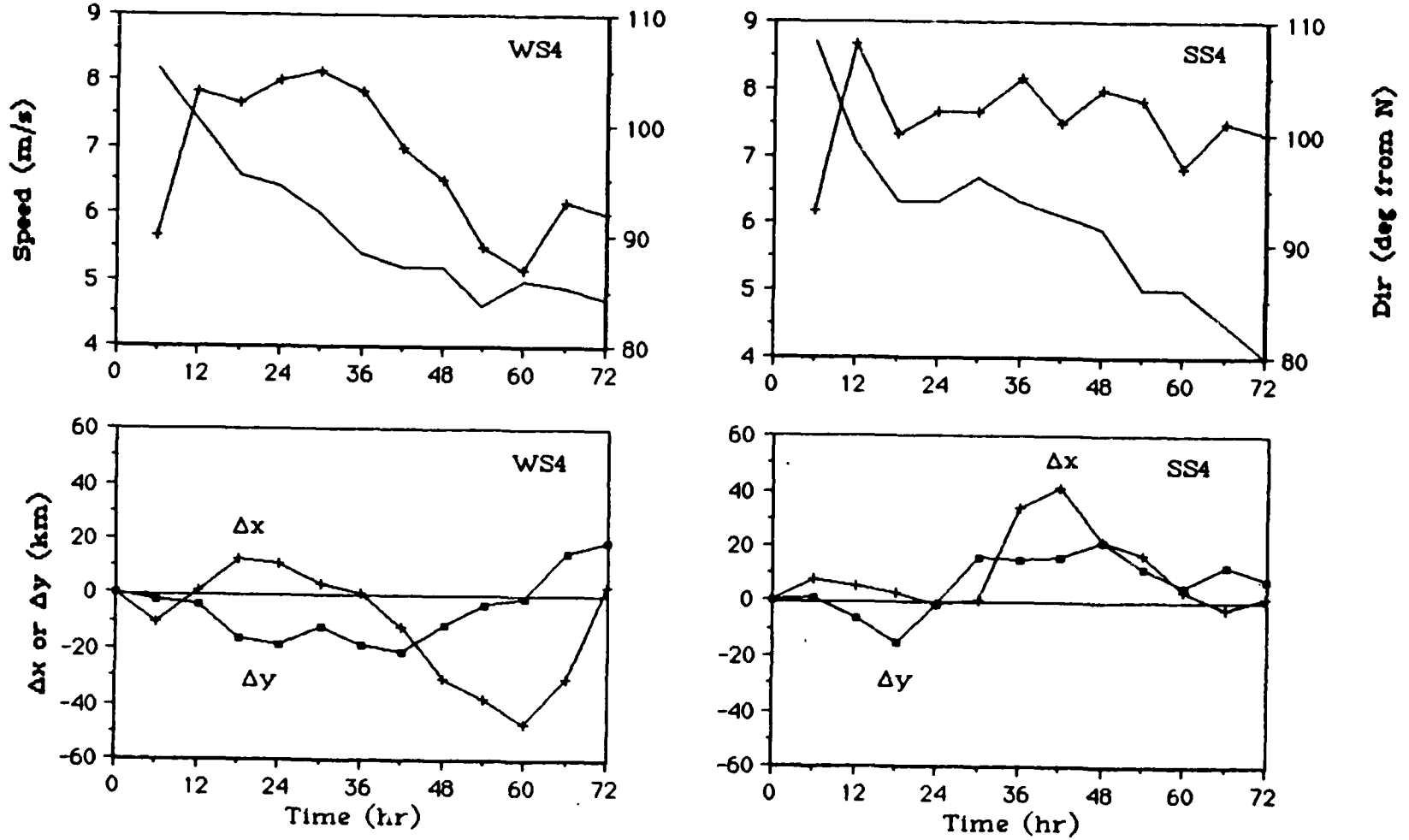

Figure 21 Time evolution of the speed (solid) and direction (hatched) of layer 1 vorticity maximum (top). Upper and lower vortex positional deviations (bottom), Δx or Δy indicates an eastward or northward displacement of the layer 2 vortex relative to the layer 1 vortex for WS4 (left) and SS4 (right).

4.4 ß-plane Simulations with Varying Magnitudes of Shear

Although highly instructional, f-plane simulations do not give an accurate portrayal of tropical cyclone movement. In Chapter 2, it was shown that the ß-effect induces a northwestward movement of a vortex embedded in a resting basic state. The influence of a variable Coriolis parameter was shown, in Chapter 3, to act in the same direction as advection and physical processes for a vortex embedded in a barotropic easterly flow and in opposition for a westerly current. The upper level vortex was also shown to advect in a different manner than its f-plane counterpart. Therefore, the simulations of the previous section are repeated with a variable, rather than constant, Coriolis parameter. A summary of these simulations is given in Table 4.

4.4.1 Results of Easterly Current Simulations

Figure 22 displays the 60-hour tracks of the layer 1 vortex centers for the weakest WS2 and strongest SS2 shear cases in easterly current. The barotropic case is presented for comparison. The tracks of the MS2 and AS2 cases ran between the two shear cases presented. Time evolution of the speed and direction of the layer 1 vortex for the weakest and strongest shear cases (Figure 23 at top) show the vortex speeds to be greater than the f-plane counterparts due to the inclusion of a variable Coriolis parameter. A southward deviation from the barotropic case is observed, although the deviation at 6 hours is less than the f-plane case due to the ß-effect which induces a component of motion towards the north in opposition to the shear effect.

An examination of positional differences beween the upper and lower vortices (Figure 23 at bottom) show very few differences from the f-plane cases. The effect of the 6 hour position differences can be seen in the track change occurring 12 hours into the integration. Hence, this deviation which was much greater for the f-plane cases seems to be tempered by the inclusion of the ß-effect. Other than the more northwesterly movement of each simulated cyclone, the greatest difference between the f- and ß-plane simulations is that the sheared cases tend to converge during the integration. This can be explained by the differences in the intensification rates of each of the simulated cyclones. As evidenced by Figure 26 (top), the greater the shear magnitude, the slower the rate of intensification with the strongly sheared case becoming more intense after the first 24 hours. As a result, both the cumulus and ß-effect will continue to induce a slightly greater northward movement of this vortex when compared to the other cases.

The results presented here are somewhat different from results presented by Madala and Piacsek (1975). In that study, two ß-plane simulations showed smaller northward displacements from the basic current with increasing shear magnitudes. However, since the vertically averaged wind was larger for the more strongly sheared case, the smaller displacement from the basic current was explained to be a result of advection by a faster steering current. In this study, the layer mean wind decreases with decreasing deviations from the basic current proving that these deviations cannot be explained by advective effects alone.

4.4.2 Results of Westerly Current Simulations

The 72-hour tracks for the westerly flow simulations are presented in Figure 24. As in previous figures only the weakest and strongest shear cases are presented along with the barotropic case. An examination of the time evolution of the speed and direction of the layer 1 vortex, displayed at the top of Figure 25, shows that initially the vortex speeds increase with an increase in the layer mean wind, which corresponds to greater shear magnitudes for westerly flow with westerly shear. However, these speeds rapidly slow so that the average speed by the end of the integration is the same for all cases.

Initial southward deviations in direction are observed which increase with increasing shear magnitude as hypothesized. Looking again at this figure shows that this initial deviation is less than its f-plane counterpart (see Figure 21) indicating that the ß-effect partially compensates for the environmental shear effects in as quickly as 6 hours. After the first 12 hours, the period of maximum intensification for all the westerly flow simulations, the vortex centers for each simulation move in a more northerly direction due to the ß-effect and a decrease in intensification rates. Figure 26 (bottom) shows the time evolution of the maximum tangential wind for SS3, WS3, and F3. As observed with all simulations, the maximum intensity increases as the magnitude of the shear decreases.

In Figure 25 (bottom), the positional deviations between the upper and lower vortices are shown. Initial position deviations do not occur, similar to the f-plane simulations but at odds with the easterly flow simulations. Oscillations of the upper vortex about the lower vortex are observed for the more weakly sheared cases, while the strongly sheared cases show a

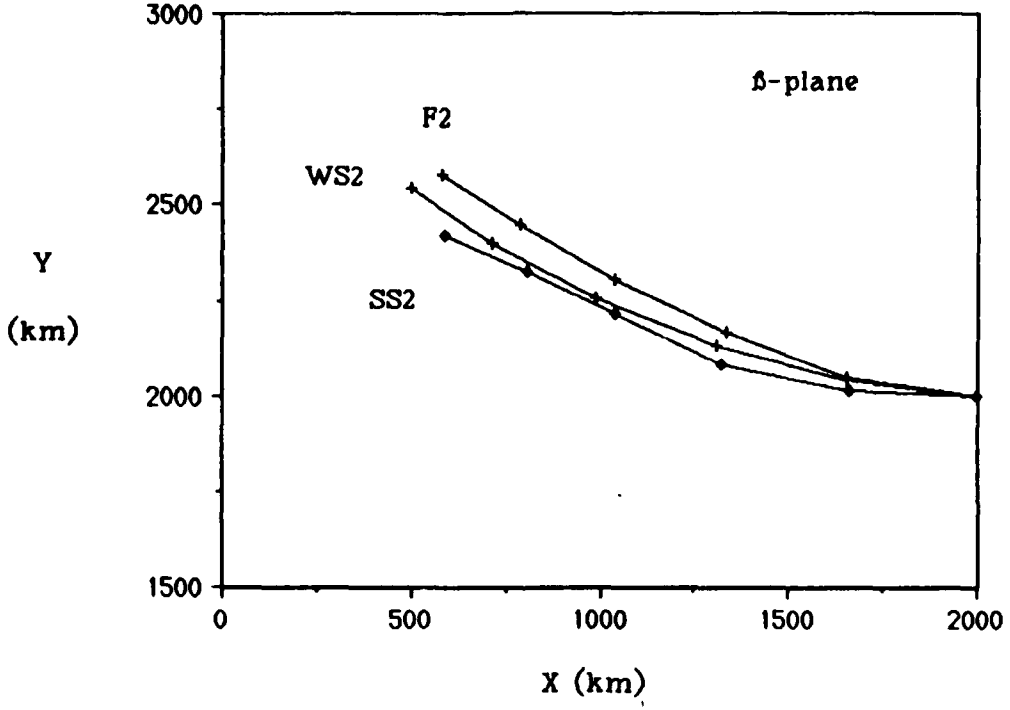

Figure 22 The 60-hour tracks of the layer 1 vorticity maximum for simulations WS2, SS2 and F2. Symbols mark the vortex position at 12-hour intervals.

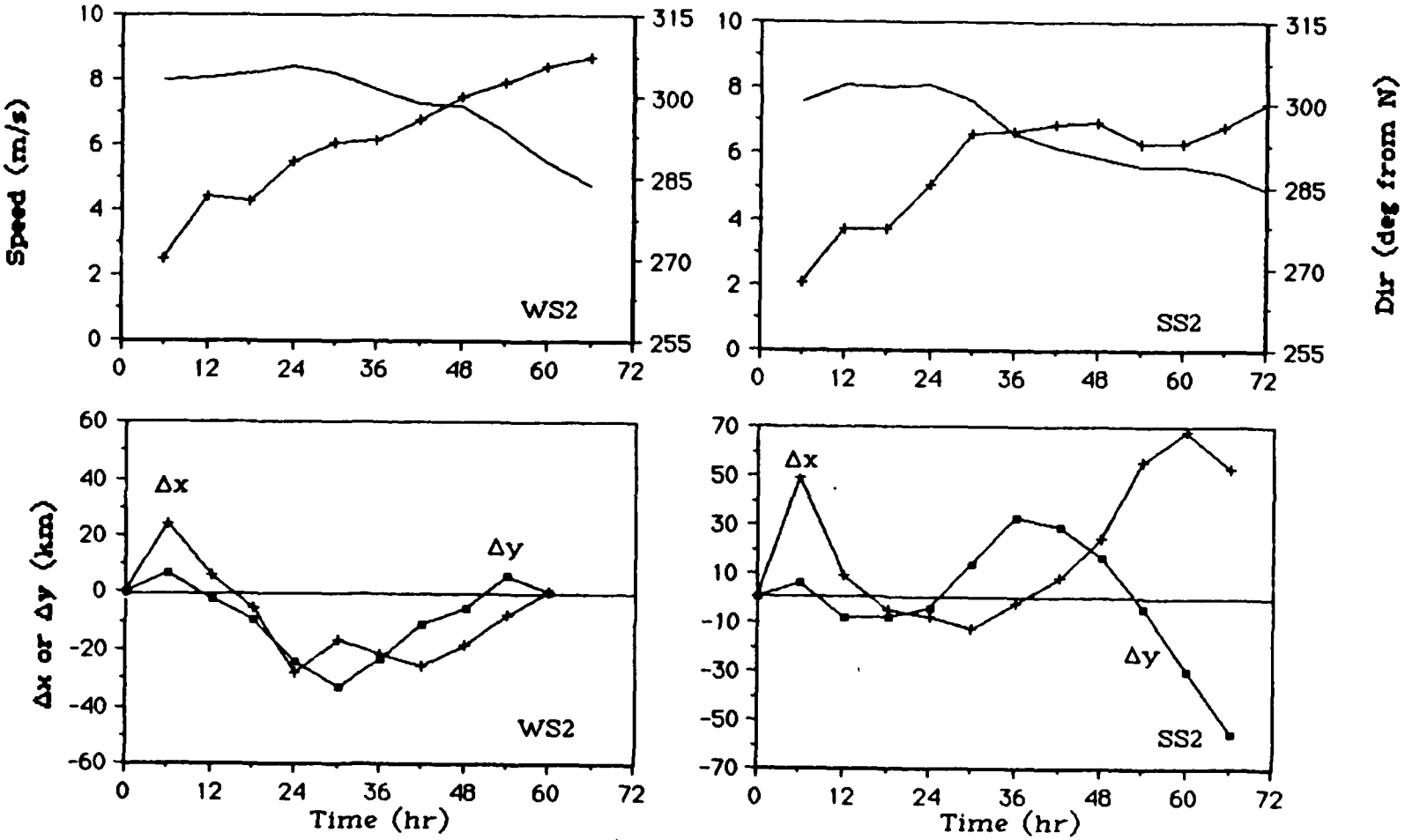

Figure 23 Time evolution of the speed (solid) and direction (hatched) of layer 1 vorticity maximum (top). Upper and lower vortex positional deviations (bottom), Δx or Δy indicates an eastward or northward displacement of the layer 2 vortex relative to the layer 1 vortex for WS2 (left) and SS2 (right).

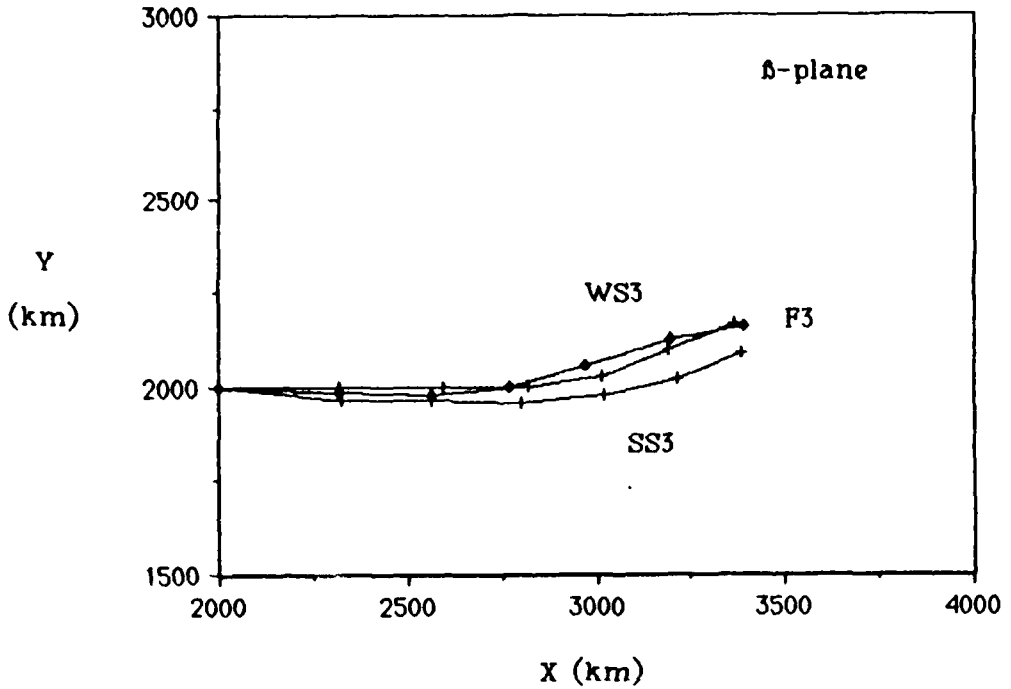

Figure 24 The 72-hour tracks of the layer 1 vorticity maximum for simulations WS3, SS3 and F3. Symbols mark the vortex position at 12-hour intervals.

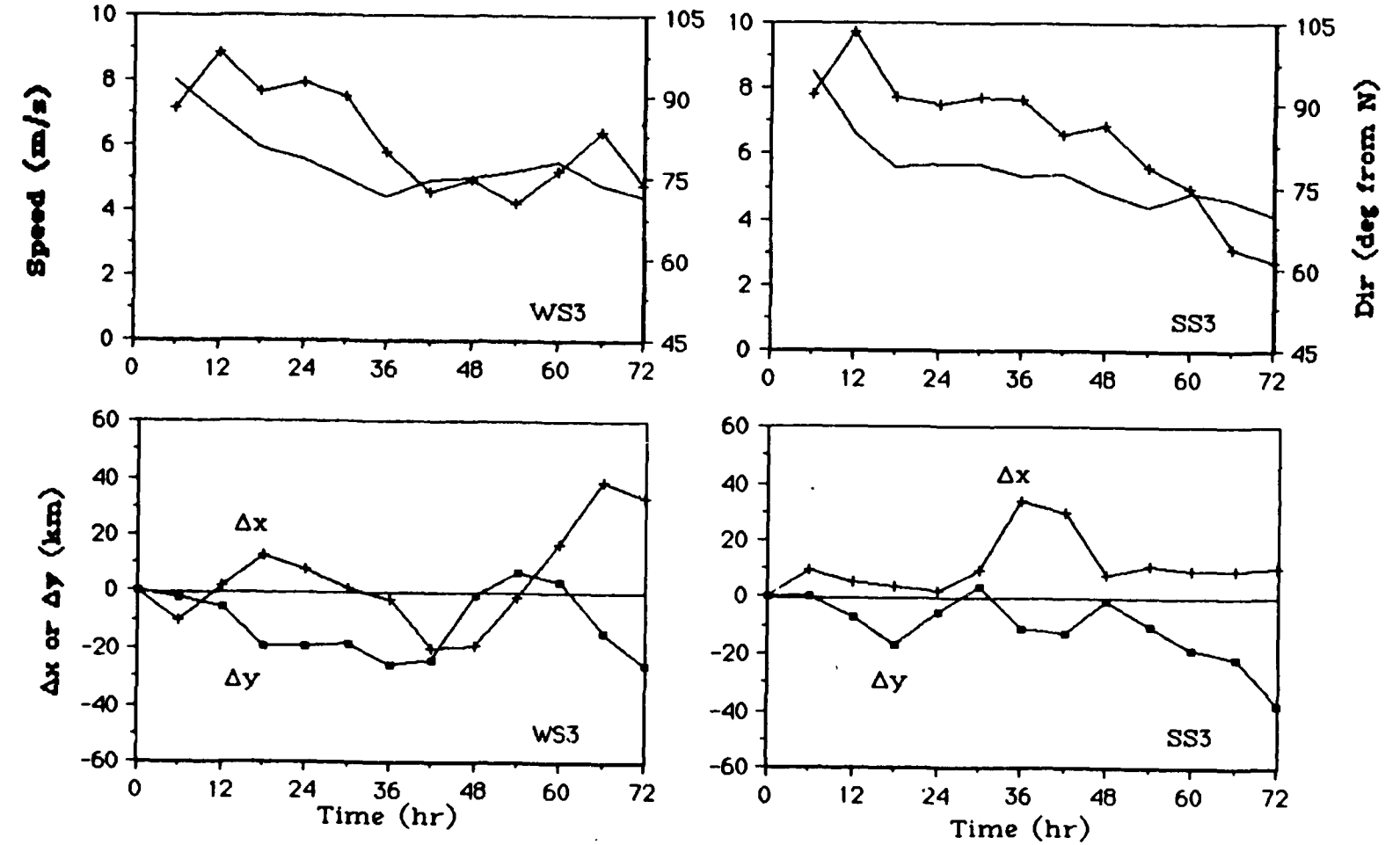

Figure 25 Time evolution of the speed (solid) and direction (hatched) of layer 1 vorticity maximum (top). Upper and lower vortex positional deviations (bottom), Δx or Δy indicates an eastward or northward displacement of the layer 2 vortex relative to the layer 1 vortex for WS3 (left) and SS3 (right).

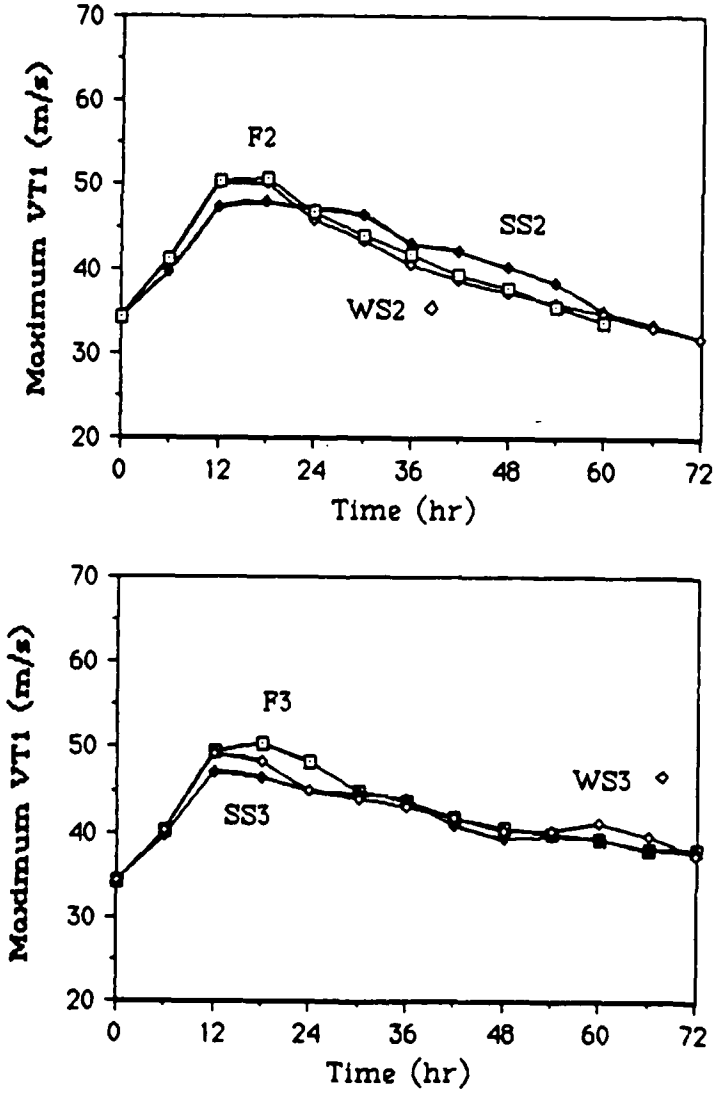

Figure 26 Time evolution of the maximum layer 1 tangential wind VT for cases F2, SS2, and WS2 (top) and F3, SS3, and WS3 (bottom).

displacement of the upper layer vortex to the southeast throughout most of the 72-hour integration.

Table 5 compares the tracks of these experiments to those of the NDBM (presented in Chapter 3) that were initialized by the layer 1 vorticity. This table indicates that with the inclusion of westerly shear in westerly flow, NDBM3 generally predicts the cyclone tracks less accurately than for the barotropic case F3. On the other hand, for westerly shear in easterly flow, NDBM2 tracks become more accurate than for the barotropic case F2. The magnitude of the positional differences between the two models is smallest for westerly sheared easterly flow at 24 hours. For intermediate forecasts, the positional differences for easterly and westerly flow are comparable in magnitude. For longer integrations, the positional differences for the westerly sheared westerly current cases are smallest in magnitude. Therefore, vertical wind shear may partially explain why the SANBAR model, which cannot incorporate the physics of a sheared environment, generally predicts low-latitude storms more accurately than high-latitude storms for short range forecasts.

4.5 Simulations with Zero Layer Mean Wind

This section investigates the effect of westerly vertical wind shear on the track of a cyclone under the condition that the layer mean wind, given by equation (4.2), is zero. To satisfy these requirements, the lower layer winds are easterly and the upper level winds are westerly and of greater magnitude than the low level winds. Given the layer 1 basic current, the upper layer current can be determined using equation (4.3). Two fully parameterized simulations, with moderate and strong shear,

are run on the f-plane and then repeated with a variable Coriolis parameter. These simulations are summarized in Table 6. Figure 27 shows the 72-hour tracks of the vorticity maximum for these cases as well as those made on the ß-plane with the resting basic state case (NS) for comparison.

Figure 28 (top) shows the speed and direction of the layer 1 vortex for the simulations made on an f-plane with moderate and strong shear, the M1 and M2 cases. An examination of this figure indicates that even though the upper level westerly winds are greater in magnitude than the layer 1 easterlies, the vortex still moves towards the west at speeds sometimes exceeding that of the layer 1 current. This indicates that as the vortex intensifies, the diabatic heating effects are more predominant towards the front of the storm rather than the right hand side as observed for previous case that were embedded exclusively in easterlies or westerlies. This may be related to the slower movement of the simulated cyclone. Shapiro (1983) showed that for slower moving storms, the maximum boundary layer convergence occurs in a broad region ahead of the storm, but becomes more concentrated on the right side as the storm speed increases. The southward deviation of the vortex from the direction of the layer 1 basic current is 16° for the M1 case and 17° for the M2 case at 6 hours, which is qualitatively similar to the previous results. However, the magnitude of this deviation is much greater than that observed for previous cases. Also, the track of the layer 1 vortex is much more erratic than that observed with exclusively easterly or westerly flow in all layers. This could be, in part, due to the slower basic current speeds used in these simulations. Observational studies (Holland, 1983) have

Table 5. Magnitude of the positional differences between NDBM and PEMOD simulations.

Simulation	Magnitude of the Positional Difference (km) 24 hours	48 hours	60 hours
F2/NDBM2	113	382	561
WS2/NDBM2	70	291	470
SS2/NDBM2	58	339	502
F3/NDBM3	90	286	394
WS3/NDBM3	122	308	378
SS3/NDBM3	135	315	411

Table 6. Summary of simulations presented in Section 4.5.

Simulation	Basic Current U_1 (ms^{-1}) U_2	$\mathbb{S}$ (ms^{-1}/km)	$\bar{U}$ (ms^{-1})	Coriolis Parameter
M1	$-1.0\hat{i}$	$2.03\hat{i}$	$.5\hat{i}$	$\Omega=0$
M2	$-3.0\hat{i}$	$6.09\hat{i}$	$1.3\hat{i}$	$\Omega=0$
M3	$-1.0\hat{i}$	$2.03\hat{i}$	$.5\hat{i}$	$\Omega\neq0$
M4	$-3.0\hat{i}$	$6.09\hat{i}$	$1.3\hat{i}$	$\Omega\neq0$

indicated that larger storm fluctuations are exhibited when the environmental winds are weak.

The oscillations in the path of the vortex illustrated in Figure 27, appear to be due to nonlinear effects. Hence, the large initial deviation appearent in the M1 and M2 cases could be due to the nonlinear effects in addition to the environmental shear effect. Any effects due to positional differences between the upper and lower layer vortices, given at the bottom of Figure 28, are not so evident. The large directional change at 24 and 36 hours, for the M1 and M2 cases respectively, is due primarily to the oscillation and partly due to slower intensification rates. The time evolution of the maximum tangential wind speeds of the layer 1 vortex, displayed in Figure 30 (top), illustrate that the intensification ends around 24 hours for the M1 case and at 36 hours for the M2 case. For all simulations having a zero layer mean wind, the maximum intensities of the storm remain greater than those storms having a nonzero layer mean wind. It appears that this particular wind configuration leads to more intense storms.

An examination of the positional deviations between the upper and lower vortices, and the speed and direction of the layer 1 vortex, Figure 29, of the ß-plane cases M3 and M4 show remarkable similarities to their f-plane counterparts. The most notable exceptions are the more northerly direction of movement and faster vortex speeds due to the ß-effect. As in all previous simulations, the greater the westerly shear magnitude, the greater the initial southward deviation from the basic current. Also, as exampliﬁed by Figure 30, the intensities of the ß-plane storms are comparable to their f-plane counterparts. This seems to indicate that, for

this wind configuration, the inclusion of a variable Coriolis parameter does not inhibit cyclone intensification.

To summarize this chapter, relative vorticity advection by the basic current is the most dominant factor controlling tropical cyclone movement. However, the addition of unidirectional vertically sheared environmental winds alters the structure of the synoptic environment which immediately induces a component of vortex motion towards the right of the direction of the wind shear vector. Thus, for westerly (easterly) vertical wind shear, the motion is directed towards the south (north). This motion is consistently observed for simulations including physical processes and those made in their absence. The magnitude of the initial deviation increases along with the magnitude of the shear vector. Furthermore, even for equivalent shear magnitudes, different vertical horizontal wind structures exhibit different deviational magnitudes. For westerly shear, the deviations are slightly greater for easterly flow simulations than for their shear magnitude counterparts in westerly flow. For zero layer mean wind simulations, the directional deviations are much greater.

As shown in Chapter 3, cumulus convection and surface drag effects induce a component of motion towards the right of the direction of vortex motion. However, the cumulus effect is somewhat inhibited when the basic currents in each layer are of opposite direction. Positional differences, caused by different advection rates, between the upper and lower vortex can further influence the direction of the layer 1 vortex. This is observed, most obviously, within the first 24 hours for the simulations with easterly flow having westerly shear. The effect is a

further southward displacement that is proportional to the shear magnitude. Cumulus transports act quickly to compensate for this initial position deviation between layers due to advection. After the initial period of rapid intensification, rightward movement due to cumulus convection slows somewhat. Short term changes in the direction of the layer 1 vortex are also observed at later times during the model integrations and seem to be correlated with large lags of the upper layer vortex behind the lower vortex.

The inclusion of a variable Coriolis parameter acts to induce a northwestward component of vortex motion in all simulations. For easterly (westerly) flow, the ß-effect acts to increase (decrease) the zonal speed of the vortex center. For the sheared experiments, the inclusion of the ß-effect does result in slightly different advection of the upper level vortex. The results show a convergence of the tracks in the shear experiments in easterly flow but a divergence in westerly flow. This indicates, again, that the vertical structure of the basic currents could play an important role in determining the track of a cyclone.

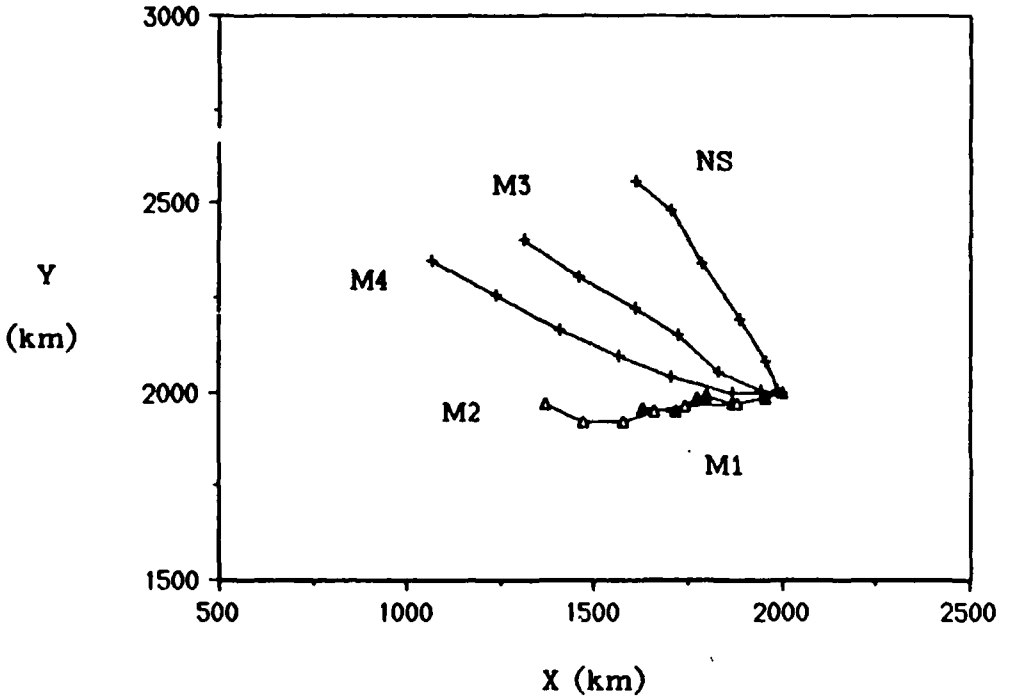

Figure 27 The 72-hour tracks of the layer 1 vorticity maximum for all $\bar{U} = 0$ simulations. Symbols mark the positions of the f-plane (triangles) and ß-plane (hatches) vortices at 12-hour intervals.

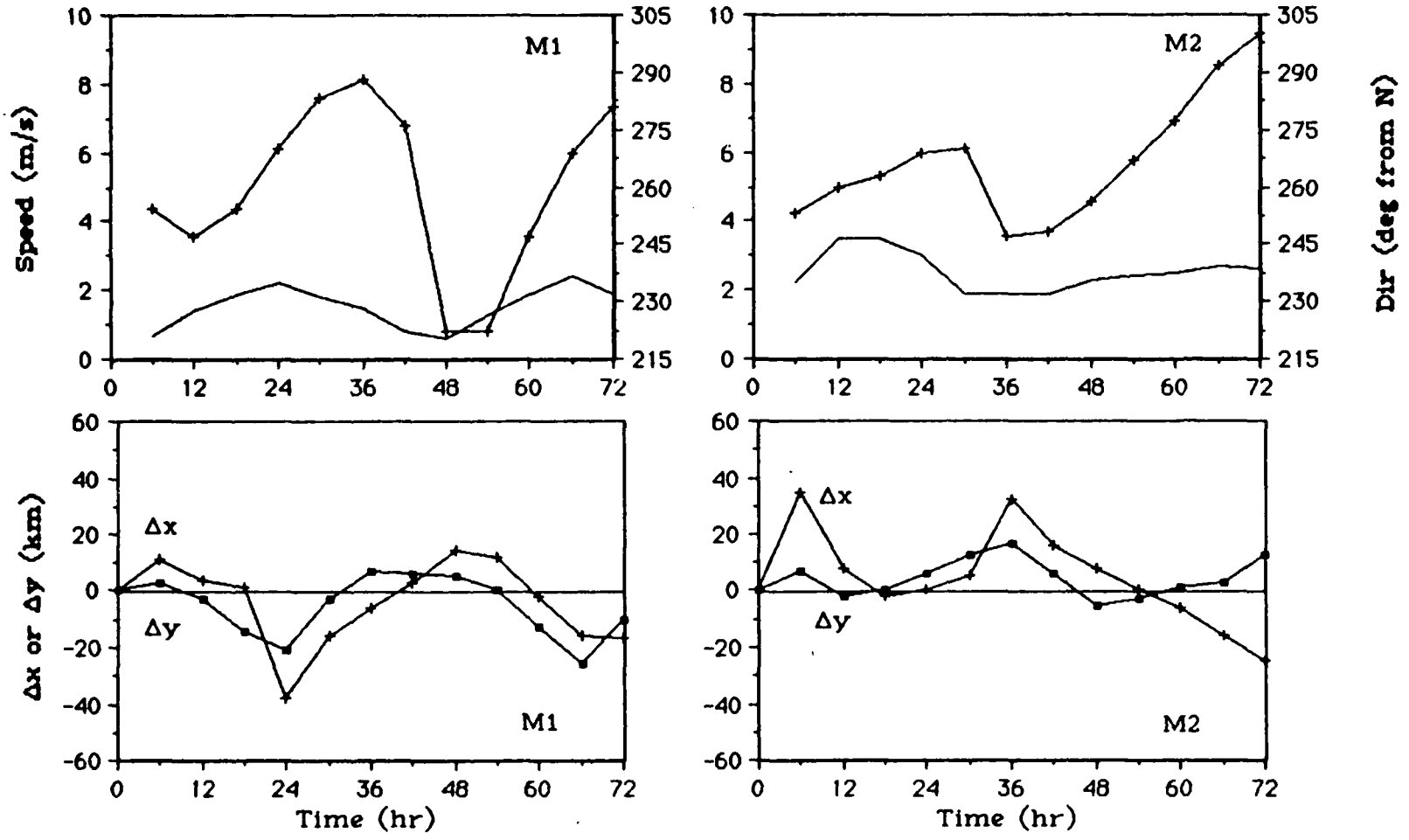

Figure 28 Time evolution of the speed (solid) and direction (hatched) of layer 1 vorticity maximum (top). Upper and lower vortex positional deviations (bottom), Δx or Δy indicates an eastward or northward displacement of the layer 2 vortex relative to the layer 1 vortex for M1 (left) and M2 (right).

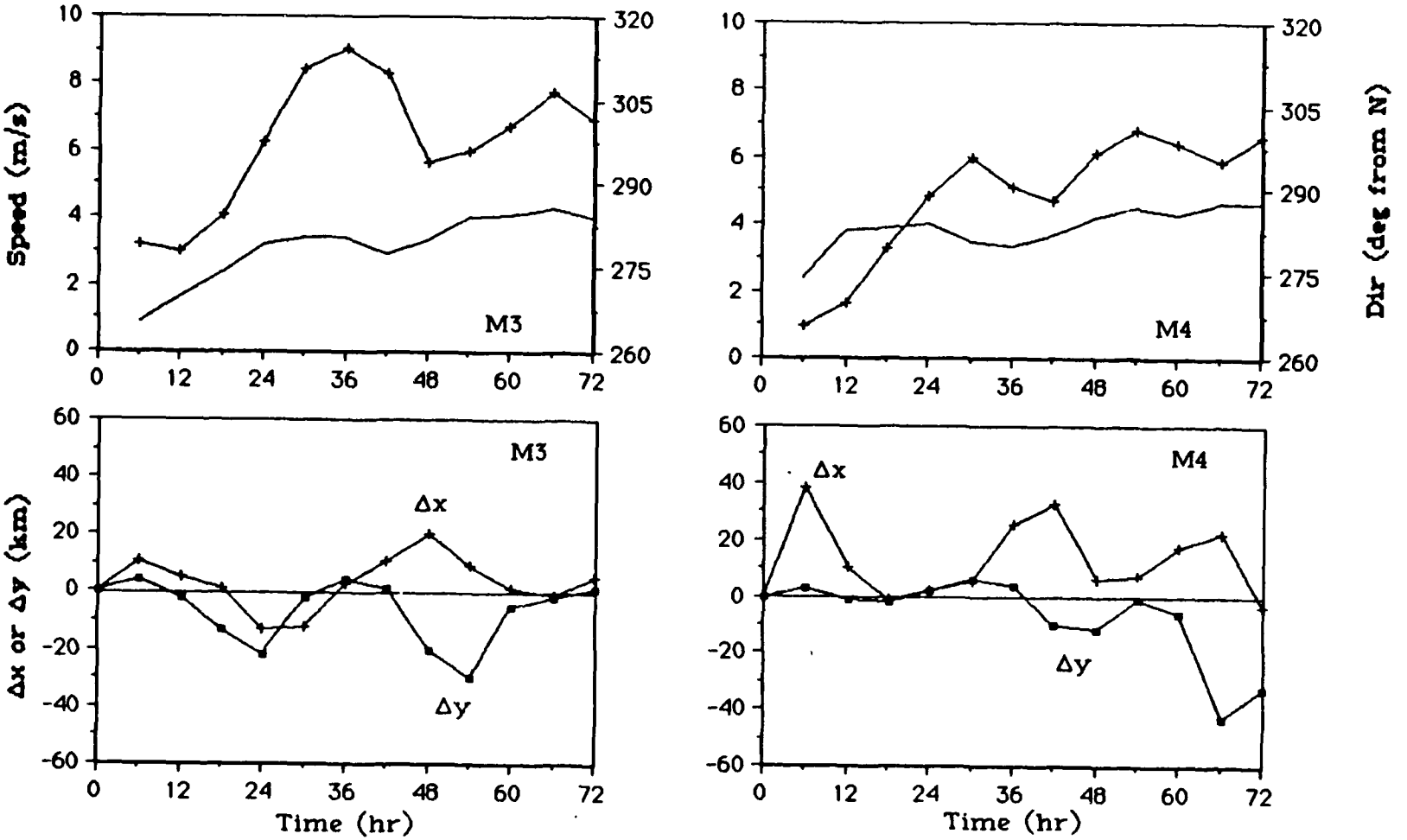

Figure 29 Time evolution of the speed (solid) and direction (hatched) of layer 1 vorticity maximum (top). Upper and lower vortex positional deviations (bottom), Δx or Δy indicates an eastward or northward displacement of the layer 2 vortex relative to the layer 1 vortex for M3 (left) and M4 (right).

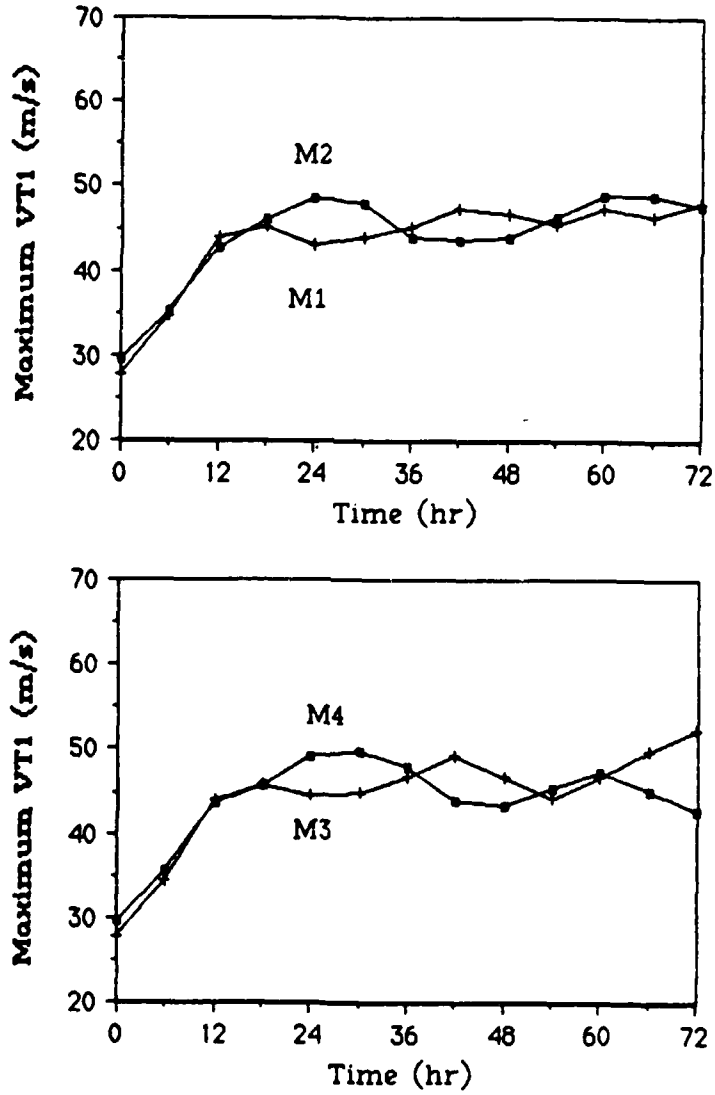

Figure 30 Time evolution of the maximum layer 1 tangential wind VT for cases M1 and M2 (top), M3 and M4 (bottom).

5. Simulations with Variable Origins and Sea Surface Temperatures

5.1. Description of Simulated Environmental Conditions

In this chapter, the movement of a simulated tropical cyclone under more realistic environmental conditions is investigated in light of previous findings. To accomplish this, an anticyclone is simulated in the low and middle levels using:

$$U_i = u \sin\left[\frac{2\pi y}{L_y}\right] \tag{5.1}$$

$$V_i = v \sin\left[\frac{2\pi x}{L_x}\right] \tag{5.2}$$

where $u = -10\,ms^{-1}$ and $v = 10\,ms^{-1}$. Therefore, the diameter of this anticyclone is 2000 km with maximum tangential winds of 10 ms^{-1} occurring at a radius of 1000 km from the anticyclone center which is located at the center of the model domain. The upper layer wind field is given by equation (5.1) which corresponds to a single sine wave in the north-south direction with simulated easterlies to the south and westerlies to the north. The maximum amplitude of the upper layer basic current is taken to be $u = -8$ ms^{-1}. The zonal component of the vertical wind shear vector is increasingly positive to the south of $y = 2000$ km and increasingly negative to the north of this position. The meridional shear magnitude is increasingly positive everywhere to the left of $x = 2000$ km and increasingly negative to the right of this position. The meridional and zonal shear fields are depicted in Figure 31.

In order to make further comparisons between the NDBM and the PEMOD, a vortex with the same structure as previous simulations is placed at the coordinates of (2000 km, 1000 km) and integrated for 72 hours

using the PEMOD. This simulation is repeated using the NDBM with an identical anticyclone simulated in its only layer. Furthermore, to determine if sensitivity experiments with barotropic models are valid, subsequent model runs are made with the vortex origin displaced by 100 km to the North, South, East, and West of the central position given above.

Research has shown that the intensity of a tropical cyclone is sensitive to the temperature of the sea surface. It is well known that tropical cyclones do not form over waters having temperatures less than 26°C. Chang and Madala (1980) ran numerical experiments which indicated that the path of a tropical cyclone was only slightly affected by changes in sea surface temperatures. In order to further investigate this effect on tropical cyclone movement, the central position PEMOD case is repeated for different values of sea surface temperatures ranging from approximately 25.5° to 29°C. Table 7 summarizes the simulations presented in this chapter.

5.2 β-plane Results with Varying Origins

The 72-hour tracks of the NDBM simulations described above are displayed in Figure 32 while those run on the PEMOD are displayed in Figure 33. Because of periodic boundary conditions, when the simulated cyclone passes beyond the left boundary, it moves into regions of northeasterly flow. Symbols mark the vortex positions at 12-hour intervals. An examination of Figure 32 shows that the NDBM simulations marked N2, C2, and S2 have nearly parallel tracks. These simulations all originated in purely zonal flow so that the initial movement is due to

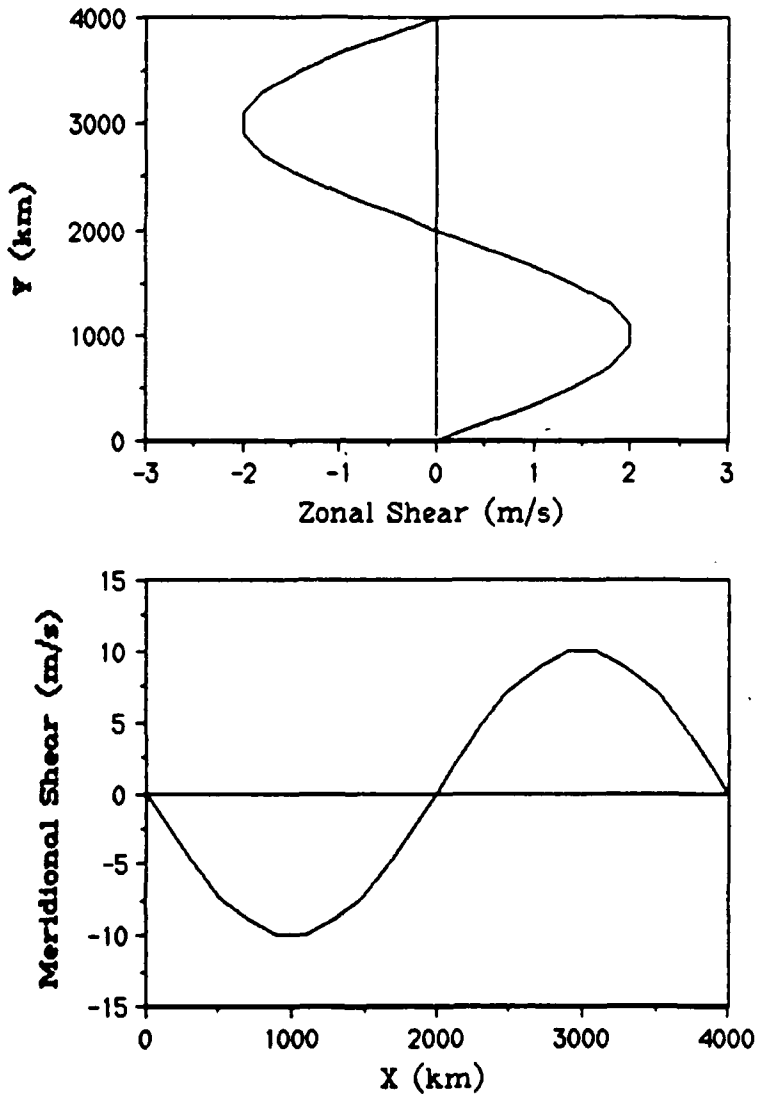

Figure 31 Zonal shear field [U_{200mb} - U_{600mb}] (top) and meridional shear field [V_{200mb} - V_{600mb}] (bottom) for all Chapter 5 PEMOD simulations.

Table 7. Summary of simulations presented in Chapter 5.

Simulation	Model	Origin x_o, y_o	Sea Surface Temperature
C1	PEMOD	2000, 1000	27.5°C
N1	PEMOD	2000, 1100	27.5°C
S1	PEMOD	2000, 900	27.5°C
E1	PEMOD	2100, 1000	27.5°C
W1	PEMOD	1900, 1000	27.5°C
C2	NDBM	2000, 1000	27.5°C
N2	NDBM	2000, 1100	27.5°C
S2	NDBM	2000, 900	27.5°C
E2	NDBM	2100, 1000	27.5°C
W2	NDBM	1900, 1000	27.5°C
C26	PEMOD	2000, 1000	25.5°C
C27	PEMOD	2000, 1000	26.5°C
C29	PEMOD	2000, 1000	28.5°C

advection by the easterly current. The cyclones then move more towards the north due to the ß-effect and advection by the increasingly southerly current. For the E2 case, being originally embedded in a northeasterly current, the initial movement, due to advection, towards the southwest is observed. The resultant track is therfore divergent from that of the C2 case. The W2 case, originating in southeasterly flow, exhibits an initial motion towards the northwest due to advection by the basic current. With the inclusion of the ß-effect, the path of the W2 vortex has an even greater component of motion towards the north. Table 8, which presents the magnitude of displacements with time, show that the E and W cases rapidly diverge.

The PEMOD simulations, N1,S1, and C1, orginating in purely zonal flow exhibit similarly parallel tracks. These three cases also originate in regions having nearly the same magnitude of westerly wind shear and no meridional wind shear. In agreement with previous discussion, these cyclones move at slower speeds than the NDBM simulations due to the inclusion of surface drag, and with greater components of motion towards the north due to the inclusion of physical processes. The magnitude of this northward movement would be somewhat tempered due to the inclusion of westerly wind shear. The biggest difference between the NDBM and PEMOD tracks is observed in the motion of the E and W cases. The paths for these cases using the PEMOD are less divergent (from one another) than those run on the NDBM. This can be explained by the inclusion of a vertically varying wind. Originally, case E1 is placed in a region where the wind shear vector is positive towards the northeast. Therefore, in light of previous discussion, the initial deviation of the vortex would have

a component of motion directed to the right of the direction of the wind shear vector, towards the southeast. Hence, the southward deviation due to wind shear is not as great for E1 as for the N1, S1, and C1 cases. However, since E1 is initially embedded in a northeasterly current, it will have an added component of motion towards the south due to advection by the basic current. With the inclusion of physical processes, which induce northward motion, this cyclone does not diverge from the central case as much as observed in the NDBM case. On the other hand, the W1 case is initially in a region of southeasterly shear, therefore, a component of motion is induced to the southwest, which serves to act in opposition to advection by the southerly current in which it is embedded. The result being that the northward movement of the cyclone lessened so that divergence on the scale of the NDBM is not observed.

The positional errors between the simulations are given in Table 8. By 72 hours the average position differences from the four cases (N, S, E and W) are similar for both models. This suggests that, at least qualitatively, the study of initial position errors in a barotropic model is valid.

5.3 Sensitivity of Cyclone Movement to Sea Surface Temperatures

Experiment C1 is repeated for three simulations each using a different value of the sea surface temperature that is held constant throughout that simulation. Figure 34 (top) shows the time evolution of the maximum tangential winds for each simulation. As evidenced by this figure, the intensity of simulated cyclone is proportional, at all times, to the sea surface temperature. The greater the sea surface temperature the greater the intensity. However, the observed deviations in the simulated cyclone

paths are so small as to be insignificant during the 72-hour model run. The magnitude of the maximum deviation of one track to that of the central position case is only 28 km. The magnitudes of the position differences from the C1 case are shown at the middle of Figure 34.

A systematically observed factor was that the higher the sea surface temperature, the greater the northward displacement of the vortex. The north-south displacements are shown at the bottom of Figure 34. This figure indicates that the magnitude of the total displacement is dominated by the north-south displacement. Furthermore, an examination of the radial profiles of the layer 1 tangential winds (not shown) indicates that the structure of the vortex changes with increasing intensities. At the final time, the greater the sea surface temperature, the larger the storm. As shown by DeMaria (1985) and Fiorino and Elsberry (1987), structural changes outside the radius of maximum winds would effect cyclone movement. However, in the case presented here, the sensitivity of the track to the sea surface temperature is very small. This suggests that accurate track forecasts might still be possible without accurately simulating the vortex intensity.

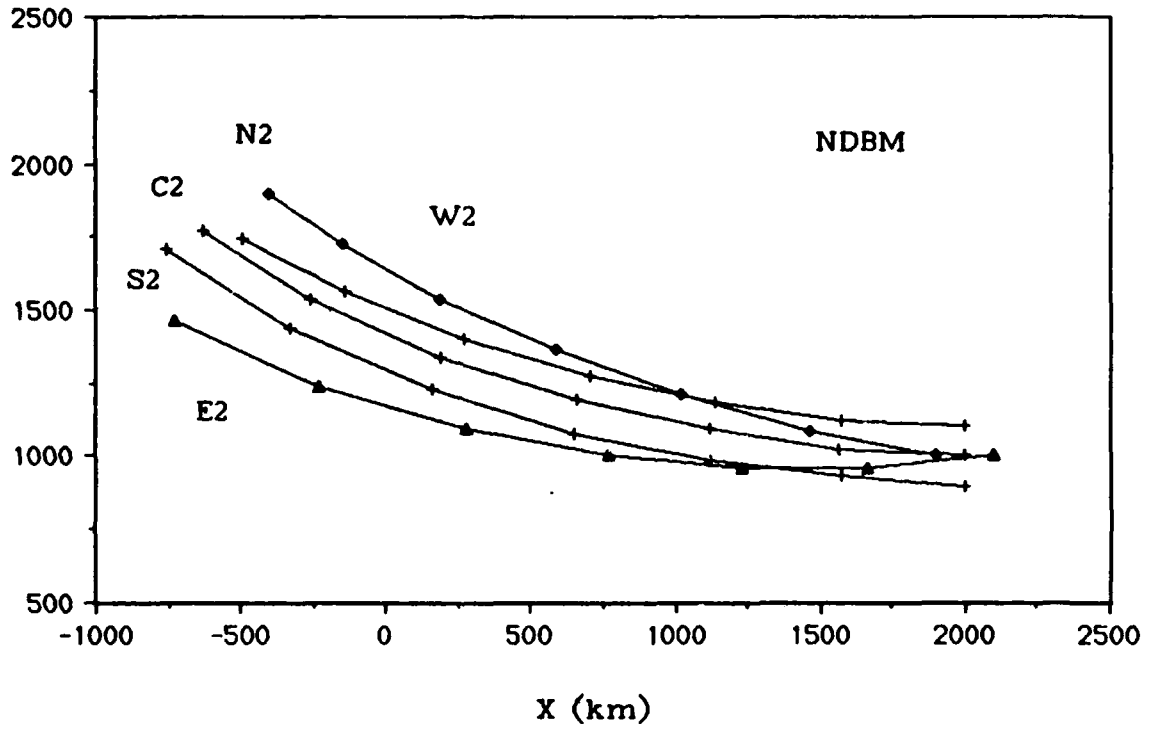

Figure 32 The 72-hour tracks of the layer 1 vorticity maximum for NDBM ß-plane simulations. Symbols mark vortex positions at 12-hour intervals.

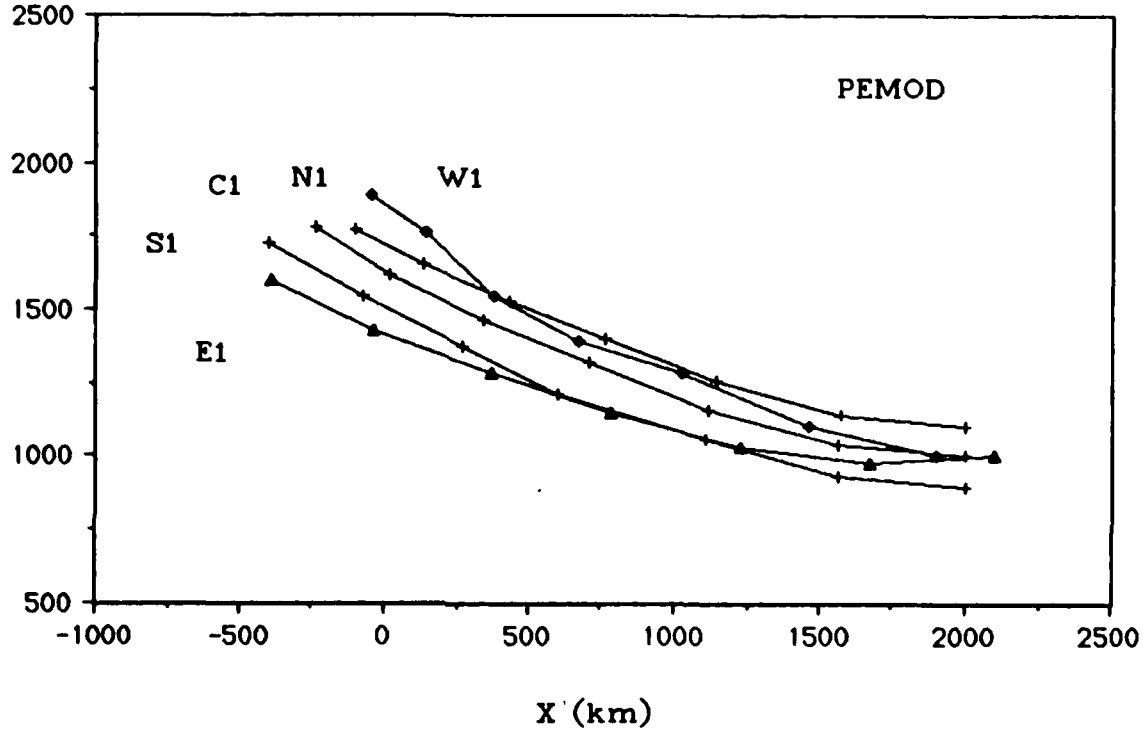

Figure 33 The 72-hour tracks of the layer 1 vorticity maximum for PEMOD simulations. Symbols mark vortex positions at 12-hour intervals.

Table 8. Magnitudes of the positional differences between C (central position case) and displaced origin cases for PEMOD and NDBM simulations.

Model	Simulations	Magnitude of Positional Difference (km)			
		0 hr	24 hr	48 hr	72 hr
PEMOD	C1/N1	100	98	110	137
	C1/S1	100	105	113	167
	C1/E1	100	163	187	233
	C1/W1	100	152	90	224
	Average		130	125	190
NDBM	C2/N2	101	96	99	138
	C2/S2	101	108	116	146
	C2/E2	101	168	262	326
	C2/W2	100	154	200	257
	Average		132	169	217

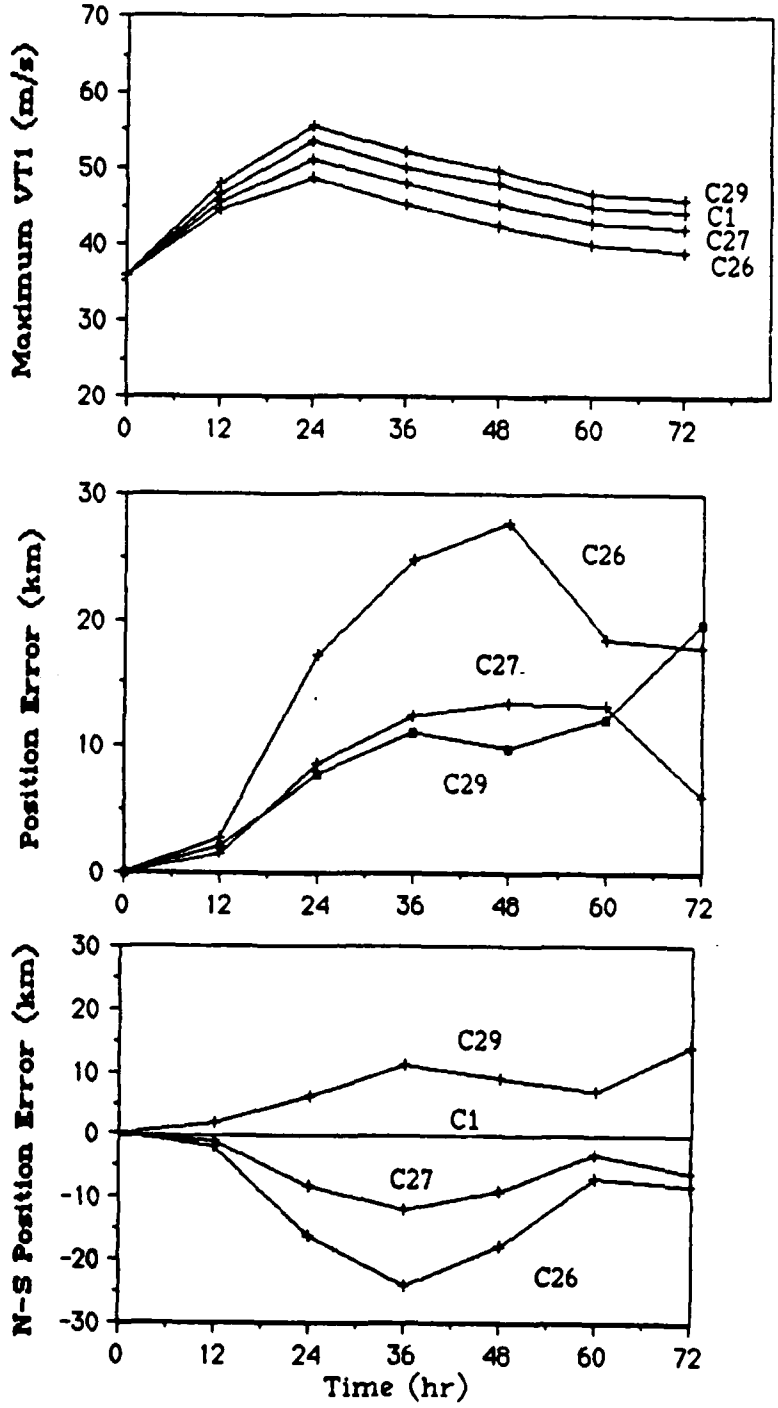

Figure 34 Time evolution of maximum tangential wind VT1 for varying sea surface temperatures (top). Magnitude of total displacement (middle) and north-south displacement (bottom) of C26, C27, and C29 cases from the C1 case versus time.

6. Discussion and Summary

A three-dimensional primitive equation model based upon Ooyama's incompressible fluid layer model is used to investigate the effect of vertical wind shear on tropical cyclone movement. The use of primitive equations allowed for the incorporation of the interactions between the large scale environment and the vortex. The vertical structure of the simulated cyclone was investigated by tracking the cyclone separately in the midtropospheric layer and in the outflow layer. In Chapter 2, a brief summary of this model was given along with results from simulations run under resting basic state conditions. These simulations, one on the f-plane and one on the ß-plane, utilized an initially strong barotropic cyclonic vortex in order to reduce the time needed for intensification to hurricane strength. The results of the simulations showed that the use of a strong vortex did not adversely affect the simulated cyclone features but did reduce the time of rapid intensification to under 24 hours in all simulations.

In order to investigate the effect of vertical shear on cyclone movement other factors affecting the movement must first be isolated. Therefore, in Chapter 3, simulations were run which successively included a linear barotropic basic current, surface drag, cumulus convection, and a variable Coriolis parameter. Simulations were run with an easterly basic current and repeated using a westerly basic current of the same magnitude. Relative vorticity advection of the vortex by the basic current was found to be the most dominant effect. As examplified by the simulations utilizing no physical processes (cases ND1 and ND4), the

vortex moved, in all layers, precisely with the basic current. Also, with no modeled physics included, the initial vortex failed to intensify further. These f-plane simulations were identical to simulations run on the NDBM under similar conditions.

With the inclusion of surface drag, all simulations showed a component of motion to the right of, and slower than, the basic current in agreement with theory (Kuo, 1968). The inclusion of cumulus convection induced movement of the cyclone towards the right front of the vortex, relative the direction of the vortex motion, due to the enhanced diabatic heating resulting from the frictionally induced boundary layer convergence. That this occurs on the right hand side of the barotropic vortex embedded in barotropic flow is a consequence of the greater wind speeds resulting from the addition of the basic current and the tangential wind speed of the vortex.

Finally, with the inclusion of a variable Coriolis parameter (ß-effect), a northwestward component of vortex motion was induced in all simulations, in agreement with results from a multitude of other numerical studies (e.g., Anthes and Hoke, 1975; Madala and Piacsek, 1975). This movement results in an enhancement of northwestward cyclone motion in easterly flow since all processes are acting in the same direction. In a westerly current, however, the ß-effect acts in opposition to both relative advection by the basic current and the motion induced by the physical processes. Furthermore, fully parameterized cases exhibited oscillations of the upper vortex about the lower vortex. The period of these oscillations increased with increasing wind speeds. Short term directional changes in the movement of the layer 1 vortex were observed

to be correlated with large deviations of the upper vortex to the rear of the lower vortex.

These results indicate that the steering current concept based on the horizontal advection of absolute vorticity (planetary plus relative), is valid in so much that it does dominate tropical cyclone motion. However, to accurately predict movement of a cyclone in barotropic current, the effects due to the physical processes of surface drag and moisture cannot be neglected. This was examplified in Table 5 which showed that the deviations between the NDBM (which excludes physical processes) cases and fully parameterized cases were quite large.

In Chapter 4, the effect of vertical wind shear on tropical cyclone movement was investigated by including increasingly greater shear magnitudes in model simulations. These experiments showed a systematic initial deviation of the cyclone towards the right of the direction of the wind shear vector, towards enhanced environmental temperatures. For westerly (easterly) wind shear, this initial deviation is towards the south (north) with westerly wind shear defined to be $[U_{200mb} - U_{600mb}] > 0$. That this effect is observed in cases with and without physical processes indicates that it results from the structure of the synoptic scale environment. This initial deviation from the basic current increases as the shear magnitude increases but is also sensitive to the vertical wind structure. Chan et. al. (1980) studied wind fields surrounding west Atlantic hurricanes. In general, the results of the shear experiments in this thesis are not in agreement with the conclusions of that study. However, an analysis of individual cases shows some similarities.

Furthermore, additional deviations are seen during the first 12 hours that are a result of the lagging of the upper level vortex behind the lower level vortex. The motion differential is a result of differing advection rates of the cyclone between layers due to the inclusion of vertically varying winds and is quickly compensated for by cumulus convection. This deviation caused by this vertical vortex displacement is observed to occur only for winds decreasing with height. With the inclusion of a nonbarotropic initial vortex, it is speculated that the motion differential would be seen for the westerly case as well. That vortex tilt does occur in nature was verified by Huntley and Diercks (1980) who correlated the vertical vortex tilt in three tropical cyclones with the vertical wind shear of the environmental winds. Furthermore, their study indicated that if the magnitude of the shear was not too strong, cumulus convection was able to overcome the motion differential. This was verified in the model simulations.

Many observational studies (e.g., Anthes, 1982; Chan and Gray, 1982; Holland, 1983) indicate that westward moving typhoons are observed to move to the left of and faster than the basic current. The majority of Atlantic hurricanes move to the right of the defined basic current, but leftward moving hurricanes are also observed. Vertical wind shear can explain this seemingly anomalous motion. For westerly wind shear, a leftward deviation is induced, if the shear magnitude was great enough in an easterly current, the shear effect could dominate over the physical processes and a leftward deviation from the basic current would be observed.

These research results are also in agreement with numerical studies by Jones (1977a). In that study, Jones attributed the rightward deviation of the vortex from the basic current (which had westerly vertical shear) to be a result of surface drag alone. In light of this research it can be considered to be a result of both the physical processes and the shear which partly compensated for the physical processes effect. Furthermore, Chan (1984) in an observational study which analyzed the vorticity budget of 22 west Atlantic hurricanes, concluded that the divergence term in the vorticity equation induced a 'propagation' of the vortex that was different from the steering current. This further indicates that vertical wind shear is an important factor effecting cyclone movement since this divergence term, in essence, couples the different layers.

Figure 35 gives a vector representation summarizing the effects of absolute vorticity advection, physical processes, and shear on the movement of a tropical cyclone. Keep in mind that this figure represents only the general effects. The magnitudes of these vectors are highly dependent upon the initial condition specifications. Although each of the effects shown in Figure 35 are probably secondary to the vorticity advection, it may be possible in some cases for all of the secondary effects to act in the same direction. (For example, a westward moving storm in easterly wind shear). In cases such as these, the storm track might be difficult to forecast. In addition, any forecasting technique which relies on climatology would probably be unreliable in such a situation.

In Chapter 5, it was shown that the inclusion of a vertically varying environment of an anticyclone lead to less sensitivity of the cyclone track

to initialization errors than for the NDBM. The effect of vertical wind shear on tropical cyclone motion was in agreement with previous discussion. Sea surface temperature experiments indicated that the effects of increasingly larger temperatures on the path of a tropical cyclone were negligible during a 72-hour integration for this case.

The implications of this research to tropical cyclone forecasting indicate that vertical wind shear can substantially alter the track of a tropical cyclone and explain some of the anomalous motion (both long and short term) observed in nature. The effect or the movement of the cyclone depends not only on the magnitude and direction of the shear, but also on the magnitude and direction of the basic current in each layer. This indicates that the use of a vertically averaged layer mean wind as the defined steering current could lead to large positional errors in track forecasting in some cases.

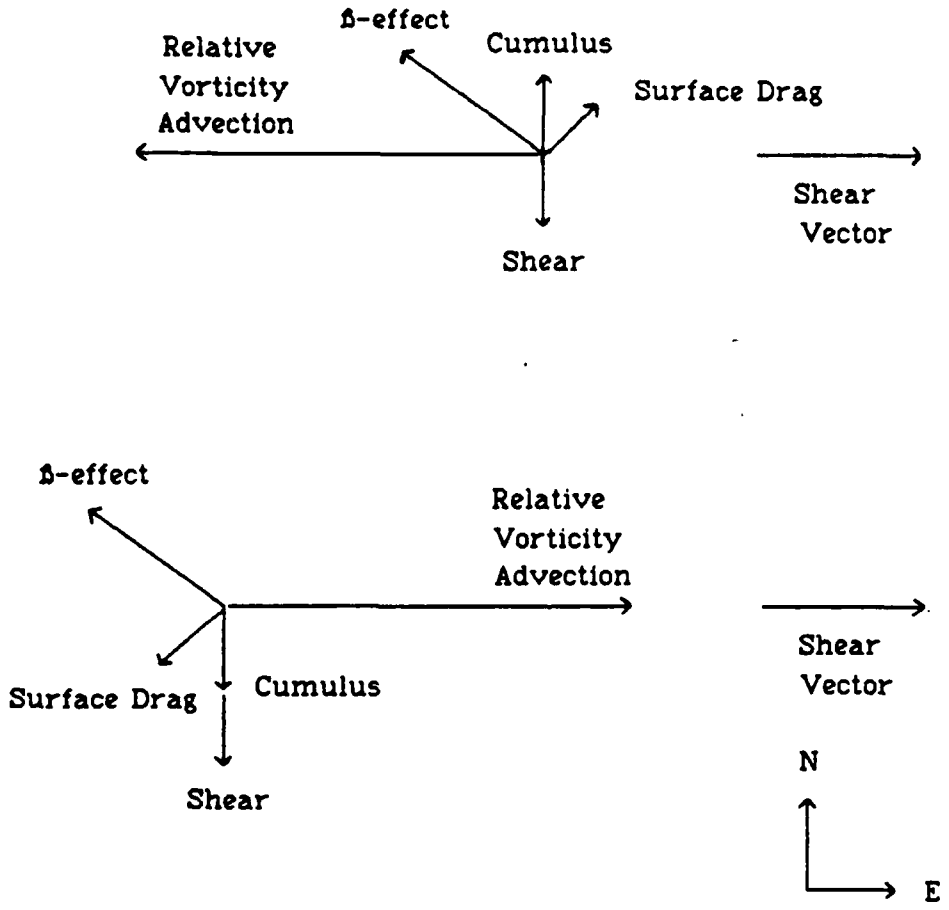

Figure 35 Vector representation of factors affecting tropical cyclone movement for a cyclone embedded in easterly (top) and westerly (bottom) current with westerly vertical wind shear.

7. List of References

Anthes, R.A., and J.E. Hoke, 1975: The effect of horizontal divergence and the latitudinal variation of the Coriolis parameter on the drift of a model hurricane. Monthly Weather Review, v. 103, p. 757-763.

Anthes, R.A., 1982: Tropical Cyclones: Their Evolution, Structure and Effects. Meteorological Monographs, No. 41, American Meteorological Society, 208 pp.

Chan, J.C.L. and W.M. Gray, 1982: Tropical cyclone movement and surrounding flow relationships. Monthly Weather Review, v. 110, p. 1354-1374.

Chan, J.C.L., 1984: Identification of the steering flow for tropical cyclone motion from objectively analyzed wind fields. Monthly Weather Review, v. 113, p. 106-116.

Chan, J.C.L., W.M. Gray and S.Q. Kidder, 1980: Forecasting tropical cyclone turning motion from surrounding winds and temperature fields. Monthly Weather Review, v. 108, p. 778-792.

Chan, J.C.L., 1986: Supertyphoon Abby - An example of present track forecast inadequacies. Weather and Forecasting, v.1, p. 113-126.

Chang S.W., and R.V. Madala, 1980: Numerical simulation of the influence of sea surface temperature on translating tropical cyclones. Journal of the Atmospheric Sciences, v. 37, p. 2617-2630.

Charney, J., and A. Eliassen, 1964: On the growth of the hurricane depression. Journal of the Atmospheric Sciences, v. 21, p. 68-75.

DeMaria, M., 1983: Experiments with a spectral tropical cyclone model. Department of Atmospheric Science Paper No. 371, Colorado State University, Ft. Collins, CO, 224 pp.

DeMaria, M., 1984: Sensitivity of a three-layer spectral tropical cyclone model to initialization procedures. Preprints 15th Conference on Hurricanes and Tropical Meteorology, Miami, FL, American Meteorological Society, p. 325-330.

DeMaria, M., and W.H. Schubert, 1984: Experiments with a spectral tropical cyclone model. Monthly Weather Review, v. 41, p. 901-924.

DeMaria, M., 1985: Tropical cyclone motion in a nondivergent barotropic model. Monthly Weather Review, v. 113, p. 1199-1210

DeMaria, M., and J. Pickle, 1987: A simplified system of equations for simulation of tropical cyclones. Submitted to Journal of the Atmospheric Sciences.

Fiorino, M., and R.L. Elsberry, 1987: The role of vortex structure in barotropic tropical cyclone motion. Preprints 17th Conference on Hurricanes and Tropical Meteorology, Miami, FL, American Meteorological Society, p. 55-59.

George, J.E., and W.M. Gray, 1976: Tropical cyclone motion and surrounding parameter relationships. Journal of Applied Meteorology, v. 15, p. 1252-1264.

Holland, G.J., 1983: Tropical cyclone motion: environmental interaction plus a beta effect. Journal of the Atmospheric Sciences, v. 40, p. 328-342.

Hastenrath, S., 1985: Climate and Circulation of the Tropics. Boston, D. Reidel, 455 pp.

Hovermale, J.B., and R.E. Livezey, 1977: Three-year performance characteristics of the NMC hurricane model. Preprints 11th Technical Conference on Hurricanes and Tropical Meteorology, Miami, FL, American Meteorological Society, p. 122-124.

Huntley, J.E., and J.W. Diercks, 1981: The occurrence of vertical tilt in tropical cyclones. Monthly Weather Review, v. 109, p. 1689-1700.

Jones, R.W. 1977: Vortex motion in a tropical cyclone model. Journal of the Atmospheric Sciences, v. 34, p. 1518-1527.

Kasahara, A., 1957: The numerical prediction of hurricane movement with the barotropic model. Journal of Meteorology, v. 14, p. 386-401.

Kasahara, A., and G.W. Platzman, 1963: Interaction of a hurricane with the steering flow and its effect upon the hurricane trajectory. Tellus, v. 4, p. 321-334.

Kitade, T., 1980: Numerical experiments of tropical cyclones on a plane with a variable Coriolis parameter. Journal of the Meteorological Society of Japan, v. 58, p. 471-488.

Kuo, H.L., 1968: Motions of vortices and circulating cylinder in shear flow with friction. Journal of the Atmospheric Sciences, v. 26, p. 390-398.

Madala, R.V. and S.A. Piacsek, 1975: Numerical simulation of asymmetric hurricanes on a ß-plane with vertical shear. Tellus, v. 27, p. 453-468.

Ooyama, K.V., 1969: Numerical simulation of the life cycle of tropical cyclones. Journal of the Atmospheric Sciences, v. 26, p. 3-40.

Orzag, S.A., 1970: Transform method for the calculation of vector-coupled sums: Application to the spectral form of the vorticity equation. Journal of the Atmospheric Sciences, v. 27, p. 890-895.

Sanders, F., and R.W. Burpee, 1968: Experiments in barotropic hurricane track forecasting. Journal of Applied Meteorology, v. 7, p. 313-324.

Shapiro, L.J., 1983: The asymmetric boundary layer flow under a translating hurricane. Journal of the Atmospheric Sciences, v. 40, p. 1984-1998.

Shea, D.J., and W.M. Gray, 1973: The hurricanes inner core region, I: symmetric and asymmetric structure. Journal of the Atmospheric Sciences, v. 30, p. 1544-1564.

Stevens, D.E., R.S. Lindzen and L.J. Shapiro, 1977: A new model of tropical waves incorporating momentum mixing by cumulus convection. Dynamics of Atmospheres and Oceans, v. 1, p. 365-425.

Yeh, T.C., 1950: The motion of tropical storms under the influence of a superimposed southerly current. Journal of Meteorology, v. 7, p. 108-113.